Faculdade de Engenharia da Universidade do Porto



Production of Functional Hollow Spheres for Bone Regeneration

Inês Moreira da Silva

Mestrado Integrado de Bioengenharia

Supervisor: Prof. Maria Ascensão Ferreira Silva Lopes

June 2020

© Inês Silva, 2020

Abstract

The human skeleton is responsible for conferring structure and protection to the human body, as well as being a deposit of important substances and ions. Despite its remarkable strength and healing properties, bone is still subject to being damaged due to external traumas or due to degeneration of bone structure caused by aging or diseases. It is thus crucial to find methods to ensure safe, efficient and complete regeneration of damaged bone, and to this end, bone substitutes are used. Though they can be of natural origin, synthetic bone substitutes have the advantage of being able to be mass produced with high reproducibility, as well as being able to have their properties be modified to be better suited for different sites of bone injury, as well as for different types of injury. Calcium phosphate-derived ceramic substitutes are particularly popular, due to the high level of biocompatibility and osteoconductive properties they have in the presence of host bone tissue.

This work aimed to produce synthetic hydroxyapatite microspheres whose structural properties would allow for proper bone growth and vascularization, as well being capable of encapsulation and controlled release of drugs that would facilitate the process of bone regeneration. The drugs used were gentamicin, an antibiotic that can prevent bone infection during and after post-operative procedures, and raloxifene, a selective estrogen receptor modulator that has been shown to prevent bone loss, mainly by deterring the activity of osteoclasts, while supposedly increasing osteoblasts' activity. In the end, two groups of drug-loaded spheres were produced: ones loaded with gentamicin, and the other loaded with raloxifene-PEG conjugate – this type of conjugate was produced to ensure that raloxifene, who has low solubility in aqueous solutions, would be properly incorporated in the drug loading solutions, and present a release profile of clinical interest. Drug loading was performed under low vacuum conditions and drug release assessed in an environment as closely as possible to clinical applications. Cell culture assays were performed, to test gentamicin's capacity of disrupting the growth of infectious bacteria, using *E. coli* ATCC 25922 bacteria, and the potential cytotoxic effects of raloxifene-PEG, using MG-63 – human osteoblast-like cells.

The results showed that microsphere porosity was appropriate for basic bone cell growth, but that overall porosity should be optimized to reliably ensure complete vascularization of new bone tissue.

Regarding the controlled release of gentamicin, sustained release did not last for as long as it was intended, lasting for 3 days instead of 1 week, but the desired levels of the released drug were achieved. For raloxifene-PEG, sustained drug release lasted for the intended period of two weeks. However, the values of concentration that were obtained have the risk of being cytotoxic to human host tissues. Based on the obtained results, further studies should be performed to tune the drug release profile of both gentamicin and raloxifene-PEG.

Keywords: Bone Regeneration, Calcium Phosphate, Porous Microspheres, Gentamicin, Raloxifene, Controlled Drug Release

Resumo

O esqueleto humano é responsável por providenciar estrutura e proteção ao corpo humano, sendo também um depósito de substâncias e iões essenciais. Apesar da sua resistência e capacidades regenerativas notáveis, o osso continua sujeito a ser danificado por traumas externos ou devido à degeneração da estrutura óssea provocada pelo envelhecimento ou por doenças. Torna-se então crucial encontrar métodos para garantir uma regeneração óssea segura, eficiente e completa, e para este fim, os substitutos ósseos são usados. Apesar de poderem ter uma origem natural, os substitutos ósseos sintéticos têm as vantagens de poderem ser produzidos em massa com alta reprodutibilidade, e de se poder alterar as suas propriedades para uma melhor compatibilidade com os diferentes locais danificados do osso e com os diferentes tipos de danos possíveis. Substitutos cerâmicos derivados de fosfatos de cálcio são particularmente populares, devido ao seu elevado nível de compatibilidade e propriedades osteocondutoras, quando na presença do tecido ósseo do paciente.

Este trabalho visa a produção de microesferas cerâmicas de hidroxiapatite, cujas propriedades estruturais permitam o crescimento e vascularização adequados de tecido ósseo, assim como o encapsulamento e libertação controlada de fármacos que facilitem o processo de regeneração óssea. Os fármacos usados foram a gentamicina, um antibiótico que consegue prevenir infeção óssea durante e após cirurgia, e raloxifeno, um modulador seletivo de recetores de estrogénio que consegue prevenir perda de material ósseo, principalmente pela inibição da atividade de osteoclasto e, potencialmente, pela estimulação da atividade de osteoblastos. No final, dois grupos de esferas carregadas de fármacos foram produzidas: umas carregadas com gentamicina e outras carregas com conjugado de raloxifeno-PEG – este tipo de conjugado foi produzido para assegurar que o raloxifeno, que possui baixa solubilidade em soluções aquosas, fosse incorporado devidamente nas soluções de carregamento de fármacos e apresentasse um perfil de libertação de interesse clínico. O carregamento de fármacos foi realizado em condições de baixo vácuo e a libertação de fármacos foi realizada num ambiente que fosse o mais próximo possível que os observados em aplicações clínicas. Ensaios de culturas celulares foram realizados para testar a capacidade da gentamicina de inibir o crescimento de bactérias infeciosas, usando a bactéria *E. coli* ATCC 25922, e para testar potenciais efeitos citotóxicos do raloxifeno-PEG, usando células humanas MG-63.

Os resultados demonstraram que a microporosidade obtida é apropriada para o crescimento essencial de células ósseas, mas que a porosidade geral deve ser otimizada para garantir com baixa margem de erro a vascularização completa de novo tecido ósseo.

Relativamente à libertação controlada de gentamicina, a libertação contínua não durou o período pretendido, durando por 3 dias em vez de uma semana, mas os níveis desejados de fármaco liberto foram alcançados. Para o raloxifeno-PEG, a libertação do fármaco durou o tempo pretendido de duas

semanas. No entanto, os valores de concentração obtidos correm o risco de serem citotóxicos para o tecido celular do paciente. Baseado nos resultados obtidos, devem ser realizados estudos adicionais para aperfeiçoar a perfil de libertação dos fármacos, tanto da gentamicina como do raloxifeno-PEG.

Palavras-Chave: Regeneração Óssea, Fosfato de Cálcio, Microsferas Porosas, Gentamicina, Raloxifeno, Libertação Controlada de Fármacos

Acknowledgements

I would like to express my thanks towards my supervisor Prof. Maria Ascensão Lopes for her continuous guidance, advice and patience throughout this study. I would also like to thank Laboratory Technician Carla Ferreira at the Department of Chemical Engineering, and Laboratory Technician Maria Cândida at the Department of Metallurgical and Materials Engineering, for providing me with materials and access to equipment that were necessary to perform the work.

I am very grateful to Prof. Liliana Grenho and her colleagues at the Department of Biomedicine of the Dental Health Faculty of the University of Porto (FMDUP), for providing the materials, space and supervision necessary for the performance of cell culture studies.

I am deeply thankful to my former work colleague Joana Reis, for all the assistance and support she gave me during the early stages of the thesis.

I extended my thanks to Investigator Miguel Rodrigues at the Department of Metallurgical and Materials Engineering, for providing me with helpful advice and valuable input during the revision stage of my thesis.

Finally, I wish to express thanks to my parents and my older sibling, for the immense encouragement and emotional support they provided me during the most arduous moments.

Table of Contents

Abstract i
Resumo iii
Acknowledgements v
Table of Contents vii
List of Figures ix
List of Tables xi
Abbreviations and Symbols xiii
Chapter 1 - Introduction 1
1.1. Aim of the Study 1
Chapter 2 - State of the Art 2
2.1. The Biology of Bone Tissue 2
2.1.1. Anatomy and Properties of Bone Tissue 2
2.1.1.1. Compact Bone and Spongy Bone 2
2.1.2. Bone Cells 3
2.2. Bone Fractures 4
2.2.1. Bone Mineral Density 5
2.2.2. Osteoporosis 6
2.3. Bone Fracture Healing 7
2.3.1. Bone Grafting 8
2.3.2. Synthetic Bone Substitutes 10
2.3.3. Drug Treatments 13
2.3.3.1. Controlled Drug Delivery 13
2.3.3.1.1. Gentamicin 15
2.3.3.1.2. Raloxifene 15
Chapter 3 - Materials and Methods 18
3.1. Materials 18
3.2. Methods 18
3.2.1. Preparation of the Microspheres 18
3.2.1.1. Syringe-Foaming 19
3.2.1.2. Co-Injection 19
3.2.1.3. Heat Treatment 21
3.2.2. Characterization of the Microspheres 22
3.2.2.1. Helium Pycnometry 22
3.2.2.2. Morphological Analysis by Scanning Electron Microscopy 22
3.2.2.3. Microsphere Size and Porosity Analysis 22
3.2.3. Drug Delivery Studies 23
3.2.3.1. Gentamicin Loading 23
3.2.3.2. Gentamicin Release Profiles of the Microspheres 23
3.2.3.3. Fluorometric Analysis 24
3.2.3.4. Raloxifene-PEG Conjugate 24
3.2.3.5. Ral-PEG Loading 25
3.2.3.6. Raloxifene Release Profile of the Microspheres 25
3.2.3.6.1. Continuous Drug Release 25
3.2.3.6.2. Non-Continuous Drug Release 26
3.2.3.7. Spectrophotometric Analysis 26
3.2.4. Cell Culture Studies 27
3.2.4.1. *E. coli* ATCC 25922 Strain 27
3.2.4.2. Effects of Gentamicin on *E. coli* ATCC 25922 Bacteria 27
3.2.4.2.1. Dose Dependent Effects of Gentamicin 27

3.2.4.2.2. Effects of Gentamicin Loaded Microspheres 27
3.2.4.3. MG-63 Cell Line 27
3.2.4.4. Effects of Ral-PEG on MG-63 Cells 27
3.2.4.4.1. Dose Dependent Effects of Ral-PEG 28
3.2.4.4.2. Effects of Ral-PEG on Collagen Production 28
3.2.4.4.3. Effects of Ral-PEG Loaded Microspheres 29
3.2.5. Statistical Analysis 30

Chapter 4 - Results and Discussion 31
4.1. Preparation of the Microspheres 31
4.2. Characterization of the Microspheres 33
4.2.1. Helium Pycnometry 34
4.2.2. Morphological Analysis by Scanning Electron Microscopy 34
4.2.3. Microsphere Size and Porosity Analysis 39
4.3. Drug Release Studies 41
4.3.1. Gentamicin 41
4.3.2. Raloxifene-PEG 44
4.4. Cell Culture Studies 47
4.4.1. Effects of Gentamicin – Indirect Studies 47
4.4.2. Effects of Gentamicin – Direct Studies 48
4.4.3. Effects of Ral-PEG 49
4.4.3.1. Dose Dependency 49
4.4.3.2. Collagen Production 52
4.4.3.3. Hollow Hap Microspheres 55

Chapter 5 - Conclusions 58

Chapter 6 - Future Works 60

References 61

List of Figures

Figure 1 - Longitudinal cut of the proximal femoral epiphysis, demonstrating how spongy bone and trabecular bone are organized within it. Adapted from [6]. 2

Figure 2 - Microstructure of a long bone. Adapted from [8]. 3

Figure 3 - Four cell types that exist within bone tissue. Adapted from [9]. 4

Figure 4 - Variation of bone mass (total mass of calcium in the skeleton in grams) with age (in years). Adapted from [9]. 5

Figure 5 - Phases of bone fracture healing, in a long bone. Adapted from [28]. 8

Figure 6 - Chemical structure of gentamicin sulphate. Adapted from [63]. 15

Figure 7 - Chemical structure of raloxifene. Adapted from [77]. 16

Figure 8 - Schematic representation of syringe-foaming procedure. a) Firstly, two 12 mL syringes are filled, one with 2.5 mL of air and the other with 3.5 mL of the foaming agent - F-127 (10%, w/v) in this case. b) Secondly, the tips of the syringes are linked together with a connecting piece, and their pistons are simultaneously pushed back and forth rhythmically for about 40 seconds, until the resulting foam phase has a volume of about 6 mL. 19

Figure 9 - Schematic representation of a longitudinal cut of the cylindrical coaxial mould. 20

Figure 10 - Schematic representation of the formation of porous microspheres with a hollow core through co-injection. The polystyrene solution (PS) is injected into the core of the ceramic foam droplets. When falling into the $CaCl_2$ solution, the droplets adopt a spherical shape and then go through reticulation, with the injected polymer at its centre. 20

Figure 11 - Heat treatment profile for porous hydroxyapatite microspheres. 21

Figure 12 - Schematic representation of a 96-well microplate seeded with MG-63 human osteoblast-like cells, for the purpose of showing the effect that hollow Hap microspheres loaded with Ral-PEG have on these cells. Columns 1 to 6 correspond to spheres loaded with different quantities of Ral-PEG, according to the different time instants at which they were collected during Ral-PEG release – 2 hours, 4 hours, 8 hours, 1 day, 3 days and 7 days. Column 7 functions as a control wherein the effect of non-loaded spheres on the MG-63 cells is examined. Column 8 function as a control wherein the spheres have not been exposed to a release medium, meaning that they are fully loaded with Ral-PEG. Column 9 functions as a control with neither spheres nor cells, acting as a blank containing only the growth medium. 29

Figure 13 - Concentration of gentamicin in aqueous release solution, plotted against time. H-3: hollow microspheres with a loading solution of 3 mg/mL; NH-3: non-hollow microspheres with a loading solution of 3 mg/mL; H-2: hollow microspheres with a loading solution of 2 mg/mL; NH-2: non-hollow microspheres with a loading solution of 2 mg/mL. Error bars indicate standard deviations in μg/mL. a) Detail of gentamicin concentration values in the first 10 hours. 42

Figure 14 - Cumulative mass of gentamicin that was measured in the aqueous release solution, plotted against time. H-3: hollow microspheres with a loading solution of 3 mg/mL; NH-3: non-hollow microspheres with a loading solution of 3 mg/mL; H-2: hollow microspheres

with a loading solution of 2 mg/mL; NH-2: non-hollow microspheres with a loading solution of 2 mg/mL. Error bars indicate standard deviations in µg. 43

Figure 15 - Concentration of Ral-PEG in PBS release solution plotted against time, during the first week of release. This drug release corresponds to both hollow and non-hollow Hap microspheres that were previously loaded in a 1m/mL solution of Ral-PEG. Error bars indicate standard deviations in µg/mL. No statistical differences between plot values were observed at any time interval ($p < 0.05$). a) Detail of Ral-PEG concentration values in the first 48 hours. 45

Figure 16 - Cumulative mass of Ral-PEG measured in the PBS release solution plotted against time, during the two weeks of release. This drug release corresponds to both hollow and non-hollow Hap microspheres that were previously loaded in a 1m/mL solution of Ral-PEG. Error bars indicate standard deviations in µg/mL. No statistical differences between plot values were observed at any time interval ($p < 0.05$). 46

Figure 17 - Results of incubation of *E. coli* cultivated in Mueller-Hinton agar alongside filter disks imbibed with gentamicin release solutions. Tags near the disks indicate the instant at which the release solution in the disk was collected. a) Release solutions that originated from microspheres initially loaded with gentamicin solutions of 2 mg/mL and b) 3 mg/mL. 48

Figure 18 - Results of incubation of *E. coli* cultivated in Mueller-Hinton agar alongside hollow Hap microspheres that were either fully loaded with gentamicin or had been exhausted of it. Tags near the spheres indicate whether the groups of three spheres are loaded with gentamicin or depleted. a) Release solutions that originated from microspheres initially loaded with gentamicin solutions of 2 mg/mL and b) 3 mg/mL. 48

Figure 19 - Relative absorbance of MG-63 osteoblast-like cells in the presence of Ral-PEG solutions with different concentrations, at different days during the MTT assays. Error bars indicate standard deviations in %. 49

Figure 20 - Relative absorbance of MG-63 osteoblast-like cells in the presence of Ral-PEG release solutions with different concentrations, at different days during the MTT assays. Error bars indicate standard deviations in %. 51

Figure 21 - Relative fluorescence of MG-63 osteoblast-like cells in the presence of hollow Hap microspheres loaded with different quantities of Ral-PEG, at different days during the resazurin assays. Error bars indicate standard deviations in %. 56

List of Tables

Table 1 - Examples of synthetic macroscopic bone graft substitutes used for bone regeneration that currently exist in the marketplace. 10

Table 2 - Examples of synthetic micro- and nano-granules used for bone regeneration that currently exist in the marketplace. 11

Table 3 - SEM micrographs of cuts of Hap non-hollow microspheres. Each row corresponds to the same sample, viewed at different scales – 1 mm for the first column and 200 μm for the second column. 35

Table 4 - Macropore diameters for non-hollow Hap microspheres, as obtained through ImageJ. Samples 1, 2 and 4 correspond to samples (a), (b) and (c) displayed on Table 3, respectively. All samples belong to different batches of microspheres. 36

Table 5 - SEM micrographs of cuts of Hap hollow microspheres. Each row corresponds to the same sample, viewed at different scales – 1 mm for the first column and 200 μm for the second column. The first row displays a sample that was cut from the base of the sphere. 37

Table 6 - Macropore diameters in the shell region and hollow core diameters for hollow Hap microspheres, as obtained through ImageJ. Samples 1, 3 and 5 correspond to samples (a), (b) and (c) displayed on Table 5, respectively. All samples belong to the same batch of microspheres. 38

Table 7 - Diameter, density and porosity values of non-hollow Hap microspheres. Different batches of microspheres were made from different ceramic foams, but all ceramic foams were prepared with the same type and quantity of materials and the same methods. For batches 1 and 2, diameter measurements were made for 6 different spheres, and Archimedes density measurements for 3 different spheres; for batch 3, diameter measurements were made for 24 different spheres, and Archimedes density measurements for 4 different spheres. 40

Table 8 - Diameter, density and porosity values of hollow Hap microspheres. Different batches of microspheres were made from different ceramic foams, but all ceramic foams were prepared with the same type and quantity of materials and the same methods. For each batch, diameter measurements were made for 6 different spheres, and Archimedes density measurements for 3 different spheres. 40

Table 9 - Results of Sirius Red staining on wells containing MG-63 cells that were incubated alongside different Ral-PEG release solutions for seven days. The darker and more reddish regions represent agglomerates of collagen. 53

Abbreviations and Symbols

α-MEM	α-Minimal Essential Medium
ANOVA	Analysis of Variance
BCP	Biphasic Calcium Phosphate
BMD	Bone Mineral Density
Cbfa	Core-Binding Factor a
DMSO	Dimethyl Sulfoxide
E. coli	*Escherichia Coli*
ER	Estrogen Receptor
F-127	Pluronic® F-127
HA	Hydroxyapatite
Hap	Hydroxyapatite Powder
MeOH	Methanol
MG-63	MG-63 Human Osteoblast-Like Cells
MIC	Minimum Inhibitory Concentration
OPA	O-Phthaldialdehyde
P. aeruginosa	*Pseudomonas Aeruginosa*
PBS	Phosphate Buffer Saline
PEG	Poly(Ethylene Glycol)
PS	Polystyrene
Ral	Raloxifene
Ral-PEG	Raloxifene-PEG Conjugate
S. aureus	*Staphylococcus Aureus*
SEM	Scanning Electron Microscopy
SERM	Selective Estrogen Receptor Modulator
TCP	Tricalcium Phosphate

Chapter 1

Introduction

1.1. Aim of the Study

Bone fractures cause an immense decrease in quality of life, especially for elderly individuals, thus explaining the development of various synthetic matrixes that can aid in bone regeneration. To allow for active bone regeneration, these matrixes can be made of a material with properties that aid in the regeneration of new bone tissue; typically, these materials are bioactive and osteoconductive [1]. As of now, the most common materials of this type are synthetic calcium phosphate-based ceramics. Besides the nature of the material, the matrix's structure must be carefully considered so that it can efficiently serve as a conduit for cell growth. Usually, matrixes with high interconnected porosity allow for this, since such structures facilitate the adhesion of cells onto their surface, as well as cellular growth and intercellular communication throughout the entire matrix.

Matrixes used to heal bone fractures can have varied geometrical shapes – such as pellets, blocks, wedges and spheres, and have dimensions in the range of micro and nanometres, allowing them to be directly placed in the site of fracture through injection or surgical insertion. One method to further increase the efficacy of the inserted matrix is to previously load it with drugs that promote bone regeneration, and that can be released on a sustained and controlled fashion when inserted into the affected area inside the human organism.

The aim of the present study was thus to develop microspheres made of osteoconductive materials - calcium phosphate-derived ceramics, with high overall porosity, high interconnected porosity and a hollow core, that were capable of encapsulating the antibiotic gentamicin, to provide anti-bacterial action during and after the operative process of microspheres insertion in the site of bone fracture, or the selective estrogen receptor modulator (SERM) raloxifene (Ral), a drug that is proven to aid in bone regeneration, and have these microspheres also be capable of releasing these drugs in a sustained and controlled manner that could potentially increase the efficiency in regeneration of fractured bone tissue.

Microsphere production was based on methodology that was previously developed by doctoral student Stéphanie Christelle Marinho Soares.

Chapter 2

State of the Art

2.1. The Biology of Bone Tissue

2.1.1. Anatomy and Properties of Bone Tissue

The human skeletal system, or skeleton, is an infrastructure mainly composed of cartilage and bone that sustains and shapes the human body, providing also protection to several vital internal organs and other tissues.

The bone component of the skeletal system is classified as a living connective tissue, comprised of a complex calcified intracellular matrix that contains collagen type I fibres and several cell types. Despite not being part of the bone tissue proper, blood-producing cells, or hematopoietic cells, are produced in bone marrow, which is stored within certain bones. Additionally, bones also function as reservoirs of phosphate and calcium, allowing for stability in plasma calcium concentrations by collecting ingested calcium, which can then be scavenged from the bone should the need arise [2-5].

2.1.1.1. Compact Bone and Spongy Bone

Bone tissue can be classified into two different types, compact/cortical bone and cancellous/spongy/trabecular bone, as illustrated in Figure 1:

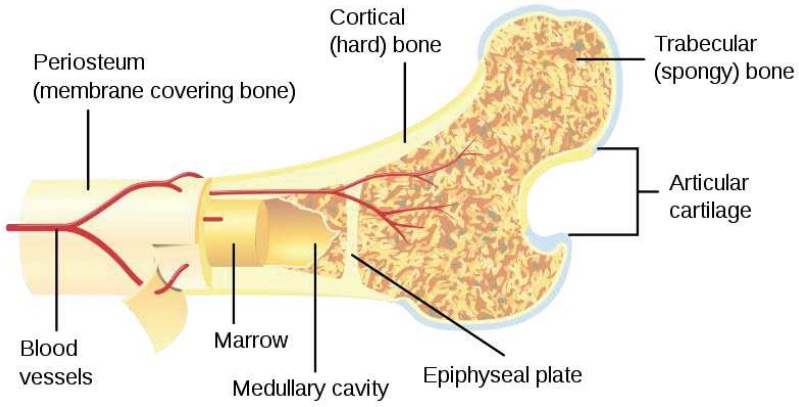


Figure 1 - Longitudinal cut of the proximal femoral epiphysis, demonstrating how spongy bone and trabecular bone are organized within it. Adapted from [6].

Compact bone and spongy bone are composed by essentially the same materials, calcium phosphates, the main difference between them being their physical structure: compact bone is denser in mineral content and has a mass that is about four times bigger than that of spongy bone, which in turn is less dense and has a total porosity of 30 to 90%, contrasting with the porosity range of 5 to 30%

of cortical bone [7]. Thus, compact bone provides more protection against physical impacts and better structural stability, while spongy bones provide a matrix that, while relatively more fragile, allows the bone to be lighter and to store and serve as a channel for cells, nutrients and several other organic or inorganic components. Therefore, cortical bone is usually found near periosteum – the outer membrane that covers bones, and envelops spongy bone, as is particularly noticeably in long bones.

At a microscopic level, compact bone is comprised of several functional units designated as cortical osteons or Haversian systems, which consist of multi-layered cylindrical composites of mineralized fibres arranged in thick concentric lamellae around a Haversian canal (Figure 2). It is through these canals that blood vessels and nerve cells are capable of being integrated inside the bone and, through Volkmann's canals, can communicate with the Haversian canals of surrounding osteons or with the environment outside of the bone. Through this network of canals, bone cells are thus capable of obtaining the necessary nutrients and substances from blood in order to grow and survive.

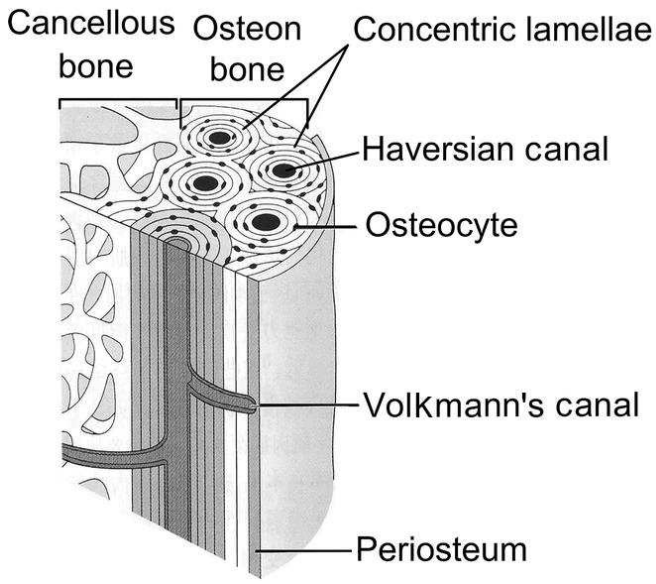


Figure 2 - Microstructure of a long bone. Adapted from [8].

2.1.2. Bone Cells

Bone tissue undergoes constant renovation throughout a person's lifetime, wherein osteoblasts, derived from another type of bone cells, the osteogenic cells, are responsible for the creation of new bone tissue, while osteoclasts, which are derived from bone marrow precursor cells, destroy old bone tissue [7]. Some osteoblasts, instead of remaining in the bone surface, migrate to the depths of the matrix by secreting new bone matrix around themselves, until they are unable to move any further and are therefore trapped in the hard matrix. From this point on, these osteoblasts gain the designation of osteocytes (Figure 3).

Osteoblasts are found on the surface of the bone matrix, from where they secrete new layers of matrix which deposit continuously on top of one another. This recently formed matrix, essentially

composed by type I collagen, is then quickly hardened by the deposition of calcium phosphate crystals, thus making it more resilient. To prevent the accumulation of unsuitable quantities of bone tissue and ensure a healthy renovation and/or growth of the bone, osteoclasts latch onto the surface of compact bone and disintegrate it, resorbing the destroyed bone and releasing its former mineral content into the blood stream. Osteoclasts are thus capable of producing cavities on the bone with considerable depth, which can later function as channels on which new blood vessels can grow through. With the combined activity of osteoblasts and osteoclasts, the skeleton is continuously remodelled, being capable of changing its dimensions over time, as well as adapting to variations of mechanical loads that are applied onto it due to various internal or external factors.

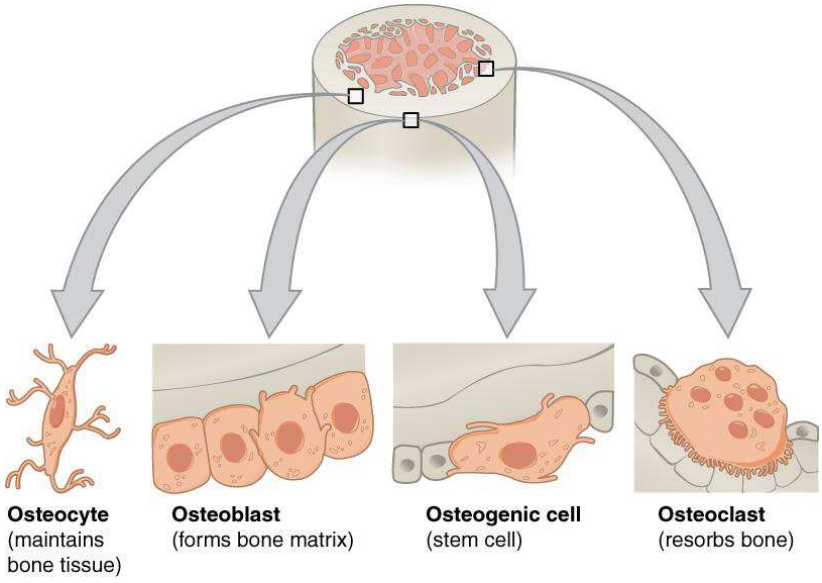


Figure 3 - Four cell types that exist within bone tissue. Adapted from [9].

2.2. Bone Fractures

The mineral and inorganic component of bone is comprised mainly of calcium phosphate crystals, which are wedged within numerous collagen fibres. It is the mineral component that confers bone its rigidity and compressive strength, while the collagen allows the bone to possess elasticity and tensile strength. These two components establish a synergistic relationship that allows the skeletal system to withstand the entire weight of the human body and to suffer external blows without suffering much damage. However, this strength is naturally not limitless, and if a force that is past the breaking point is exerted onto the bone, it may crack – if the force is just nearly past the breaking point, or fracture.

There are different types of bone fractures, which can be classified according to the angle at which the fracture occurs in relation to the bone – transversal, linear, oblique; according to whether the skin is pierced by the broken bone, to the point where the bone may be visibly exposed to – open or compound; according to the degree of fragmentation of the bone post-fracture – comminuted, among other criteria.

Fractures are commonly caused by physical trauma, which can vary in severity, with major trauma fractures usually being due to motor vehicle crashes, fast-moving projectiles or falls from greater

than standing heights [10]. Furthermore, depending on the average bone mineral density (BMD) of the individual, the likelihood of the fracture can also change, with smaller values of BMD being associated with, not only a higher risk of bone fractures, but also a higher likelihood of the fracture being more severe.

2.2.1. Bone Mineral Density

Although crucial for bone health and stability, BMD and, by extension, bone strength and size vary greatly depending on an individual's age and sex, mainly due to the activity of osteoblasts relative to osteoclasts changing across these two parameters, as demonstrated in Figure 4. On average, from the moment they are born until they reach 25 years of age, the bones of a healthy individual increase in size, since osteoblast activity is greater than that of osteoclasts, that is, the rate of formation of new bone tissue is greater than the rate of disintegration of old tissue. Between 25 and 35 years of age, the rate of bone formation is practically equivalent to the rate of its degradation, meaning that the skeleton is continuously renewed, but suffers no perceptible variations in size or in BMD. From 35 years of age and onward, the activity of osteoclasts is greater than that of osteoblasts, leading to an overall increase in bone tissue degradation and a consequential decrease BMD over time. This loss of density is more pronounced in individuals of the female sex, since around 50 years of age these individuals experience menopause, a process that is characterized by the drastic decrease in production of oestrogens. Oestrogens are a type of hormones that have the ability to, among others, attenuate apoptosis – controlled cell death, of osteoblasts [11-12]; therefore, the reduction of the concentration of these hormones in the organism lead to the decrease of viable osteoblasts, which in turn lead to a sudden decrease in bone mass after menopause.

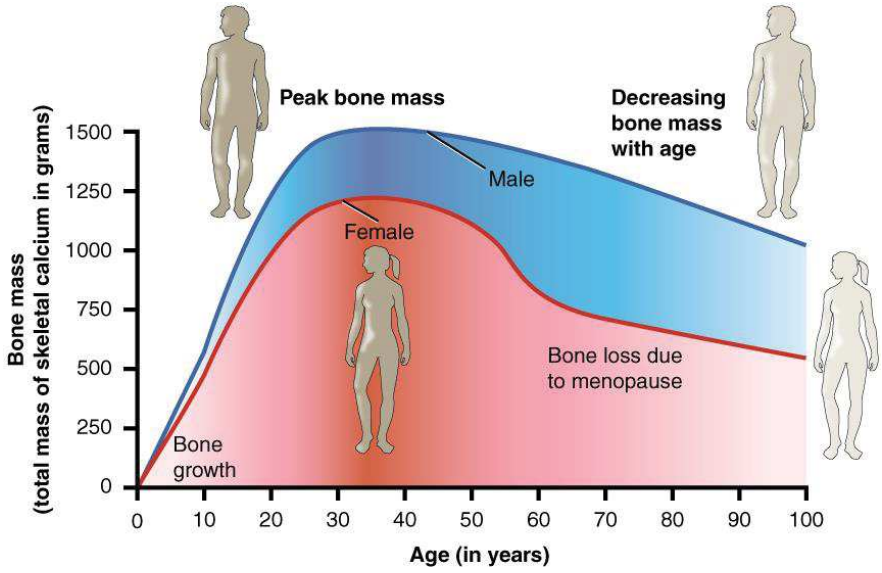


Figure 4 - Variation of bone mass (total mass of calcium in the skeleton in grams) with age (in years). Adapted from [9].

Since elderly individuals tend to have a more sedentary life style, due to becoming fatigated more easily and no longer being capable of doing activities that require a certain degree of physical effort,

their skeletal system undergoes less stimulation when compared to that of a younger and healthier individual. As a living tissue, stimulation is essential for the health and growth of bones, which must be continuously subjected to certain physical loads in order to develop properly [13-14] and the absence of such external loads leads the bones to degenerate – to lose BMD. Thus, elderly people continuously lose bone mass, not only due to the tissues aging, but also due to the lack of mechanical stimulation. It also due to this high influence of mechanical stimulation on BMD that other people with mobility issues, such as paraplegic individuals, are subjected to physiotherapy - so that the bones and muscles of the affected limbs do not atrophy due to lack of activity.

Although bone degeneration is a process that occurs naturally with age, it can worsen if the individual suffers from osteoporosis, a skeletal disease characterized by an accentuated decrease in bone mass and structural deterioration of bone tissue, leading to increased fragility of bone and risk of fracture, more prominently on the hip, spine, and wrist [15].

2.2.2. Osteoporosis

According to the International Osteoporosis Foundation, osteoporosis caused more than 8.9 million fractures per year worldwide in the year 2000 [16-17], with around 75 million people in the United States, Europe and Japan combined being affected by osteoporosis in 1997 [18]. In the USA, by 1995, it was estimated that there were about 1.5 million fractures caused by osteoporosis per year [19], and in six European countries, the estimated total of individuals over the age of 50 that suffered from osteoporosis was 20 million in the year 2015 [20]. The risk of osteoporosis tends to increase with age and has a markedly higher probability of occurrence in women, although men have a tendency for higher mortality rates after bone fracture [21-22].

The underlying causes of osteoporosis are currently unknown, but there are correlations between this condition and low levels of sex hormones – estrogen in women and testosterone in men, low intake of vitamin D and calcium, intake of medications that include glucocorticoids, low physical activity, alcohol consumption and cigarette smoking; in other words, behaviours and consumption of substances that are associated with decreases in BMD appear to show a relation with a higher incidence of osteoporosis.

Even for fractures of lower severities, an individual with a bone fracture can have their quality of life greatly compromised. Individuals may develop serious physical disabilities and become unable to live independently. Additionally, studies have shown that people who have suffered fractures in the past are more likely to develop future fractures, and the more fractures a person suffers, the higher the risk of future fractures and of developing osteoporosis becomes [10, 23]. In the worst-case scenario, bone fractures may increase the risk of early mortality; despite the fractures induced by osteoporosis themselves being a possible cause of death, comorbidities, and poor physical and general health that are exacerbated post-fracture may be the factors that ultimately lead to death. Furthermore, in the case of hip fractures, a review on deaths linked to osteoporosis remarked that postoperative complications, such as infections and cardiovascular diseases, lead to a notably high

risk of mortality [22]. Thusly, the development and refinement of fast and efficient medical treatments for bone fractures is imperative.

2.3. Bone Fracture Healing

The human body has natural biological mechanisms for fracture healing, which can be classified as either indirect/secondary or direct/primary. Primary fracture healing is less likely to occur without surgical intervention, since it requires anatomical reduction of the ends of the bone fragments, very strong stability and fixation conditions and interfragmentary compression, whereas secondary fracture healing occurs more often, as a result of lower stability of fractured bone during the healing process [24-26].

As shown in Figure 5, secondary fracture healing follows a specific set of phases, some of which overlap with each other. It starts with an acute inflammatory response shortly after the physical trauma occurs; a hematoma is formed that consists of bone marrow cells and cells that originate from peripheral and from intramedullary blood. This hematoma coagulates between and around the fracture ends, and within the bone marrow, setting up the template for the formation of a soft callus structures. In the meantime, mesenchymal stem cells, which are believed to originate from the surrounding soft tissue and bone marrow, start gathering at the fracture area, proliferating and differentiating into osteogenic cells. Following hematoma, granulation tissue rich in fibrin develops between the fracture ends and on external periosteal sites. This tissue then differentiates into fibroblasts and chondroblasts, which produce an extracellular matrix of fibrous and of cartilaginous tissue, originating an internal soft callus that provides the fracture with some structural stability. Meanwhile, between the periosteum and the distal and proximal ends directly adjacent to it, intramembrane ossification occurs that results in the formation of an external hard callus, a semi-rigid structure that allows the healing site to withstand a higher level of weight-bearing. As the soft callus is formed, it simultaneously suffers chondrocyte apoptosis and cartilaginous degradation, to allow for the formation of angiogenic pathways and blood vessel in-growth, thus allowing revascularization of the internal tissue – a crucial step, since an adequate blood supply is essential for the bone remodelling process that occurs later on. As the healing progresses, the extracellular matrix of the soft cartilaginous callus starts to calcify, due to chondrocyte hypertrophy. This mineralized cartilage is then gradually resorbed, as osteoblasts begin to replace it by depositing woven bone – bone that is composed of unorganized collagen fibres, which allows the inner callus to become more solid and mechanically rigid. The external hard callus, on the other hand, undergoes a remodelling process suffering resorption due to osteoclasts and being ultimately replaced by lamellar bone deposited by osteoblasts – lamellar bone presents collagens fibres that are aligned parallelly to the axis of the bone, and is thus more compact and mechanically stronger than woven bone. Thus, the newly formed bone is now lined with a rigid structure that virtually completely restores the biomechanical properties of normal bone [24, 26-27].

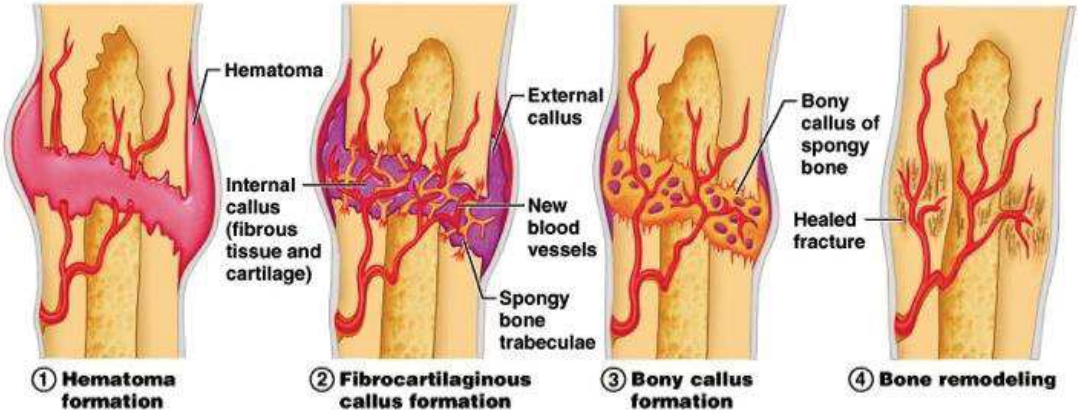


Figure 5 - Phases of bone fracture healing, in a long bone. Adapted from [28].

Due to the complexity and length of the process, secondary fracture healing may not be successful. If there is not an adequate supply of blood, an atrophic fibrous non-union may develop; if there is good vascularity but unstable fixation, resulting in gross motion between fracture fragments, a cartilaginous callus may still form, but it may lead to a hypertrophic non-union or a pseudoarthrosis. To ensure that there is at least a good level of stability, fixation devices can be surgically implemented, such as intra-medullary nails, bridging plates and external fixators.

In primary fracture healing, there is an almost immediate regeneration of anatomical lamellar bone, Haversian systems and associated blood vessels, without the need of remodelling steps. Primary fracture healing is commonly subdivided into contact healing and gap healing, the former of which occurs when the gap between the fractured bone ends is less than 10 μm and interfragmentary strain is lower than 2 %, and the latter tends to occur when the gap is 800 μm to 1 mm long. To achieve primary healing, fixation devices that cause interfragmentary compression, such as lag screws and compression plates, are typically used.

Despite bone having a natural healing process that can be optimized with the use of external fixators, there are bone fractures that are far too complex to be healed regularly through secondary healing, and, in cases where healing failure occurs, a follow-up corrective surgical procedure is necessary. In situations such as these, the most common solution is to internally implement a bone graft in the affected area, to primarily function as a scaffold which host bone tissue can use to enable proper fracture healing.

2.3.1. Bone Grafting

Overall, bone grafting consists of removing a part of bone tissue from one bone and placing it in an area of a different bone, which has been fractured or has had some of its tissue removed due to disease. Before being implemented in the host site, the bone graft may be subjected to certain treatments, in order to ensure that the eventual healing process occurs as optimally as possible. Currently, bone grafts can be divided into three main types, those being autografts, allografts and xenografts.

In autologous grafting, the graft originates from a healthy bone of the patient itself and is then transplanted into the defected area of the injured bone. In this case, the chosen healthy donor bones are those that are usually considered non-essential, such as the iliac crest [29-31]. The lack of rejection due to immune responses and possibility of maintaining the osteogenic cells and bone growth factors present in the graft, as well as the structural integrity of the graft, make autografts the current gold standard for grafts, in terms of bone healing. To elaborate, autologous bone grafts have an external and internal structure that allows the host bone tissue to adhere to and to grow on top of and within it – osteoconductive properties, they are capable of stimulating undifferentiated pluripotent cells into osteogenic cells, due to the availability of bone growth factors – osteoinductive properties, and can contain bone cells, such as osteoblasts, that, through the conferred osteoinduction, are capable of working together with the cells of the host site to greatly facilitate bone growth – osteogenic properties. Despite its many favourable properties, autografts have the disadvantages of having a very limited supply and of inducing tissue morbidity and possible post-operative infections and complications in the donor bone from which the graft is removed. Autografts are even discouraged in the case elderly patients, since their overall low levels BMD make it dangerous to attempt removal of any kind of bone.

Allografts are classified as grafts that are taken from the body of another individual from the same species. Usually, bone allografts are obtained from cadaveric tissue that is preserved in bone banks [29-30]. Some of the major advantages of allografts over autografts is the significantly larger availability of material and the possibility to remove grafts from a larger variety of different bones, allowing for the collection of allografts of various shapes, sizes and structures. Since the vast majority of allografts is obtained from cadavers, there is also no morbidity associated with the donor sites. However, due to allografts coming from a different human being, there are risks of rejection of the graft as a result of immune responses, as well as risks of disease transmission from the donor tissue to the host. To solve these issues, allografts undergo various types of sterilization and can also be frozen or submitted to freeze-drying, processes used for graft preservation which have the added benefit of eliminating certain infectious agents. Nevertheless, there always remains a risk of rejection, and due to eradication of living osteogenic cells and weakening of the mechanical properties of the bone after rigorous sterilization and storage processes, allografts tend to have very weak osteoinductive properties and almost no osteogenic properties, serving mostly as osteoconductive scaffolds for bone regeneration. Allografts are common targets for demineralization, a process that leads to the formation of demineralized bone matrixes (DBMs); due to absence of the osseous mineral component, DBMs are very lacking in compressive strength, but still maintain the collagenous structure and some of the growth factors and proteins that were originally present. As such, there is potential in using DBMs in conjunction with other materials, such as autologous bone grafts.

Xenografts are grafts obtained from an individual of a different species. In the case of bone grafts for humans, the most common types of xenografts are of either bovine or porcine origin [29-30, 32].

Given the large availability of cattle animals and the ease at which they can be raised at certain controlled conditions, xenografts have an overwhelming advantage in terms of availability when compared to allo- and autografts. However, they also present an even higher chance of rejection due to immune response, when compared to allografts, and a risk of transmission of diseases that were present in the donor animal, that would not be transmittable to a human being under normal circumstances. Therefore, in a similar manner to allografts, xenografts are required to undergo intensive sterilization process, making the resulting graft only efficient for osteoconductive purposes.

Despite the very favourable bone healing properties that autologous bone grafts provide, their very limited lack of supply is a major disadvantage, and although allografts and xenografts have a higher availability, the properties of these latter types of graft are sub-optimal for the purpose of bone regeneration. As a means to circumvent all these issues, various types of synthetic bone substitutes have been created, and many more studies and experiments have arisen to perfect them.

2.3.2. Synthetic Bone Substitutes

In the current marketplace, there already exist a large variety of synthetic bone substitutes for the purpose of bone regeneration. Besides being capable of being produced at a large scale and with high reproducibility, and of being made with materials that are biocompatible with human bone, synthetic bone substitutes can come in the form of pastes, putties, gels or 3-dimensional solid scaffolds, the latter of which can be created in a variety of shapes, such as blocks, wedges, cylinders, pellets or spheres, and can have scales that range from macro, to micro, to nanometres. In the case of nanoparticles, pastes and gels, some can be directly injected in the site of injury. Tables 1 and 2 respectively show examples of synthetic macroscopic bone graft substitutes and of synthetic micro- and nanogranules used for bone regeneration that are already available in the market.

Table 1 - Examples of synthetic macroscopic bone graft substitutes used for bone regeneration that currently exist in the marketplace.

Product	Company	Composition	Characteristics	Application
ENGipore	Jri Orthopaedics	HA	Porosity = 90% Shaped like disks, blocks, wedges or hollow cylinders	Orthopaedics
MBCP Synthetic Bone Graft Substitute	Biomatlante	BCP	Porosity = 70% Shaped like disks, blocks, wedges or cylinders	Orthopaedics
Osteocera Bone Graft Substitute	Hannox International Corp.	ß-TCP	Porosity > 70% Micro-porosity = 300 – 600 µm Shaped like blocks	Dental Care

Table 2 - Examples of synthetic micro- and nano-granules used for bone regeneration that currently exist in the marketplace.

Product	Company	Composition	Characteristics	Application
nanoXIM TCP	FLUIDINOVA	≥ 95% β-TCP	Surface area ≥ 80 m^2/g Particle size = 4,0 ± 2,0 μm High porosity	Orthopaedics
nanoXIM.HAp		HA	Surface area ≥ 100 m^2/g Particle size = 5,0 ± 1,0 μm = 10,0 ± 2,0 μm High porosity	Orthopaedics
nanoXIM.Granules		≥ 95% HA	Particle size = 0,5 -1,0 mm = 1,0 – 2,0 mm High porosity	Orthopaedics
BoneCeramic	Straumann	60% HA 40% β-TCP	Particle size = 0,4 – 0,7 mm = 0,5 – 1,0 mm = 0,8 – 1,5 mm Porosity = 90% Pore size = 100 – 500 μm	Dental Care
Artosal Granules	app	60% HA 40% β-TCP	Particle size = 1,0 – 4,0 mm High porosity Pore size = 200 – 800 μm	Orthopaedics
Osmosys	Medicrea	60% HA 40% β-TCP	Particle size = 2,0 – 3,0 mm Macro-porosity = 90 – 95% Micro-porosity = 5 – 10% (5 μm) Interconnected porosity = 60 – 80%	Orthopaedics
GlassBONE	Noraker	Bioactive glass 45S5: 45 wt% SiO_2 24,5 wt% CaO 24,5 wt% Na_2O 6,0 wt% P_2O_5	Particle size = 0,04 - 0,5 mm = 0,5 - 1,0 mm	Dental Care
			Particle size = 0,5 - 1,0 mm = 1,0 - 3,0 mm	Orthopaedics

The customization capacity that synthetic materials is a very desirable advantage, since it allows the bone substitutes to be personalized to some extent, depending on the type and extent of fracture and the type of affected bone. However, the selected materials and structure of the substitute are required to have certain properties; the bone substitute must be biocompatible, must be osteoconductive, must allow for vascularization and angiogenesis of new bone tissue (ideally, it should be able to actively promote it), must be bioresorbable and have a degradation rate that matches with

the growth rate of new bone tissue, and must be cost efficient and have great reproducibility and availability. Bone substitutes should also have mechanical properties that are as close as possible to those of real bone, since a substitute that is made of a material that is more brittle and has less tensile strength than bone can lead to lower fracture stability, while materials with higher biomechanical strength can lead to stress shielding. Other desirable biological properties are for the substitute to be osteoinductive and osteogenic, although these are exceedingly difficult to achieve, especially for the latter which, in practice, is currently observed essentially in autografts that contain the patient's own osteogenic cells.

Many of the materials used to create synthetic bone substitutes are of a ceramic nature, of which calcium phosphates are commonly used for bone regeneration, due to high biocompatibility between these materials and natural bone [33-35]; hydroxyapatite (HA), tricalcium phosphates (TCP, of which α-TCP and ß-TCP are its most common crystalline structures), and biphasic calcium phosphates (BCP) – mixtures of HA and TCP, are widely used to create a variety of ceramic bone substitutes. Mineral bone is essentially composed of HA, although the major difference between natural HA and synthetic HA ($Ca_{10}(PO_4)_6(OH)_2$) is that the former contains certain impurities, as well as carbonated ions or silicates in place of some of the phosphate or hydroxyl groups [34, 36] Nevertheless, synthetic HA has been shown to develop strong bonds with host bone tissue without the formation of fibrous tissue in the substitute/bone interface – great osteointegration, to have good osteoconductive properties, to have compressive strength properties similar to those of spongy bone, to be non-toxic and present little to no inflammatory responses, to be highly stable at physiological conditions (such as pH, temperature and composition of physiological fluid) and overall highly resistant to pH changes [35] [37-40]. Drawbacks of HA include its relatively weak tensile strength and its low dissolution rate, especially when compared to TCP, meaning that HA may be resorbed too slowly by the body in some circumstances, and thus render fracture healing inefficient [30, 41]. However, dissolution rate of a HA scaffold can be increased by increasing its porosity and pore interconnectivity.

Besides influencing bioresorption, the porosity of a bone substitute greatly promotes osteoconductivity and is fundamental for proper vascularization of new bone tissue, making it a structural property that is crucial for the regeneration of bone tissue. There must be a hollow network within the synthetic scaffold that allows for cell transportation throughout it, as well as the growth of new blood vessels that can offer the nourishment essential for new tissue proliferation and survival. This network is achieved through the existence of interconnected pores, that must have diameters above certain values: 50 to 100 μm is considered the minimum range of macropore diameters necessary to promote bone cell migration and angiogenesis of small blood vessels, and diameters above 150-300 μm are thought to be optimal for proper vascularized bone ingrowth [41-45]. Meanwhile, micropores – pore diameter lower than 5 μm, are associated with the bioresorbability of the structure [41, 44]. Pore size and volume are crucial when creating a bone substitute, since although a higher porosity tends to be more favourable for cell migration and vascularization, large porous volumes can lead to a decrease in mechanical strength; an adequate balance between porosity

and structural strength is thus required. There are several methods used to create varying degrees of porosity in materials for synthetic bone replacements, such as: implementation of porogens, which are inert substances whose elimination creates pores in the material in which they are incorporated [46-47]; rapid prototyping, a group of techniques which utilize 3-dimensional computer models to create matching 3-dimensional scaffolds, which are constructed layer by layer [38, 48]; foaming through bubble generation, in which air bubbles are formed either through the physiochemical properties of a foaming agent or the through stirring of the material mixture, usually coupled with the addition of a surfactant agent that stabilizes the bubbles' structure [47, 49]. A specific method of foaming, syringe foaming, will be explored in greater detail further on.

Besides being essential for the growth of new cell tissue and blood vessels, the existence of interconnected porosity has the potential for allowing the incorporation, into the substitute's structure, of drugs and other substances that can aid in bone regeneration or lead to lower risks of infection during surgical fracture treatment.

2.3.3. Drug Treatments

As mentioned previously, the control over scaffold porosity offers great potential for the introduction of drugs inside the synthetic bone substitutes, which can aid in the overall surgical procedure and bone regeneration. One important factor to take into account is the interaction that the drugs have with the material itself, since it is favourable that the drug does not compromise the integrity of the scaffold's structure and that it has decent adhesion properties to the material, so that it can be loaded into the scaffold more easily.

2.3.3.1. Controlled Drug Delivery

Drug administration through non-invasive routes, such as through the mouth or skin, tends to be preferred due to the high ease of self-administration, low risk of infection, and overall lower costs of manufacture. However, there are a variety of medications, such as proteins, antibodies and vaccines, that cannot be delivered through those non-invasive routes, since the substances involved are susceptible to enzymatic degradation or are unable to be absorbed into systemic circulation efficiently if administered in those manners, and thus, vaccines and many protein based drugs are, for example, delivered through direct injection into the blood stream. Furthermore, even in the case for drugs that are generally safe to be administered through non-invasive routes, at times the absorption of the active ingredient can still be considered inefficient, in the sense that a large dosage of the drug must be consumed, often for long periods, only for a relatively small percentage of it to be incorporated into the systemic circulation. In this scenario, greater care must be taken with the quantity of the drug that is consumed, so as not to increase the risk of adverse side-effects, further straining the efficiency of the medication. Controlled drug delivery thus emerges as a highly promising solution to the inefficiency of a drug's healing properties, since it puts forth methods for the drug to be released over a period of time in a controlled manner, preferably near or on the site of disease if

the issue is localized. There is thus a local delivery of the drug at a constant rate, with less drug quantity required to treat the disease and less frequency of administration, leading to the decrease of risks of side-effects and a higher level of efficiency [50-51].

To achieve a controlled drug delivery, a delivery device that carries the drug is first required. This device must thus be loaded with the intended quantity of drug that is required for the treatment – drug loading, so that, after incorporation into the organism, the carrier may then release the drug at the desired rate – drug delivery.

There are two main types of drug loading: the drug can be incorporated within the material before the scaffold is made, so that, when it is completed, the drug is already part of it. The materials and methods of fabrication must be such that they do not compromise the active ingredient of the drug. On the other hand, the scaffold can already be completed, and the drug is then incorporated within it and/or on its surface through diffusion. In this type of loading, centrifugation or application of vacuum can promote drug loading inside the scaffold, by forcing penetration of the drug within the porous network. Thus, porosity properties play a crucial role once again, since larger pore volume and pore interconnectivity will allow for more quantity of drug to be loaded within the scaffold more easily. Additionally, porosity greatly affects the kinetic properties of drug loading, with higher level of porosity being associated with faster loading [52-53]. Other structural properties of the scaffold, such as specific surface area, also affect drug loading; in most cases, a higher specific surface area leads to higher drug adsorption [54]. However, the chemical interaction between the surface's material and the drugs play an even higher role in absorption. In a study by Santos et al. [55], they obtained 10 times more drug absorbed per surface unit on calcinated HA granules than on non-calcinated HA granules, despite the former having a lower specific surface area (6.2 m^2/g) than the latter (150 m^2/g). Further on the topic of chemical bonds, a study by Queiroz et al. [56] showed that the antibiotic ampicillin had a higher level of adsorption on HA samples then on glass-reinforced HA samples, likely due to the higher concentration of OH- groups on the formers surface, thus interacting more strongly with the NH_3^+, Na^+ and H^+ groups present in sodium ampicillin.

Most properties that influence drug loading also influence the kinetics of drug release. A higher specific surface area will tend to lead to a faster drug release; a strong chemical bond between drug and surface will lead to a slower release; higher pore volume, open porosity and pore diameter lead to a faster drug release, whereas increased microporosity leads to slower drug release [52-54]. Drug release from a synthetic scaffold can usually be divided into two phases: the initial phase is characterized by a burst, were large quantities of drug are released in a relatively short period of time, due to the greater ease with which the molecules present on the surface and on the macropores on the surface detach into the surrounding medium. The second phase is characterized by a slower and more linear release, due to diffusion of drug through the porous network to the outside medium, and through dissolution of the material that contains the drug. However, the degree of this linearity varies depending on the rate of diffusion vs the rate of material disintegration. In the case of less soluble materials, it is more likely that diffusion will take place and end much sooner than drug

release through material disintegration, thus varying the rate at which drug will be release, due to the different properties of the release phenomena.

2.3.3.1.1. Gentamicin

Gentamicin is an aminoglycoside antibiotic, characterized by being not a single molecule, but rather a complex of three molecules with differing major components, as shown in Figure 6, wherein R represents the different degrees of methylation that differentiate those three molecules [57]. It is mainly indicated for the treatment of infections caused by strains of bacteria such as *Pseudomonas aeruginosa*, *Proteus* species, *Escherichia coli*, *Klebsiella*, *Enterobacter* and *Serratia* species, and *Staphylococcus* (including strains resistant to other antibiotics) [58]. The minimum inhibitory concentrations (MIC) for reference strains are the following [59]: 0.25 and 0.5 µg/mL for *E. coli* NCTC and ATCC, respectively; 1 µg/mL for *P. aeruginosa* NCTC and ATCC; 0.12 and 0.25 µg/mL for *S. aureus* NCTC and ATCC, respectively. Gentamicin is also commonly used in the treatment of osteomyelitis (bone infection), which is usually caused by bacterial infection following surgical fracture treatment or orthopaedic implants [60-62].

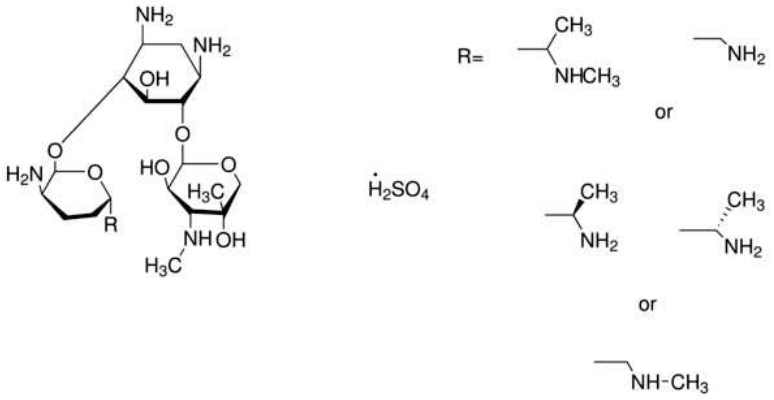


Figure 6 - Chemical structure of gentamicin sulphate. Adapted from [63].

Regarding potential cytotoxicity, concentrations of gentamicin below 100 µg/mL appear to not significantly decrease cell number of human osteoblast cultures for a period of ten days, according to a study performed by Rathbone et al. [64]; gentamicin concentrations below 200 µg/mL appeared to not affect cell number nor cell viability of murine C2C12 cells – myoblast cell line, for a two-day period, in a study by Ince et al. [65]; thirdly, in a study by Chang et al. [66], for a period of seven days, cell viability of marrow-derived human mesenchymal stem cell was not affected by gentamicin concentrations equal to and below 200 µg/mL, although cell proliferation remained unaffected for concentrations below 100 µg/mL.

2.3.3.1.2. Raloxifene

Selective estrogen receptor modulator (SERMs) are a group of compounds that act on estrogen receptors (ERs), behaving as either agonists or antagonists to these receptors depending on the type of cell tissue – SERMS tend to behave as agonists in regards to ERs in bone or liver tissues, while

commonly behaving as antagonists to ERs in uterine or mammary tissues [67-70]. Raloxifene (Ral) (Figure 7) is a nonsteroidal benzothiophene derivative that is classified as a second-generation SERM. The effects of Ral on bone for tissue regeneration have been studied at length, and it has been determined that Ral leads to an increase in bone mineral density and prevents bone loss, while also reducing estrogen activity of breast and uterine tissues [71-76].

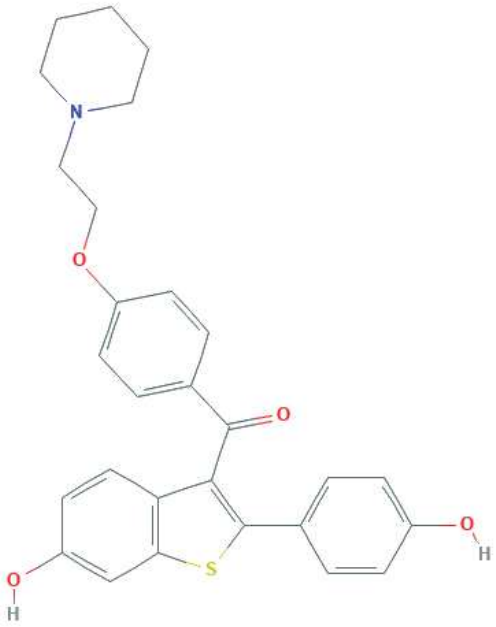


Figure 7 - Chemical structure of raloxifene. Adapted from [77].

The exact mechanisms of action of Ral are currently unknown, but it is theorized that they behave in the following manner [75]: similarly to estrogen molecules, Ral likely enters the nucleus of the target organ cells and binds itself to the ERs that are present, through its benzothiophene ring. This bond, in addition to preventing access of the estrogen estradiol to the ERs, which would lead to the activation of genes responsible for synthesising proteins that trigger the estrogen-related activity of reproductive cell tissue, also inflicts a change in the spatial configuration of the ER that makes it unable to interact with the same specific DNA sequence that would lead to the activation of the aforementioned genes, thus leading to the antagonist estrogenic effect that Ral has on breast and uterine tissues. Additionally, in bone and other non-reproductive tissues, the resulting ER-Ral receptors activate a specific DNA sequence known as the Raloxifene Responding Element, with the aid of a series of activating, helping and/or adapting proteins, which is theorized to lead to the synthesis of specific cell proteins that are responsible for the estrogen agonist effect that Ral has on these tissues [78-79]. Moreover, regarding bone tissue, raloxifene appears to be capable of decreasing the resorptive activity of osteoclasts, the production of interleukin-6 and the production of tumor necrosis factor α, with the latter two corresponding to substances that are important mediators of bone resorption, as well as increasing the production of transforming growth factor β_3, which would lead to a decrease in the number of osteoclasts and their resorptive activity [80-83], thus preventing loss of bone mass and loss of bone mineral density.

Although the effects of Ral on osteoclastic activity is greatly documented, Ral may also have an agonist estrogenic effect on osteoblasts. A study by Taranta et al. [84] reported that Ral stimulated proliferation of osteoblasts derived from CD-1 female neonatal mice, as well the transcription of genes relevant to the osteoblast phenotype (Cbfa1 and collagen I).

Regarding drug cytotoxicity, a study by Kavas et al. [85] showed that, for 14 days, concentrations of Ral equal to or below 0.05 μg/mL appear to not have any toxic effects in adipose-derived mesenchymal stem cells obtained from female Sprague-Dawley rats, whereas Ral concentrations that equal to 0.47 or 4.74 μg/mL have noticeable cytotoxic effects (although do not appear to cause great differences in cytotoxicity among themselves). A study by Lo Muzio et al. [86] showed that, for 7 days, MG-63 human osteoblast-like cells did not experience cytotoxicity for Ral concentrations of 0.120 and 0.240 μg/mL – in fact, for the former concentration, cell viability appeared to increase compared to the control, whereas MC3T3-E1 murine osteoblasts experienced cytotoxicity for both of those concentrations.

Raloxifene is currently available in the marketplace under the trade name EVISTA® (Eli Lilly and Company) in the form of 60 mg tablets, and it is commonly prescribed for the treatment or prevention of osteoporosis in postmenopausal women, as well as for the reduction of risk of invasive breast cancer in postmenopausal women at high risk of developing such cancer or who have osteoporosis [87].

Chapter 3

Materials and Methods

3.1. Materials

Hydroxyapatite powder (Hap, $Ca_5(OH)(PO_4)_3$, Mw: 502.31 g/mol, CAS Number: 1306-06-5, SKU: 04238), Pluronic® F-127 (F-127, CAS Number: 9003-11-6, SKU: P2443), Polystyrene (PS, $[CH_2CH(C_6H_5)]n$, average Mw: 350,000 g/mol, CAS Number: 9003-53-6, SKU: 441147), Sodium phosphate dibasic heptahydrate ($Na_2HPO_4.7H_2O$, Mw: 268.07 g/mol, CAS Number: 7782-85-6), Poly(ethylene glycol) (PEG, $H(OCH_2CH_2)_nOH$, CAS Number: 25322-68-3, SKU: 95172-250G-F), Phosphate buffer saline tablets (PBS, MDL Number: MFCD00131855, SKU: P4417-50TAB), 2-mercaptoethanol for electrophoresis ($HSCH_2CH_2OH$, Mw: 78.13 g/mol, CAS Number: 60-24-2, SKU: M7154), Gentamicin sulfate salt (CAS Number: 1405-41-0, SKU: G3632), Raloxifene hydrochloride ($C_{28}H_{27}NO_4S.HCl$, Mw: 510.04 g/mol, CAS Number: 82640-04-8, SKU: PHR1852) and Phthaldialdehyde for fluorescence ($C_8H_6O_2$, Mw: 134.13 g/mol, CAS Number: 643-79-8, SKU: 79760) were obtained from Sigma-Aldrich.

Dichloromethane (CH_2Cl_2, Mw: 84.93 g/mol, CAS Number: 75-09-2, Catalogue Number: 32222-2.5L) was obtained from Honeywell Research Chemicals.

Methanol (MeOH, CH_3OH, Mw: 32.04 g/mol, CAS Number: 67-56-1, Art. Number: 8388.5) was obtained from Carl Roth.

Alginic acid sodium salt ($(C_6H_7O_6Na)_n$, Mw: 10000 - 600000 g/mol, CAS Number: 9005-38-3 , Order Number: A3249,0250) was obtained from PanReac AppliChem.

Potassium hydroxide (KOH, Mw: 56.11 g/mol, CAS Number: 1310-58-3, EC Number: 215-181-3), Boric acid (H_3BO_3, Mw: 61.83 g/mol, CAS Number: 10043-35-3, EC Number: 233-139-2) and Calcium chloride dihydrate ($CaCl_2.2H_2O$, Mw: 147.01 g/mol, CAS Number: 10035-04-8, SKU: 1023821000) were obtained from Supelco.

3.2. Methods

3.2.1. Preparation of the Microspheres

It is desired that the production system of the ceramic microspheres should be accessible, cheap and scalable for industrial applications. A foaming method, followed by co-injection moulding were implemented to produce porous calcium phosphate-derived ceramic microspheres with and without a hollow core, which was followed by a heat treatment that allowed the ceramic component of the microspheres to undergo sintering, while fully combusting and eliminating any existing organic

substances. This entire process was based on the methodology that was previously optimized by doctoral student Stéphanie Christelle Marinho Soares.

3.2.1.1. Syringe-Foaming

It was critical to ensure that the resulting microspheres had a high porosity and interconnected macroporosity, so that adhesion and cell proliferation into the sphere's structure was allowed, a more efficient drug loading and controlled drug delivery could be achieved, and bone reabsorption of the ceramic component could be adjusted. To this end, a syringe-foaming method was used, based on the works of Vásquez et al [88-89] and Zhang et al [90].

1.5 g of hydroxyapatite powder (Hap) was mixed with 3 mL of alginic acid sodium salt (10%, w/v) and 1 mL of sodium phosphate (2.5%, w/v). The mixture was stirred with a magnetic stirrer for 30 min, until the mixture was a homogenous ceramic suspension.

When the above mixture became homogenous – still maintaining stirring to prevent the resulting paste from undergoing sedimentation, one 12 mL sterile plastic syringe was filled with 2.5 mL of air, while another was filled with 3.5 mL of the surfactant Pluronic® F-127 (10%, w/v), as exemplified in Figure 8-a. The two syringes were then connected at the tip with a plastic syringe connector, and the contents of the syringes were pumped into each other with a constant and coordinated movement for about 40 seconds, creating a foam, as illustrated in Figure 8-b. The contents of both syringes were then transferred to only one of them, which marked a volume of around 6 mL of the resulting foam.

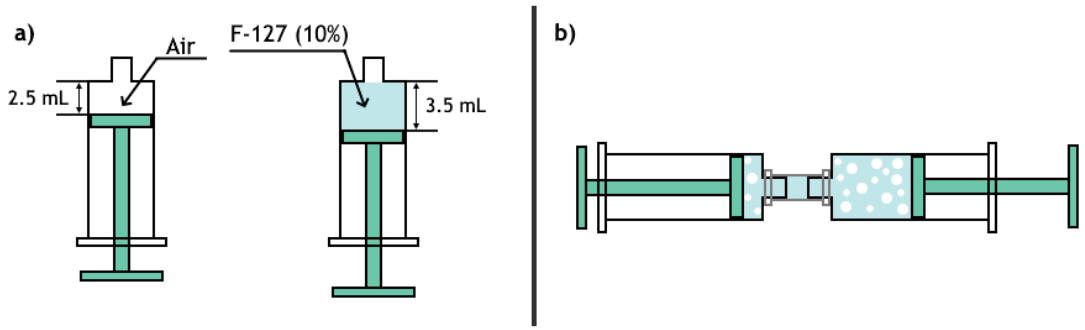


Figure 8 - Schematic representation of syringe-foaming procedure. **a)** Firstly, two 12 mL syringes are filled, one with 2.5 mL of air and the other with 3.5 mL of the foaming agent - F-127 (10%, w/v) in this case. **b)** Secondly, the tips of the syringes are linked together with a connecting piece, and their pistons are simultaneously pushed back and forth rhythmically for about 40 seconds, until the resulting foam phase has a volume of about 6 mL.

5.4 g of the produced ceramic suspension were then inserted into a third 12 mL sterile plastic syringe, which was then connected with a plastic syringe connector to the syringe that contained the recently formed foam. These two syringes were pumped as described previously, for about 40 seconds, resulting in the formation of a ceramic foam. Again, the contents of both syringes were transferred into only one of them.

3.2.1.2. Co-Injection

To shape the ceramic foam into droplets, a cylindrical coaxial mould was used. The coaxial mould had two entry holes: one which guided fluids through the mould's outer channel and the other which guides fluids through the inner channel, as shown in Figure 9. The syringe with the ceramic foam was

thus mounted onto an infusion pump (PHD ULTRA™ Syringe Pump, Harvard Apparatus) and connected to the outer channel of the coaxial mould. A 12 mL sterile plastic syringe containing a solution of polystyrene in dichloromethane (PS, 4%, w/v) was mounted onto a second infusion pump and connected to the inner channel of the coaxial mould. The two infusion pumps were activated, with the pump that had the syringe containing the ceramic foam being programmed with a flow rate of 25 µL/s, while the second pump with the syringe containing PS was programmed with a flow rate of 2.5 µL/s. A container with calcium chloride ($CaCl_2$,10%, w/v) was placed beneath the coaxial mould, so that the resulting droplets would fall onto the $CaCl_2$ solution where they reticulate, resulting in the production of microspheres with a core filled with PS, the precursors for the hollow microspheres. This entire process is illustrated in Figure 10.

To produce non-hollow microspheres, the process is similar to that of the hollow ones, but only the ceramic foam is pumped through the coaxial mould, through the outer channel at a flow rate of 2.5 µL/s.

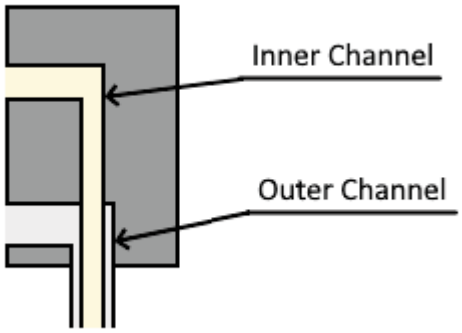


Figure 9 - Schematic representation of a longitudinal cut of the cylindrical coaxial mould.

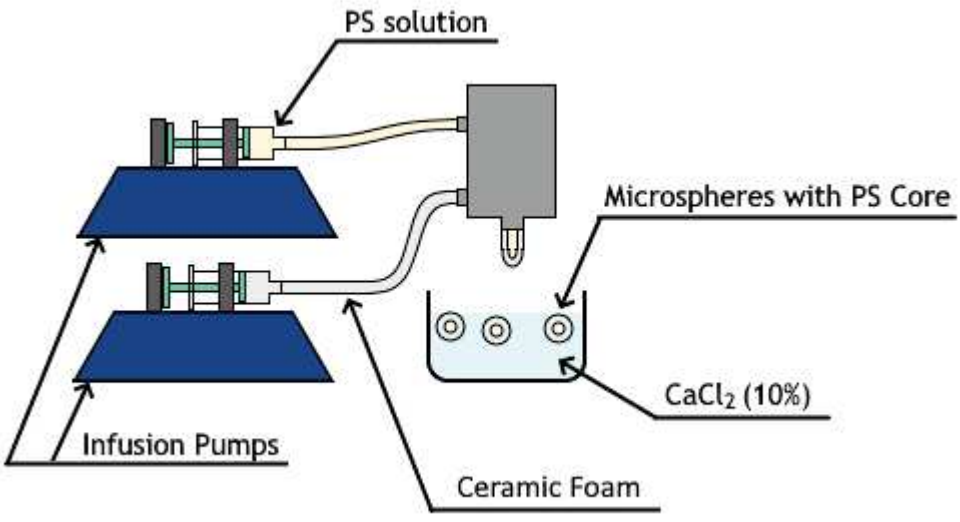


Figure 10 - Schematic representation of the formation of porous microspheres with a hollow core through co-injection. The polystyrene solution (PS) is injected into the core of the ceramic foam droplets. When falling into the $CaCl_2$ solution, the droplets adopt a spherical shape and then go through reticulation, with the injected polymer at its centre.

After the syringe containing the Hap paste and the foam was emptied, the newly formed microspheres were transferred into containers.

3.2.1.3. Heat Treatment

Once the reticulation process was complete, the microspheres were removed from the $CaCl_2$ solution and washed gently with distilled water, to remove traces of $CaCl_2$, and then immersed in ethanol for 5 to 10 minutes, to prevent electrostatic bonds to form between the spheres, thus aiding in their separation.

Afterwards, the spheres were carefully placed onto a clean ceramic slab, which was placed in an oven to commence heat treatment. This heat treatment consisted of five steps, as illustrated in Figure 11: in the first step, the spheres were placed inside the oven and heated to 700 ºC, with a rate of 0.5 ºC/min; in the second step, the spheres remained at 700 ºC for 3 hours; in the third step, the temperature was raised to 1300 ºC, with a rate of 4ºC/min; in the fourth step, the temperature remained at 1300 ºC for 1 hour; in the fifth and final step, the oven's heating system was turned off and the spheres remained inside it to naturally cool to room temperature, taking up to 12 hours.

The first and second steps are necessary for the complete combustion of the PS, to allow for the formation of a hollow core in the centre of the sphere, and of the alginate, to allow for the formation of pores in the surface and shell of the sphere. For this combustion to be successful without resulting in the microsphere's implosion due to the release of CO_2 gas, there must be an initial slow heating ratio (0.5 ºC/min), and the resulting microsphere's structure must be porous enough to safely allow escape of the gas. The third and fourth steps of the heat treatment are essential for the Hap particles to sinter and thus form a cohesive and firm microstructure.

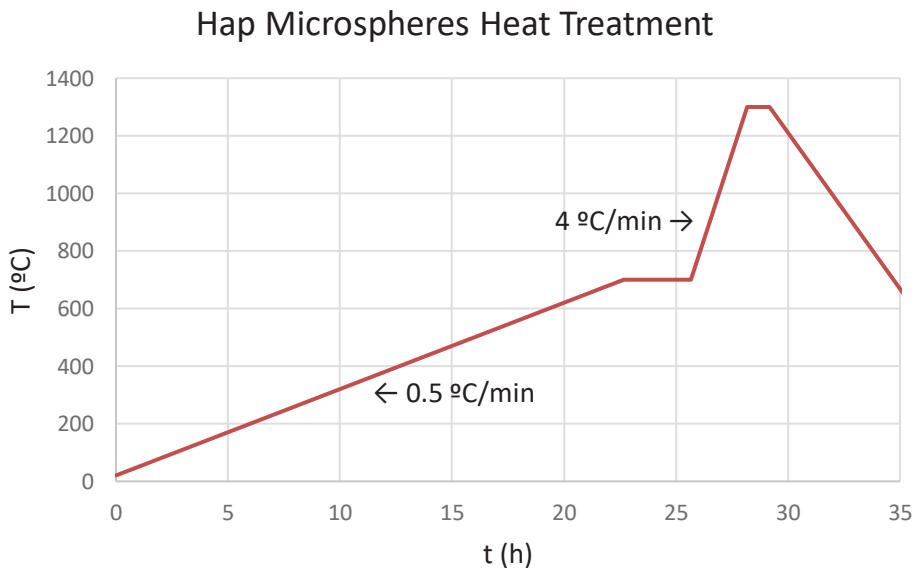


Figure 11 - Heat treatment profile for porous hydroxyapatite microspheres.

3.2.2. Characterization of the Microspheres

3.2.2.1. Helium Pycnometry

The density of the hydroxyapatite powder that was used to create the microspheres was measured through helium pycnometry (AccuPyc 1330, Micromeritics) at the Faculty of Engineering of the University of Porto, FEUP.

3.2.2.2. Morphological Analysis by Scanning Electron Microscopy

The morphology and topography of microspheres with a hollow core and microspheres without a hollow core were examined qualitatively by scanning electron microscopy (SEM) (High resolution (Schottky) Environmental Scanning Electron Microscope with X-Ray Microanalysis and Electron Backscattered Diffraction analysis: Quanta 400 FEG ESEM / EDAX Genesis X4M) at the Materials Centre of the University of Porto, CEMUP. Before analysis, the microspheres were cut in half and glued onto a metal stub with epoxy resin Araldite and coated with a fine layer of gold/palladium with a sputter coating device (SPI Module Sputter Coater) - samples were coated with Au/Pd for 120 seconds and with a 15mA current.

3.2.2.3. Microsphere Size and Porosity Analysis

Microsphere diameter (d) was measured directly with a calliper, after which the mean and standard deviation of such diameters were calculated for each different batch of microspheres, with six different microspheres being measured per batch.

Microsphere geometric density (ρ_g) was determined according to equation (1):

$$\rho_g = \frac{\overline{m}}{\frac{4}{3}.\pi.(\frac{d}{2})^3} \qquad (1)$$

$\overline{m}$ denotes the mean mass of six different spheres from the same batch.

Microsphere Archimedes' density (ρ_a) was determined by measuring the mass of six different unsubmerged spheres from the same batch (m_6) and then measuring the mass of those same six spheres while submerged in distilled water (apparent immersed mass, m_a) (Density determinator kit METTLER TOLEDO), followed by the application of Archimedes' principle (2):

$$\rho_a = \frac{m_6}{m_a}.\rho_w \qquad (2)$$

ρ_w denotes the density of the distilled water at the given room temperature.

To quantitively determine the microspheres' closed porosity and open porosity, the above corresponding densities were used in conjugation with equations (3) and (4), respectively:

$$Closed\ Porosity\ (\%) = \left(\frac{1}{\rho_a} - \frac{1}{\rho_m}\right) . 100 \qquad (3)$$

ρ_m denotes the density of the microsphere's base material (Hap), determined by helium pycnometry as denoted in *3.2.2.1. Helium Pycnometry*.

$$Oen\ Porosity\ (\%) = \left(1 - \frac{\rho_g}{\rho_a}\right) . 100 \qquad (4)$$

3.2.3. Drug Delivery Studies

3.2.3.1. Gentamicin Loading

Both microspheres with and without a hollow core were loaded with gentamicin, to determine if the existence of a hollow core allowed for a larger quantity of gentamicin to be stored within the spheres.

Two concentrations of gentamicin loading solution were utilized: 2 mg/mL and 3 mg/mL, in distilled water. Three assays were performed for each condition of concentration and sphere type.

For each assay, about 30 mg of microspheres were placed in open containers with 2 mL solutions of gentamicin in distilled water. These containers were then placed in a small closed chamber that was connected to a vacuum pump (KNF LABOPORT® N 820 FTP Diaphragm Vacuum Pump) that produced low vacuum – 99 mbar, at room temperature and for 1 h 30 min, in order to force the liquid solution of gentamicin to enter the interconnected porous infrastructure of the microspheres, thus loading the spheres with this drug. Afterwards, the solutions from each container were drained and the spheres where dried at 37 ºC.

3.2.3.2. Gentamicin Release Profiles of the Microspheres

The drug release from the microspheres loaded with gentamicin was analysed, in order to understand the efficiency of this release from these microspheres into an aqueous medium.

Two batches of 30 mg of spheres that had been loaded with gentamicin, with the method previously described in *3.2.3.1. Gentamicin Loading*, for each condition of concentration and sphere type, were placed in containers with 2 mL of distilled water in an orbital shaker (IKA® KS 4000 ic control) with a constant temperature of 37ºC at 130 rpm.

Microspheres were kept in the orbital shaker for a total of 3 days. The entirety of the drug release solution was removed from the containers in the following time intervals, since the time microspheres were first placed inside the orbital shaker: 2, 4 , 6, 8, 10 , 22, 46 and 70 hours. Each time the solution was taken, the corresponding container was refilled with 2 mL of fresh and clean distilled water.

The drug release solutions that had been removed were placed in clean containers and stored at 4ºC.

3.2.3.3. Fluorometric Analysis

In order to determine the quantity of gentamicin released from the loaded microspheres with respect to time, the fluorometric method described by Jerzy Gubernator et al. [57] was implemented. This method is mainly based on the reaction between amino groups in the gentamicin molecules and o-phthaldialdehyde (OPA), under basic pH conditions.

Firstly, boric acid buffer solution was prepared by dissolving 24.7 g of boric acid (0.4 M) in 900 mL of distilled water, followed by adjusting the solution pH to 10.4 (pHenomenal pH.Cond.O2 1000L VWR®) with the addition of potassium hydroxide (50%, w/v). Afterwards, more distilled water was added to produce a total solution volume of 1000 mL.

The OPA reagent was prepared by dissolving 0.2 g of o-phthaldialdehyde in 1 mL of MeOH, which was then mixed with 19 mL of the previously prepared boric acid buffer solution. Next, 0.4 mL of 2-mercaptoethanole were added and the solution pH was adjusted to 10.4 with potassium hydroxide (50%, w/v).

To quantitively measure the concentration of gentamicin present in a solution, a calibration curve was constructed using gentamicin solutions in water with known concentrations, in the range of 0-50 µg/mL. 1 mL of each calibration gentamicin solution was directly mixed with 0.6 mL of MeOH, while 0.1 mL of OPA reagent were diluted in 0.8 mL, and the two resulting solutions were then mixed together for a total of 2.5 mL, with the use of a vortex mixer. 200 µL of resulting solution were then transferred to a well in a 96-well plate, left to incubate for 10 minutes, and, afterwards, its relative fluorescence was measured in a microplate reader (Synergy™ HTX Multi-Mode Microplate Reader by BioTek Instruments, Inc.), at an excitation wavelength of 360/40 nm and emission wavelength of 460/30 nm. The relative fluorescence of the drug release solutions was measured in the same manner, and the obtained calibration curve was then used to determine the concentration of gentamicin in them.

3.2.3.4. Raloxifene-PEG Conjugate

To reduce the hydrophobic properties and the crystallinity of Ral, in order to facilitate Ral loading into the porous ceramic microspheres and subsequent Ral release into a mock physiological medium, a conjugation reaction was performed between Ral and PEG (an amorphous substance that is highly hydrophilic), to obtain a raloxifene-PEG conjugate (Ral-PEG). This conjugate is thought to be achieved through hydrogen bonds that form between the amine and phenolic -OH groups of Ral and the hydroxyl groups of PEG [85, 91].

The solvent evaporation method described by Ayşegül Kavas et al. [85] was used to prepare a Ral-PEG conjugate with a weight ratio of 1:2. 36 mg of Ral were dissolved in 3.4 mL of MeOH, while 52 mg of PEG were dissolved in 2.4 mL of MeOH. The Ral solution was put under constant stirring with a magnetic stirrer, while the PEG solution was added to it. The resulting solution kept being stirred at room temperature for 6 hours. Afterwards, the solution was dried overnight with a water bath at 35 ºC, and any solvent vestiges were then removed by placing the conjugate in a vacuum drying chamber

(BINDER Vacuum Drying Oven, Model VD 53) for 2 hours. For the purpose of safe storage, the resulting Ral-PEG must be kept at 4ºC.

3.2.3.5. Ral-PEG Loading

Both microspheres with and without a hollow core were loaded with Ral-PEG, to determine if the existence of a hollow core allowed for a larger quantity of Ral-PEG to be stored within the spheres.

As explained further on, two different release conditions were established, resulting in three assays being performed for each sphere type (hollow or non-hollow), and two assays being performed for hollow spheres for 19 different time intervals.

For each assay, about 30 mg of microspheres were placed in open containers with 1 mL solutions of Ral-PEG in MeOH, with concentrations of 1 mg/mL. These containers were then placed in a small closed chamber that was connected to a vacuum pump (KNF LABOPORT® N 820 FTP Diaphragm Vacuum Pump) that produced low vacuum – 99 mbar, at room temperature and for 1 h 30 min, in order to force the Ral-PEG solution inside the porous microspheres infrastructure.

To determine the loading efficiency of Ral-PEG, the volume of the solution remaining in the containers, after loading the spheres, and the concentration of Ral-PEG were measured, which allowed for the quantification of the mass of Ral-PEG. The efficiency was then calculated by dividing this value per the initial mass of Ral-PEG available in the loading solution.

3.2.3.6. Raloxifene Release Profile of the Microspheres

The drug release from the microspheres loaded with Ral-PEG was analysed, in order to understand the efficiency of its release, in a mock physiologic medium.

In order to study continuous drug release, and to be able to preserve spheres with different percentages of encapsulated drug and their corresponding drug release solutions, two different release conditions were established: continuous and non-continuous.

3.2.3.6.1. Continuous Drug Release

For continuous drug release, spheres that differed in type (hollow or non-hollow) were used, for a total of 3 assays for each sphere type. Each 30 mg of microspheres that were loaded with Ral-PEG, with the method previously described in *3.2.3.5. Ral-PEG Loading* were placed in containers with 1 mL of PBS solution in an orbital shaker (IKA® KS 4000 ic control) with a constant temperature of 37ºC at 130 rpm.

Microspheres were kept in the orbital shaker for a total of 2 weeks, with the drug release solutions being removed in their entirety from their containers in 2-hour time intervals, until the 10^{th} hour, from which point the solutions were removed in daily intervals, for a total of 19 measurements per assay. The containers with the microspheres would be then refiled with 1 mL of clean PBS solution.

900 µL of the removed drug release solution would then be mixed with 900 µL of MeOH, in order to obtain solutions with a PBS:MeOH ratio of 1:1.

The Ral-PEG solutions resulting from this continuous release were later used to measure the concentration of Ral-PEG present in them - *3.2.3.7. Spectrophotometric Analysis*, and to study their effects in osteoblast-like cells' activity - *3.2.4.4.1. Dose Dependent Effects of Ral-PEG*, *3.2.4.4.2. Effects of Ral-PEG on Collagen Production*.

3.2.3.6.2. Non-Continuous Drug Release

For non-continuous drug release, only hollow spheres were used, for a total of 38 assays. Each 30 mg of microspheres that were loaded with Ral-PEG, with the method previously described in *3.2.3.5. Ral-PEG Loading,* were placed in containers with 1 mL of PBS solution in an orbital shaker (IKA® KS 4000 ic control) with a constant temperature of 37ºC at 130 rpm.

Microspheres were kept in the orbital shaker for a total of 2 weeks, with two containers being removed in 2-hour time intervals, until the 10th hour, from which point the containers were removed in 24-hour intervals – 19 different time intervals. The solutions of every removed container were discarded, while the spheres were left in each container, dried overnight at 37 ºC and later stored at 4 ºC.

The microspheres resulting from this non-continuous drug release were later used in cell culture studies to analyse their potential cytotoxicity on osteoblast-like cells - *3.2.4.4.3. Effects of Ral-PEG Loaded Microspheres*.

3.2.3.7. Spectrophotometric Analysis

The amount of Ral-PEG that was released by the Ral-PEG loaded microspheres, during continuous drug release - *3.2.3.6.1. Continuous Drug Release*, was determined by measuring the absorbance of the resulting Ral-PEG solutions in PBS:MeOH (1:1) through spectrophotometry.

To quantitively measure the concentration of Ral-PEG present in a solution, a calibration curve was constructed using Ral-PEG solutions in PBS:MeOH (1:1) with known concentrations, in the range of 0-4 µg/mL. 200 µL of the calibration Ral-PEG solutions were transferred to a 96-well UV-transparent microplate (96 Well UV-Star® Microplates, clear) per well, and the plate was placed inside a microplate reader (PowerWave XS2, Microplate Spectrophotometer by BioTek Instruments, Inc.). The absorbance was measured at a wavelength of 287 nm, as Ayşegül Kavas et al. [85] have validated that PEG does not interfere with Ral optical measurements at this wavelength. The absorbance of the Ral-PEG solutions obtained during continuous drug release was determined using this same method and the obtained calibration curve was then applied to determine their concentrations of Ral-PEG.

The measurements were made with a PBS:MeOH (1:1) solvent, instead of just PBS, since it was determined that Ral-PEG had higher solubility in a PBS:MeOH (1:1) solution than in a PBS solution. By having PBS:MeOH (1:1) as the solvent, it was thus more safely ensured that the Ral-PEG would be completely dissolved and, therefore, appropriate for absorbance reading through spectrophotometry.

3.2.4. Cell Culture Studies

3.2.4.1. E. coli ATCC 25922 Strain

E. coli ATCC 25922 strain bacteria were purchased from ATCC®. They were cultivated in Luria Bertani (LB) agar – purchased from Liofilchem®, in a carbon dioxide incubator at 37ºC.

3.2.4.2. Effects of Gentamicin on E. coli ATCC 25922 Bacteria

E. coli bacteria were suspended in tryptic soy broth (TSB) and measured with an initial colony density of 10^8 cfu/mL. 80 µL of this solution were diluted with TSB to a density of 10^6 cfu/mL, resulting in a total volume of about 8 mL.

3.2.4.2.1. Dose Dependent Effects of Gentamicin

A qualitative assay was performed to observe the dose-dependent effect of gentamicin. It used filter disks embedded with 5 µL of gentamicin release solutions placed on a petri dish with Mueller-Hinton agar cultivated with *E. coli*, which was then incubated at 37ºC overnight – the purpose being to observe the radius of bacterial toxicity of each solution.

3.2.4.2.2. Effects of Gentamicin Loaded Microspheres

A qualitative experiment was performed to examine the effects of gentamicin loaded microspheres on *E. coli*, wherein, for each initial gentamicin loading concentration (2 mg/mL and 3 mg/mL) three groups of three hollow microspheres were placed on a petri dish with Mueller-Hinton agar cultivated with *E. coli*, which was then incubated at 37ºC overnight. The first group had microspheres fully loaded with gentamicin, and the second and third group were comprised of microspheres which had been releasing gentamicin into distilled water for 3 days.

3.2.4.3. MG-63 Cell Line

MG-63 – human osteoblast-like cells, purchased from ATTC®, were cultivated in growth medium - α-Minimal Essential Medium (α-MEM), supplemented with 10% of foetal bovine serum (FBS), 2.5 µg/mL of Amphotericin B and 100 UI/mL of penicillin/ 100 µg/mL of streptomycin (all supplements purchased from Gibco), at 37 ºC in a carbon dioxide incubator.

3.2.4.4. Effects of Ral-PEG on MG-63 Cells

Human osteoblast-like cells were incubated in essential growth medium, as previously described, inside a culture flask at 37 ºC.

3.2.4.4.1. Dose Dependent Effects of Ral-PEG

To examine MG-63 cells' viability with the Ral-PEG release solutions obtained in *3.2.3.6.1. Continuous Drug Release*, cell suspensions were incubated in a 96-well microplate alongside those drug release solutions with different concentrations of Ral-PEG.

In a 96-well microplate, a quantity of cells per well surface of 10^4 cells/cm^2 was seeded. 50 µL of prepared MG-63 cell suspension + 50 µL of each Ral-PEG release solution were added per well, with an additional column seeded with 50 µL of suspension + 50 µL of PBS to act as a control, and the microplate was left to incubate overnight in a carbon dioxide incubator at 37 ºC.

To analyse cell metabolism depending on the concentration of Ral-PEG of each release solution, an MTT assay was performed. MTT assays consist of colorimetric assays that rely on the reduction of MTT, a yellow water-soluble tetrazolium dye, primarily by the mitochondrial dehydrogenases, to purple coloured formazan crystals – the higher the quantity of formazan crystals formed, the higher the quantity of mitochondrial dehydrogenases present in the suspension, meaning that there is a higher metabolic cellular activity. The crystals are analysed spectrophotometrically (550 nm) after dissolution in dimethyl sulfoxide (DMSO), giving an estimate of the extent of cytotoxicity [92]. Thusly, 10 µL of MTT were added to each well, and the plate was left to incubate at 37 ºC for 2h 30 min. Afterwards, the plate was removed from the incubator and all volume of solution was removed from each well and replaced with 100 µL of DMSO. Three clean and empty wells were also filled with 100 µL of DMSO, to act as a negative control. After a 15 min wait in order to allow proper formazan dissolution in DMSO, the absorbance of each well was read in a microplate reader (Synergy™ HTX Multi-Mode Microplate Reader by BioTek Instruments, Inc.) at a wavelength of 550 nm.

3.2.4.4.2. Effects of Ral-PEG on Collagen Production

Cell suspensions were incubated in a 48-well microplate alongside the Ral-PEG release solutions obtained in *3.2.3.6.1. Continuous Drug Release*. A quantity of cells per well surface of 10^4 cells/cm^2 was used. 250 uL of the prepared cell suspension + 250 µL of Ral-PEG release solution were then placed in each well, and the plate was left to incubate for seven days at 37 ºC.

To qualitatively analyse collagen production, a staining assay with Sirius Red was conducted. After removing the 48-well plate from the incubator, all the wells were fully drained of their liquid solutions and were then gently washed with 400 µL of PBS per well. After the PBS was discarded, 400 µL of of glutaraldehyde (1.5% in sodium cacodylate) were placed in each well and the plate was left to incubate for 15 minutes at room temperature, in a dry area shielded from light. The glutaraldehyde was then removed, and each well was gently washed with 400 µL of PBS. Following PBS removal, 400 µL of Sirius Red dye were added to each well and the plate was left to incubate for 1 hour at room temperature, in a dark and dry area. The dye was then removed, and each well was carefully rinsed with HCl 0.01 N twice, until all dye residues had been washed away. The plate was left to dry for a few minutes and then, through inverse microscopy, the contents of each well were observed and photographed.

3.2.4.4.3. Effects of Ral-PEG Loaded Microspheres

After the experiments performed in *3.2.3.6.2. Non-Continuous Drug Release*, hollow Hap microspheres loaded with varying quantities of Ral-PEG were obtained, according to the time instant that drug release was suspended, and later underwent ethylene oxide sterilization. In order to determine MG-63 cell metabolic activity when in contact with, not only the remainder of Ral-PEG that is released from the microspheres, but also with the sphere's material and microstructure, a 96-well microplate was seeded with MG-63 cells and left to incubate in essential medium, whilst in the presence of the microspheres.

A quantity of cells per well surface of $5x10^4$ cells/cm^2 was used. In each well with 100 µL of cell suspension, 5 Hap microspheres were added, with each column of the microplate corresponding to different quantities of Ral-PEG loaded onto the spheres (Figure 12). The microplate was then placed in a CO_2 incubator at 37 ºC, to incubate overnight.

To analyse cell metabolism depending on the quantity of Ral-PEG that each sphere yielded, three resazurin assays were performed on different days. Resazurin is an oxidation-reduction indicator with a blueish color, that becomes pink when reduced to resorufin by cellular oxidoreductases [93] – therefore, the higher the cell metabolism, the higher the concentration of cellular oxidoreductases that are produced, and, thus, the pinker the indicator will be. For each assay, firstly, 3.6 mL of essential growth medium were mixed with 0.4 mL of resazurin. Then, all liquid medium was removed from each well and replaced with 100 µL of the resazurin dilution. The microplate was then incubated at 37 ºC for 2 h 30 min and, afterwards, 60 µL of the liquid contents of each well were transferred to a solid black 96-well microplate, in order to protect the solutions from the effects of visible radiation. The microplate was then inserted into a microplate reader and fluorescence was read at at an excitation wavelength of 530/25 nm and emission wavelength of 590/35 nm.

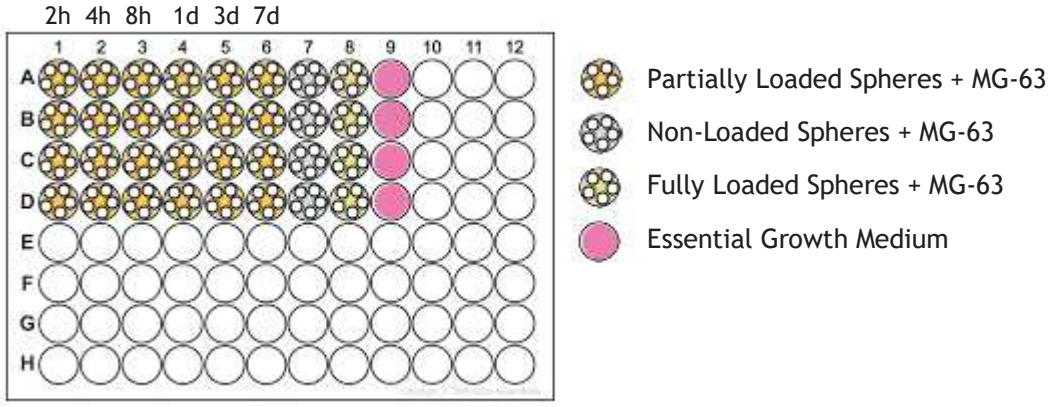


Figure 12 - Schematic representation of a 96-well microplate seeded with MG-63 human osteoblast-like cells, for the purpose of showing the effect that hollow Hap microspheres loaded with Ral-PEG have on these cells. Columns 1 to 6 correspond to spheres loaded with different quantities of Ral-PEG, according to the different time instants at which they were collected during Ral-PEG release – 2 hours, 4 hours, 8 hours, 1 day, 3 days and 7 days. Column 7 functions as a control wherein the effect of non-loaded spheres on the MG-63 cells is examined. Column 8 function as a control wherein the spheres have not been exposed to a release medium, meaning that they are fully loaded with Ral-PEG. Column 9 functions as a control with neither spheres nor cells, acting as a blank containing only the growth medium.

3.2.5. Statistical Analysis

The obtained numerical data was analysed with the software IBM® SPSS® Statistics 26.0.0.0.

For gentamicin drug release tests and Ral-PEG cell culture studies, one-way analysis of variance (ANOVA) tests with post hoc analysis employing Tukey's range test were used for statistical analysis, with a 95% ($p < 0.05$) confidence level being adopted for statistical significance.

For Ral-PEG drug release tests, an independent-samples T test was used for statistical analysis, with a 95% ($p < 0.05$) confidence level being adopted for statistical significance.

Chapter 4

Results and Discussion

4.1. Preparation of the Microspheres

To obtain calcium phosphate-derived ceramic microspheres that had a high degree of interconnected porosity, syringe-foaming followed by a co-injection method were applied, the latter of which made use of a coaxial mould and programmable fusion pumps.

In the syringe-foaming process, hydroxyapatite powder was mixed with an aqueous solution of alginic acid sodium salt and sodium phosphate, resulting in a ceramic suspension, as previously described. Through a syringe-foaming method, this suspension was mixed with the surfactant F-127 to create a ceramic foam, which was then injected into a coaxial mould through an infusion pump at a fixed flow rate. For the creation of non-hollow spheres, it is only necessary to attach the syringe with the ceramic foam into the mould's outer channel. For hollow spheres however, an additional syringe, filled with polystyrene, is pumped into the mould's inner channel at the same time as the ceramic foam is injected into the outer channel (co-injection), leading to the incorporation of PS inside the ceramic foam. The ceramic foam then exits the mould in the form of small spheres, which are later on subjected to a heat treatment wherein all polymeric components combust and hydroxyapatite sinters.

Hydroxyapatite was used as the calcium phosphate-derived material that would compose the microspheres' matrix, due to its well-documented properties as a biocompatible and bioactive substance (as previously described in section *2.3.2. Synthetic Bone Substitutes*), meaning that it supports and stimulates bone ingrowth as well as osteointegration. Additionally, hydroxyapatite is currently used as the main material for many synthetic bone substitutes available in the marketplace (Tables 1 and 2).

The alginic acid sodium salt dissolution in water allows for the creation of an alginate hydrogel which increases the cohesion of the calcium phosphate ceramic suspension and, by extension, the cohesion of the ceramic foam [94-97]. Additionally, despite leading to a decrease in foamability that could potentially lead to a decrease in porosity, the alginate hydrogel can counterbalance this effect by allowing for higher stability and elasticity of the ceramic foam [89]. Finally, it is the hydrogel that allows for the reticulation process brought by the $CaCl_2$ solution, due to a reduction in elasticity that is bought by the incorporation of free calcium ions into the gel's network [98]. Thus, the alginate hydrogel proves to be critical to the ceramic foam's rheological properties, allowing for a cohesive structure that does not overly disrupt the foam produced by the surfactant, and for the formation of pores shaped by the foam bubbles, upon alginate combustion during the heat treatment.

The addition of the sodium phosphate solution allows for the Hap to dissolve more easily in the alginate hydrogel, by acting as a buffer solution that reduces the pH of the Hap and hydrogel mixture. Sodium phosphate also affects the rheology of the ceramic foam in such a way that it prevents the coalescence of foam bubbles, thus leading to a potential lower pore size distribution within the structure of the resulting microspheres [88-89].

To induce sphere porosity, a foam solution of the surfactant agent Pluronic® F-127 was added to the alginate-Hap mixture. As a surfactant, Pluronic® F-127 is water-soluble, FDA-approved for use on humans and has the advantage of being fully synthetic and biocompatible. Although the subsequent heat treatment would likely eliminate any substances that could cause immunogenic responses, if the foaming agents were protein-based and derived from a natural source [99], the synthetic origin of the used surfactant allows it to inherently have higher reproducibility and a more tight control of its chemical properties. Moreover, this surfactant is non-ionic, making it less sensitive to changes in pH and less likely to be subjected to electrical repulsion of its molecules, resulting in the formation of more stable foams that have a higher degree of compatibility with other materials [88, 99].

Through syringe-foaming, the surfactant agent produces foam in the ceramic suspension, with the resulting internal air bubbles that are formed being the basis for the high degree of porosity that is created in the spheres later in the production process. As a foaming method, syringe-foaming is a mechanical process, which gives it the advantages of a better general distribution of pores and a higher degree of pore interconnectivity, when compared to other pore-inducing alternatives [97, 100-101]. Syringe-foaming is also a simple, direct and non-expensive method, that allows for the control of the air volume that is injected into the sample, something which cannot be controlled in the case of solutions that are foamed with mechanical agitators.

One notable disadvantage of syringe-foam is, due to the immiscibility of the ceramic suspension and the surfactant solution, these two phases start to separate from each other when together in the syringe, meaning that if a flux is not quickly applied into the syringe, or if this flux is too slow, the two phases will become too far apart to produce microspheres with the desired structure and composition, meaning that resulting spheres can become either too dense (not enough foam phase) or too porous (overabundance of foam phase). Therefore, for the spheres to present an optimal structure, the operator must be quick to mount the syringe with the cement foam onto the infusion pump after its formation, and the volume of cement foam inside the syringe and the speed of the applied flux must be adjusted accordingly to one another, in order to efficiently use as much ceramic foam as possible. Due to the possibility of adjusting the volume of air and, consequently, of foam that is produced with this syringe-foaming method, this obstacle has a high potential of being surpassed.

Before the production of microspheres with a hollow core, non-hollow porous microspheres were initially produced, since this allowed for the analysis of the microspheres infrastructure, without the need to use two different infusion pumps at different flow rates; for non-hollow spheres, only the syringe that contains the foam and ceramic past is connected to the co-axial mould, into its outer channel, and a flow rate of 2.5 μL/s is applied. Both non-hollow and hollow microspheres that were

obtained presented an overall spherical structure, although most non-hollow spheres were slightly ellipsoidal at one axis. Since the droplet's shape is greatly dependent of the action of gravity, this may be due to a non-optimal distance between the exit point of the coaxial mould and the surface of the reticulation solution of $CaCl_2$, which must be carefully adjusted so that the droplet assumes an optimal spherical shape when dropped into the $CaCl_2$.

The polymer PS was inserted into the centre of the droplets of alginate-Hap that are formed trough co-injection, so that later, during the first steps of heat treatment, PS would be fully combusted and leave a hollow space in the centre of the resulting microsphere. In the case of hollow spheres, when observing the co-injection droplets, some would have their PS component dislocated from the droplet's centre, which resulted in a decentralized hollow core; droplets that had their PS component properly located at their centre still had a risk of ending with a decentralized core, since fallen droplet observation only allows for an analysis that is closer to a 2-dimensional plane. The inappropriate positioning of the hollow core can have later repercussions when trying to analyse drug encapsulation and drug release, since the obtained microsphere model is not properly concentric. A potential solution would be to change the solvent in which the PS solution is prepared: dichloromethane has a tendency to evaporate quickly, leading to PS potentially solidifying inside the mould's channels and disrupting the flow of the solutions in them, so a less volatile solvent, that does not react with the ceramic foam, would be recommended. Furthermore, it is suspected that the inner channel and outer channel of coaxial mould used during co-injection appeared to not be properly aligned to each other; since the work done is at a microscale, small misalignments in the used instruments can result in noticeable faults in the finished products, so the use of a coaxial mould that is certified to be aligned properly is crucial for the production of the hollow microspheres.

Post-heat treatment, the microspheres overall presented a porous infra-structure, although porosity was not homogenous throughout the structure of some spheres and, in the case of hollow spheres, there was a tendency for a less porous wall to form between the hollow core and the rest of the sphere's ceramic structure. This will be explained and exemplified with more detail in section *4.2.3. Morphological Analysis by Scanning Electron Microscopy*.

4.2. Characterization of the Microspheres

In order to determine if the obtained microspheres had the desired structural properties to potentially be used as bone substitutes, as well as having the capability for drug encapsulation and controlled drug release, several analyses on the spheres' microstructure were performed, including: helium pycnometry to determine the density of the used Hap; morphological analysis of the microspheres through SEM to qualitatively examine their porosity, morphology and topography; examination of the microspheres' size and degree of porosity through direct measurement of their diameter and through density measurements utilizing the Archimedes' principle.

4.2.1. Helium Pycnometry

The density of the hydroxyapatite powder that was used for microsphere production was measured to be 3.1723 $g.cm^{-3}$ ± 0.0035 $g.cm^{-3}$. The theoretical density of pure phase hydroxyapatite is stated to be about 3.16 $g.cm^{-3}$ [102-104], meaning that the obtained density of the used Hap is credible, given that this specific powder has an assigned purity of ≥ 90 % and it is thus expected that there might be slight impurities that result in a density that is, on average, 0.39 % higher than the theorical values.

4.2.2. Morphological Analysis by Scanning Electron Microscopy

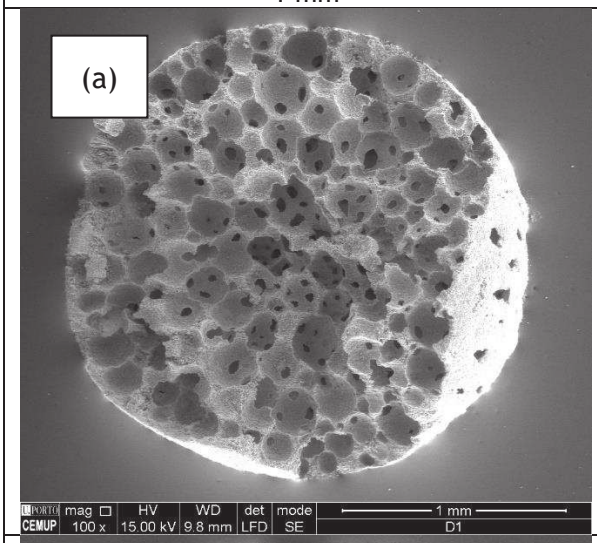
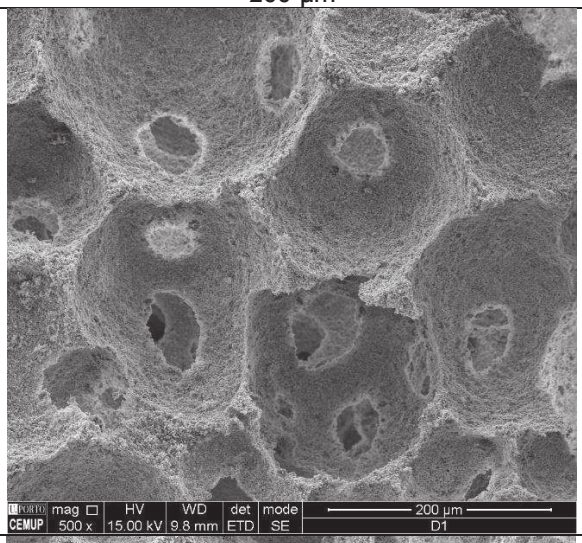
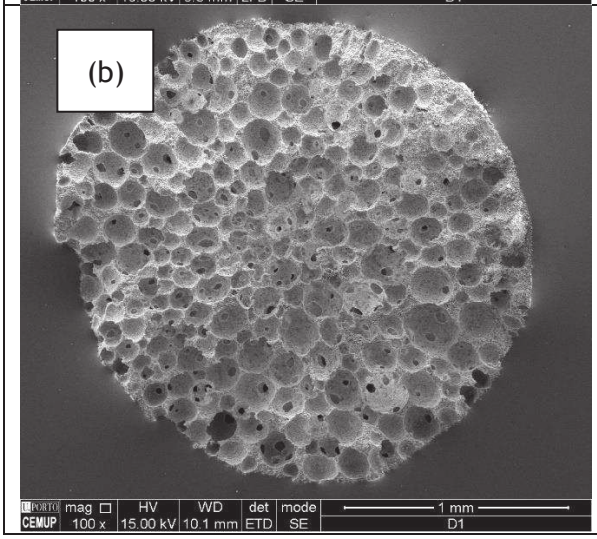
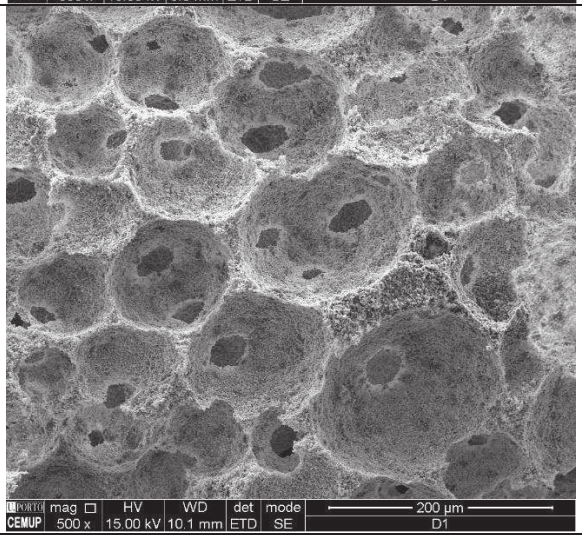
SEM analysis was performed to qualitatively examine the morphological and topographical properties of the obtained microspheres, both those with and without a hollow core. Sphere macroporosity and pore interconnectivity is crucial for the purpose of bone growth and vascularization, and for encapsulation of relatively large volumes of drug, so it is desired that the produced spheres have a large network of interconnected macropores with diameters that are favourable for bone regeneration to occur. In the case of hollow spheres, the existence of a hollow core will theoretically allow for a larger volume of drug to be loaded within the spheres, and it is desired that this core is localized at the very centre of the sphere and that the surrounding ceramic matrix has a relatively low pore size distribution, since an eventual drug release will easier to control if the carrier is as close as possible to a perfectly concentric sphere, wherein the structural properties of its shell are homogenous and consistent.

Regarding non-hollow Hap microspheres, SEM analysis shows a high density of macropores within the spheres' structure, along with micropores within the macropores, allowing for a greater degree of interconnectivity (Table 3). Using ImageJ software, the maximum and minimum diameters of the macropores were measured for non-hollow spheres of different batches (Table 4), showing that these values range from around 80 to 250 µm, 60 to 250 µm, 80 to 300 µm and 60 to 380 for each different batch. Since it is usually required a minimum pore diameter of 50 to 100 µm to promote bone cell migration and angiogenesis of small blood vessels, and diameters above 150-300 µm for proper vascularized bone ingrowth [41-45] the obtained microspheres have a suitable porosity to potentially allow for a proper regeneration of bone tissue. Both high values of macropore diameter and high apparent interconnectivity suggest that the obtained non-hollow Hap microspheres may have great capability of also allowing for drug loading and release.

Macropore size distribution in non-hollow spheres appears to be generally low, as a qualitative analysis of the SEM micrograms (Table 3) seems to indicate. It is favourable that this size distribution is low, since it allows for a better prediction and, thus, control of a subsequent drug release. A slight outlier is sample 4 (sample (c) in Table 3), which presents a larger variety of macropore sizes, including both the lowest and the highest macropore diameters measured in all samples – 61 µm and 381 µm, respectively. This difference is likely due to this sample corresponding to a microsphere that was produced from ceramic foam whose foam phase was greater than its ceramic suspension phase

in comparison to the other samples: during the process of injection of the ceramic foam into the coaxial mould, as time passes by, the two phases of the ceramic foam inside the syringe start to slowly separate due to their immiscibility, meaning that, when the syringe is closer to being emptied, there is a greater percentage of foam than of ceramic suspension. A larger percentage of foam in the ceramic suspension leads to a destabilization of the bubbles, which, through coalescence, form slightly large bubbles and increase the variety in overall bubble size. Consequently, the resulting microspheres have, on average, a larger pore size and a greater macropore size distribution.

Table 3 - SEM micrographs of cuts of Hap non-hollow microspheres. Each row corresponds to the same sample, viewed at different scales – 1 mm for the first column and 200 µm for the second column.

Scale	
1 mm	200 µm
	
	

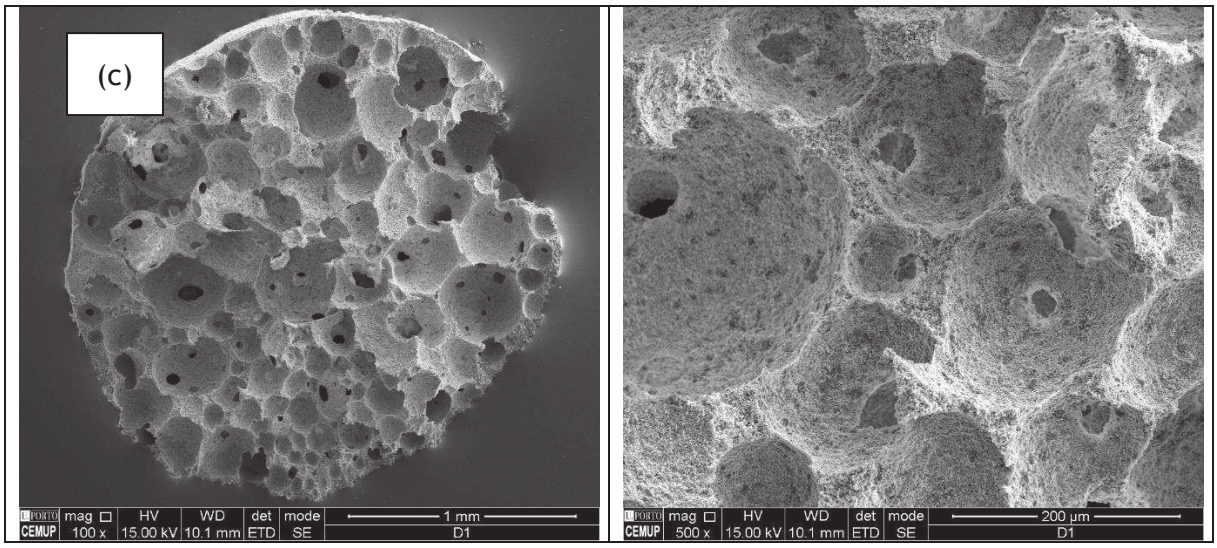


Table 4 - Macropore diameters for **non-hollow** Hap microspheres, as obtained through ImageJ. Samples 1, 2 and 4 correspond to samples (a), (b) and (c) displayed on Table 3, respectively. All samples belong to different batches of microspheres.

Sample	Min Diameter (µm)	Max Diameter (µm)
1	83	247
2	64	248
3	85	307
4	61	381

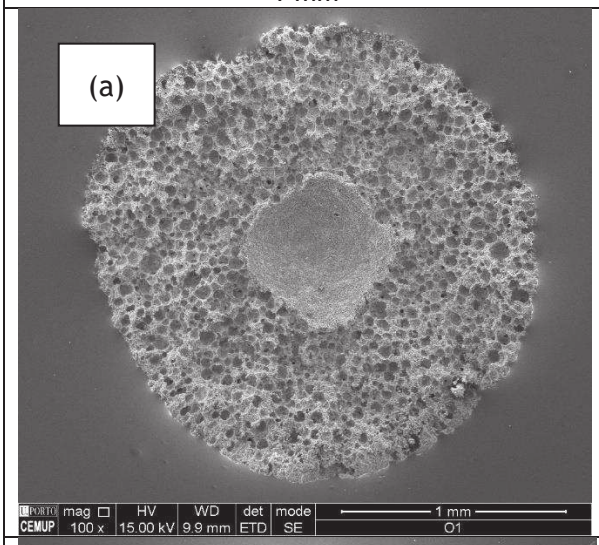
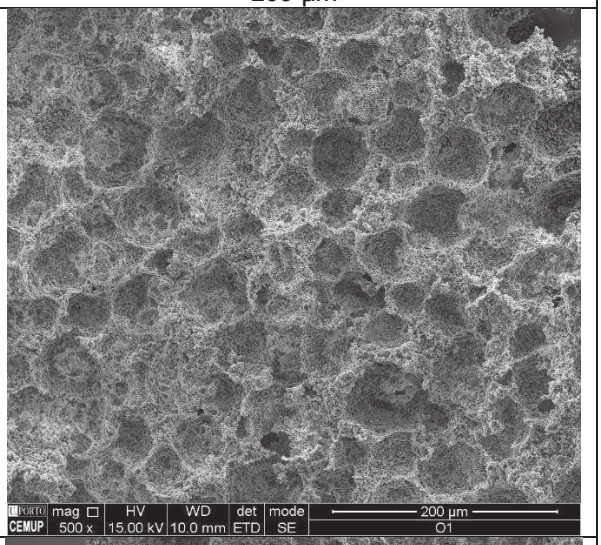
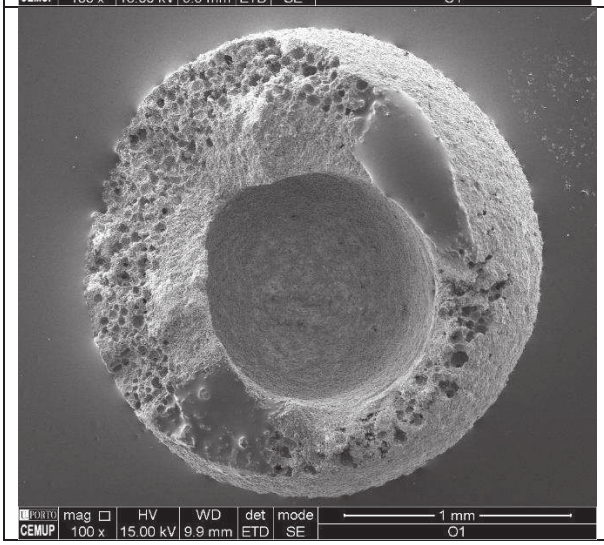
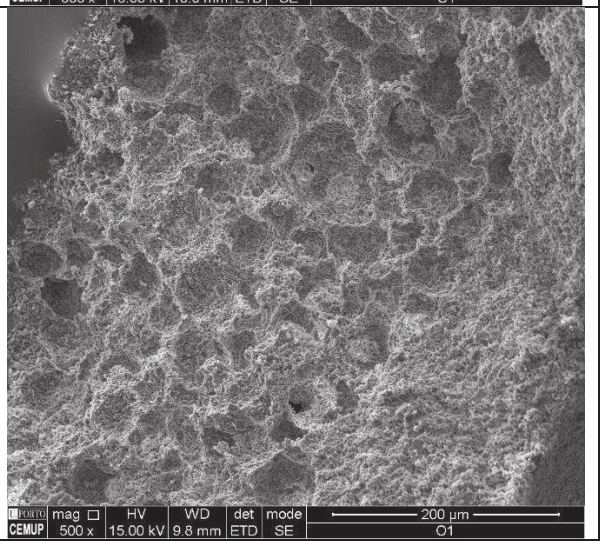
Regarding hollow Hap microspheres, the SEM micrographs show that they present an overall smaller macropore size in the sphere's shell – the area surrounding the hollow core (Table 5), smaller interconnectivity between macropores and smaller micropore size, when compared to the non-hollow microspheres. The first assertion is further supported by the values of macropore diameter obtained through the ImageJ software, as shown in Table 6. Despite the smaller values, macropore diameter for the obtained hollow microspheres varies from about 30 to 90 µm, managing to cover the range of pore diameter that is necessary to promote bone cell migration and basic vascularization. As the samples presented in Tables 5 and 6 belong to the same batch, both micrographs and numeric data suggest that, for the same batch, there is a decent level of reproducibility for hollow Hap microspheres.

On Table 5, the micrographs show that the sphere's cores are divided from the shell by a surface with few openings – this skin, that is also present in the outer surface of the microspheres themselves, is likely formed during heat treatment, due to migration of the finer particles of Hap to the interfaces between the ceramic material and the atmosphere/the hollow core, which then form the skin when sintered [105]. Still, closer observation of samples b) and c) in particular show that there exists porosity in that inner surface, meaning that it is possible for loaded drugs to be stored inside the hollow core. Furthermore, as observed in Table 6, the cores present a diameter that is in the range of 900 to 1100 µm, meaning that the core can potentially store the desired drug volumes, that may

vary from to 3.00 to 5.50 µL. Thus, the interference in drug loading that a smaller level of porosity in the surface between the shell and core might cause could potentially be overcome by a longer period of drug loading, as well as by applying a larger pressure during the loading process, to enhance drug diffusion into the microspheres' core.

Macropore size distribution in the shell region is very low, with the shell having a relatively uniform structure. There are, however, some problematic regions next to the surface that separates the shell from the core, that present a noticeable different gradient of porosity and have relatively high density – Table 5, samples b) and c). Coupled with the smaller level of porosity of the inner core's skin when compared to the shell, this seems to suggest that the part of the sphere's infrastructure that is closer to the core has a risk of being less porous, and may thus negatively interfere with drug loading and release.

Table 5 - SEM micrographs of cuts of Hap hollow microspheres. Each row corresponds to the same sample, viewed at different scales – 1 mm for the first column and 200 µm for the second column. The first row displays a sample that was cut from the base of the sphere.

Scale	
1 mm	200 µm
	
	

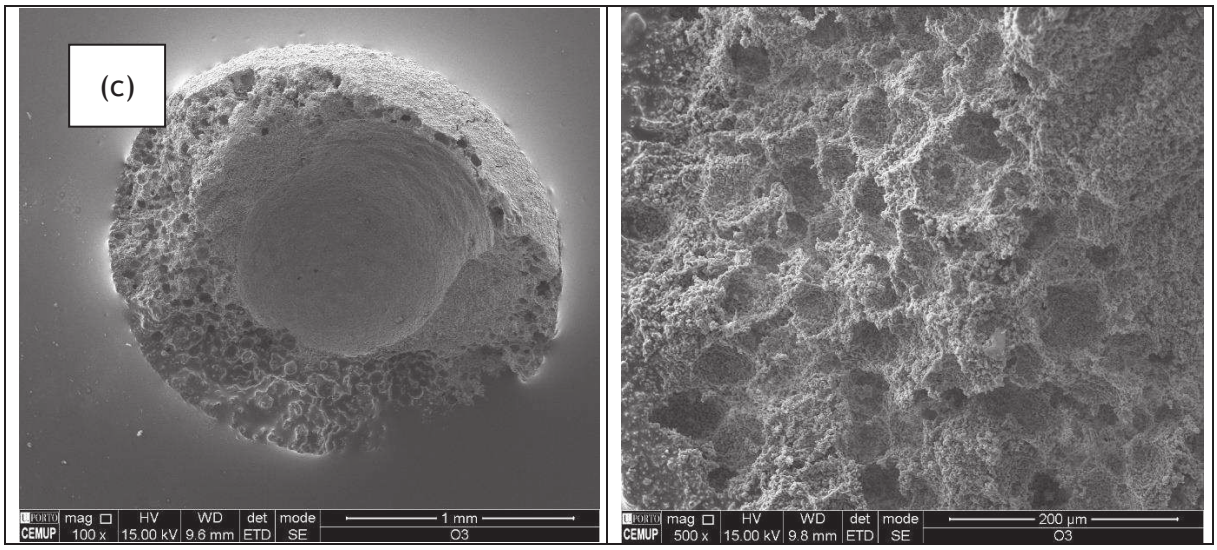


Table 6 - Macropore diameters in the shell region and hollow core diameters for **hollow** Hap microspheres, as obtained through ImageJ. Samples 1, 3 and 5 correspond to samples (a), (b) and (c) displayed on Table 5, respectively. All samples belong to the same batch of microspheres.

Sample	Min Diameter (µm)	Max Diameter (µm)	Core Diameter (µm)[1]
1	35	94	N/A
2	38	90	1181 ± 87
3	31	111	1042 ± 63
4	35	81	944 ± 78
5	31	88	1018 ± 37
6	32	88	1031 ± 48

The differences in macropore size and distribution between hollow and non-hollow spheres is not unexpected, seeing as their production methods, although similar, were markedly different in terms of the processing of the ceramic foam. In the production of hollow microspheres, two infusion pumps were used, with ceramic foam being pumped with a flow rate of 25 µL/s into the coaxial mould's outer channel, while the PS was pumped with a flow rate of 2.5 µL/s into the coaxial mould's inner channel. In the production of nonhollow microspheres, only one pump was used, pumping only the ceramic foam contained in the syringe into the outer channel of the coaxial mould at a flow rate of 2.5 µL/s. This difference in flow rates of the ceramic foam, as well as the presence of an additional material in hollow sphere fabrication, are likely the main causes behind the differences in porosity properties between the two types of spheres.

Overall, the macropore size and interconnected porosity suggest that these microspheres would allow for bone growth and some degree of vascularization. Still, larger macropores with diameters in the range of 150-300 µm would be preferable to ensure that a good vascularization of the bone tissue

[1] Diameter was measured up to six times for the same core, for each different sample.

would take place [41-45]. One way to remedy this situation would be by adjusting the concentration of surfactant during the syringe-foaming stage, so that the resulting air bubbles are larger, and thus lead to the production of larger macropores in the microspheres' structure. Another option would be to use a different foaming agent, such as Tween 80, which has been shown to have good foam stability and lead to high open and total porosities in calcium phosphate derived scaffold [49, 99, 106]. However, an important detail to keep in mind is that excess macroporosity can result in microspheres that are too frail to be handled manually without breaking apart, so an appropriate balance between porosity and structural strength must be found. For hollow microspheres in particular, the irregularity of the hollow core's location is troublesome, since an optimal core should be able to be consistently formed at the very centre of the sphere, ensuring the method's reproducibility and a proper prediction of how drug release would take place. Furthermore, the existence of denser regions near the core can also affect drug release analysis, as well as serving as a potential deterrent for proper drug loading and cellular tissue migration.

4.2.3. Microsphere Size and Porosity Analysis

Microsphere diameter was measured with a calliper, with average diameters being determined for different batches of microspheres – microspheres that were produced with the exact same methods, but at different times. By combining these values with the sphere densities measured using the Arquimedes' principal, closed, open and total porosities for different batches of spheres was determined, with closed porosity corresponding to the percentage of porosity in a sphere that is due to isolated pores, open porosity the percentage of porosity in a sphere that is induced by the interconnected network of pores that is also connected to the exterior surface, and total porosity the sum of those two.

In terms of dimensions, hollow microspheres tend to be slightly larger than non-hollow ones, having a diameter that is about 0.1 mm larger (Tables 7 and 8). It is possible that hollow microspheres present a slightly larger diameter due to an additional expansion of the sphere's structures that occurs during heat treatment, caused by the combusted PS pushing the ceramic component from the inside, when it has yet to have undergone sintering. However, has stated previously, hollow and non-hollow spheres have differences in their production method, regarding the processing conditions of the ceramic foam, meaning that it is not entirely unexpected that the diameters are different between the two types of spheres.

In terms of porosity, both non-hollow and hollow spheres present similar values: for closed porosity, the values range from about 7 to 16 % for non-hollow microspheres, and from 3 to 20 % for hollow ones; for open porosity, the percentage ranges from about 35 to 60 % for non-hollow microspheres, and from 55 to 65 % for hollow ones.

At first glance, similar values of open porosity for both hollow and non-hollow spheres appear to contradict the data that was presented in *4.2.3. Morphological Analysis by Scanning Electron Microscopy*. However, the results do, in fact, complement and support each other: as it was previously

observed, non-hollow microspheres present a significant level of macropores and of interconnected porosity, which is in accordance with the values of open porosity in Table 7, but hollow microspheres have smaller macropores and smaller apparent interconnectivity between them. These smaller values, however, are mainly applicable to the shell of the microspheres, and the bulk of the open porosity measured for these spheres lies mainly in the hollow core, meaning that it is not surprising that both hollow and non-hollow that were obtained present similar percentages of open porosity. What this does indicate is that both SEM and geometrical analysis are essential to determine the porosity of the hollow microspheres, since the measured open porosity alone does not fully account for the different structural properties between the hollow sphere's shell and its core.

Table 7 - Diameter, density and porosity values of **non-hollow** Hap microspheres. Different batches of microspheres were made from different ceramic foams, but all ceramic foams were prepared with the same type and quantity of materials and the same methods. For batches 1 and 2, diameter measurements were made for 6 different spheres, and Archimedes density measurements for 3 different spheres; for batch 3, diameter measurements were made for 24 different spheres, and Archimedes density measurements for 4 different spheres.

Batch	Sphere Diameter (mm)	Geometric Density ($g.cm^{-3}$)	Archimedes' Density ($g.cm^{-3}$)	Closed Porosity (%)	Open Porosity (%)	Total Porosity (%)
1	1.65 ± 0.22	1.50 ± 0.62	2.75 ± 0.42	8.4 ± 1.7	44.7 ± 7.9	50.1
2	1.73 ± 0.16	1.10 ± 0.32	2.76 ± 0.33	6.9 ± 2.6	59.9 ± 4.6	65.0
3	1.63 ± 0.08	1.33 ± 0.17	2.13 ± 0.30	16.1 ± 6.5	36.6 ± 8.6	52.8
Average	1.70 ± 0.16	1.20 ± 0.39	2.53 ± 0.44	11.3 ± 6.2	47.3 ± 12.4	56.5

Table 8 - Diameter, density and porosity values of **hollow** Hap microspheres. Different batches of microspheres were made from different ceramic foams, but all ceramic foams were prepared with the same type and quantity of materials and the same methods. For each batch, diameter measurements were made for 6 different spheres, and Archimedes density measurements for 3 different spheres.

Batch	Sphere Diameter (mm)	Geometric Density ($g.cm^{-3}$)	Archimedes' Density ($g.cm^{-3}$)	Closed Porosity (%)	Open Porosity (%)	Total Porosity (%)
1	1.83 ± 0.08	0.937 ± 0.137	2.61 ± 0.46	7.6 ± 6.6	63.3 ± 6.2	70.9
2	1.87 ± 0.12	0.961 ± 0.162	2.15 ± 0.24	15.4 ± 5.6	54.9 ± 5.4	70.3
3	1.82 ± 0.8	1.00 ± 0.15	2.46 ± 0.66	3.8 ± 1.0	64.6 ± 1.1	68.4
4	1.73 ± 0.04	1.14 ± 0.07	2.50 ± 0.06	8.4 ± 1.0	54.3 ± 1.2	62.7
Average	1.81 ± 0.09	1.01 ± 0.15	2.43 ± 0.42	11.0 ± 7.9	57.6 ± 8.1	68.6

In the final paragraph of *4.2.3. Morphological Analysis by Scanning Electron Microscopy*, it was discussed that macropore size in the microspheres should be larger, in order to ensure proper bone tissue growth and vascularization. On this note, if macropore size were to increase, open porosity would increase as well, given that, not only would the pores have a larger volume, bigger pores are more likely to intersect with each other on a small matrix, allowing for higher pore interconnectivity.

Ideally, such changes would thus lead to pores that would be isolated to become part of the interconnected pore network, thus shifting the values of closed porosity towards open porosity. However, as previously mentioned, if such adjustments take place, great care must be taken so that total porosity does not become so high to the point where the microspheres become too fragile to be used in a therapeutic setting.

4.3. Drug Release Studies

Since ceramic bone substitutes are required to have a high level of porosity to allow for proper bone regeneration, this opens the possibility to load these bone substitutes with substances that facilitate the healing process, such as antibiotics that prevent post-operative infections or drugs that actively enhance production of new healthy bone tissue. Thus, the produced microspheres were loaded with either the antibiotic gentamicin sulphate or with the drug raloxifene hydrochloride, to potentially create two sets of microspheres, each containing different medication, and either one or both sets of spheres could then be inserted, depending on the desired treatment, in the site of bone injury to promote a safer and more efficient healing process.

Drug release studies were then performed for the different drugs, in order to understand the rate at which each drug was released from the microspheres, for how long those releases lasted, and what quantity of drug was effectively released.

4.3.1. Gentamicin

Gentamicin is an aminoglycoside antibiotic that is mainly indicated for the treatment of infections caused by strains of bacteria such as *Pseudomonas aeruginosa*, *Proteus* species, *Escherichia coli*, *Klebsiella*, *Enterobacter* and *Serratia* species, and *Staphylococcus* [58], and is also commonly used in the treatment of osteomyelitis, which is usually caused by bacterial infections following surgical fracture treatment or orthopaedic implants [60-62]. The MIC of gentamicin for reference bacteria strains varies from 0.12 to 1.0 μg/mL [59], and concentrations below 100 μg/mL are advised when in contact with human bone tissue, so as to avoid citotoxicity [64-66].

In practice, it was desired that the gentamicin would be able to be released at a concentration above the common MICs and below concentrations that would be cytotoxic, and that this drug release could be sustained for at least 7 days, so that, in a hypothetical surgical scenario, there would be enough time for the antibiotic to eliminate infectious bacteria.

To study the release profile of gentamicin for the produced hollow and non-hollow microspheres, loading solutions with different concentrations – 2mg/mL and 3 mg/mL, were used to determine if any of these concentrations have potential to get a release profile of clinical interest.

As depicted in Figures 13 and 14, both non-hollow and hollow spheres show the same release pattern and similar release rate. Regarding the effect of loading conditions , it was observed that the released levels were statistically different only up to hour 8 and hour 22 for non-hollow and hollow spheres, respectively, with the highest loading concentration leading to the highest released levels.

The release profiles indicate that hollow spheres had a higher uptake of the drug compared to non-hollow spheres for both loading conditions under study. It is possible that this is due to the existence of the hollow core in the former spheres, which may allow for a larger storage of gentamicin within its structure.

For hollow spheres, there is a peak of concentration at hour 2, which greatly decreases until hour 10, after which concentration begins to diminish more slowly, until there is no noticeable release of gentamicin between hour 46 and hour 70 (between 2 to 3 days). The concentration peaks observed at hour 2 are likely due to the release of gentamicin molecules that are adsorbed directly onto the spheres' surface and onto the pores connected to the surface, which due to interacting more readily and freely with the release medium, are thus dissolved more quickly, resulting in an early burst of gentamicin.

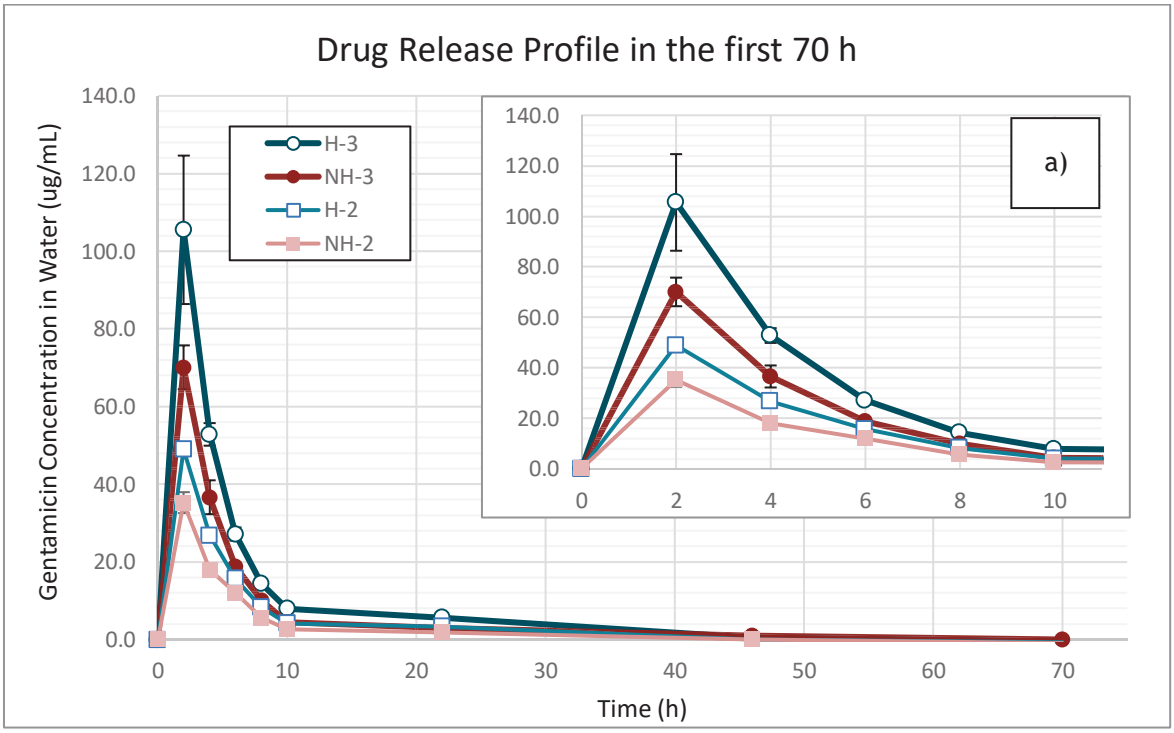


Figure 13 - Concentration of gentamicin in aqueous release solution, plotted against time. **H-3**: hollow microspheres with a loading solution of 3 mg/mL; **NH-3**: non-hollow microspheres with a loading solution of 3 mg/mL; **H-2:** hollow microspheres with a loading solution of 2 mg/mL; **NH-2:** non-hollow microspheres with a loading solution of 2 mg/mL. Error bars indicate standard deviations in µg/mL. a) Detail of gentamicin concentration values in the first 10 hours.

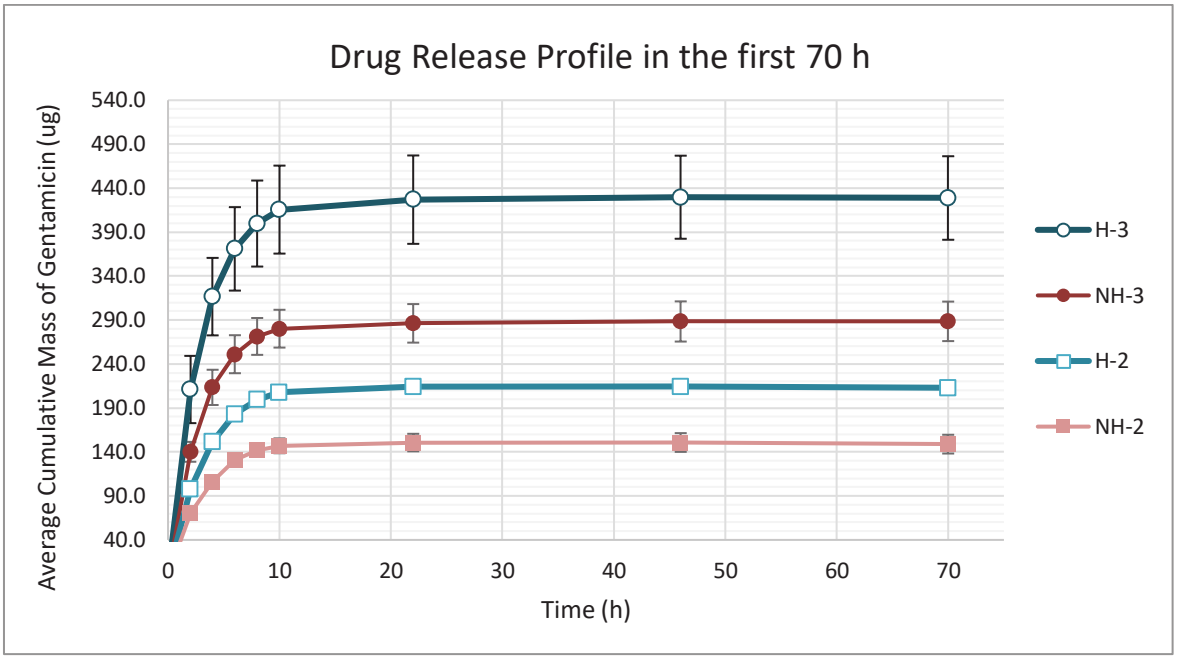


Figure 14 - Cumulative mass of gentamicin that was measured in the aqueous release solution, plotted against time. **H-3**: hollow microspheres with a loading solution of 3 mg/mL; **NH-3**: non-hollow microspheres with a loading solution of 3 mg/mL; **H-2:** hollow microspheres with a loading solution of 2 mg/mL; **NH-2:** non-hollow microspheres with a loading solution of 2 mg/mL. Error bars indicate standard deviations in µg.

In the performed experiments, considering the variables that were implemented, hollow Hap microspheres loaded with a 3 mg/mL gentamicin solution result in higher values of released gentamicin. In this case, the highest concentration of gentamicin in the aqueous medium was an average of 105.5 ± 19.1 µg/mL, reached at the 2-hour mark, from which point there is decrease to 7.92 ± 0.57 µg/mL at the 10-hour mark, with a total of 429.7 ± 47.2 µg of gentamicin released between 2 to 3 days, beyond which there is no more significant drug release. These values, while significantly higher than the MIC of gentamicin for several strains of bacteria (0.12 - 1.0 µg/mL), may present a small degree of cytotoxicity to the human host tissue, due to the peak concentration potentially being above 100 µg/mL. To safely ensure that the release concentration of gentamicin does not exceed 100 µg/mL while still being significantly above the MICs, it may be advised to load hollow microspheres with a solution with a concentration below 3 mg/mL, since, for a loading concentration of 2 mg/mL, the peak concentration of release is 48.96 ± 1.08 µg/mL, and presents a concentration above the MICs until hour 22 (3.32 ± 0.46 µg/mL).

Despite the obtained concentration values showing that this method can result in microspheres with a strong antimicrobial activity, while being safe for the host bone tissue, the obtained rate of release was not as intended: regardless of initial loading concentration and sphere type, gentamicin was only released for a maximum of about 3 days, a period much lower than the intended 7 days that would be required to more safely ensure the lack of bacterial proliferation. Given the similar release rates that were obtained for 2 mg/mL and 3 mg/mL, increasing the concentration of the loading solution will not solve this issue, which would also likely lead to the release of a cytotoxic quantity of gentamicin. It can be hypothesized that the use of a material that can entrap gentamicin molecules

into the Hap drug carries could solve this issue, since it would very likely lead to a slower drug release. However, although the desired release period was not as intended, it does not mean that the obtained release of gentamicin for about 3 days is useless; if the target area of bone healing is relatively small, a less prolonged antibiotic release may still be appropriate for preventing bacterial infection. Thus, it becomes a matter of examining the quantity and exposure of gentamicin that is necessary according to the dimensions of the site of injury.

4.3.2. Raloxifene-PEG

Raloxifene is a SERM that has been reported to increase bone mineral density and prevent bone loss, while also reducing estrogen activity of breast and uterine tissues [71-76]. The effect that Ral has on bone turnover is mainly due to its effect on osteoclast activity: Ral is capable of reducing the resorptive activity of osteoclasts, as well as their production [80-83], allowing for rate of destruction of bone tissue to decrease in relation with the creation of new bone tissue, thus preventing loss of bone mass and loss of bone mineral density. Ral has also been reported to potentially stimulate the proliferation of osteoblasts, although there is still little research on this topic [84].

Although Ral is available for administration in the form of 60 mg tablets, mainly for the treatment or prevention of osteoporosis on postmenopausal women [87], about 60 % of that Ral is absorbed after oral administration and the absolute bioavailability of the drug is only 2 %. The poor bioavailability of this drug is mainly attributed to Ral's low water solubility and dissolution, as well as due to high presystemic clearance [85, 91]. In order to increase the solubility of Ral in an aqueous medium, so that an eventual release of this drug in physiological fluid could be efficient, a conjugation reaction was performed between raloxifene hydrochloride and PEG (an amorphous substance that is highly hydrophilic) to obtain a raloxifene-PEG conjugate with a weight ratio of 1:2, using the solvent evaporation method described by Ayşegül Kavas et al. [85]. The microspheres were then loaded with the obtained Ral-PEG solution under a low vacuum environment, with an encapsulation efficiency of nearly 50 %.

In practice, it was desired that the Ral-PEG would be released below concentrations that would be cytotoxic, and that this drug release could be sustained for at least 2 weeks, so that, in a hypothetical surgical scenario, there would be enough time for raloxifene to efficiently promote bone regeneration.

The Ral-PEG release profile of both non-hollow and hollow spheres was compared. Regarding both sphere types, the quantity of Ral-PEG that they released was statistically identical (Figures 15 and 16). Their behaviour regarding the rate of drug release is also identical, exhibiting a burst of release at the 2-hour mark – in which the highest concentration of Ral-PEG in the release medium is observed - 12.6 ± 1.1 µg/mL for non-hollow spheres and 15.0 ± 4.8 µg/mL for hollow spheres, and stabilizing at the 48-hour mark, from which point on Ral-PEG release is still observed throughout 2 weeks, with the cumulative mass of Ral-PEG increasing at a rate of about 0.66 ± 0.39 µg/day for non-hollow spheres and 0.66 ± 0.34 µg/day for hollow spheres. At the end of those 2 weeks, the measured cumulative

mass of release Ral-PEG was determined to be around 34.9 ± 3.1 µg for non-hollow spheres and 38.2 ± 3.5 µg for hollow spheres.

As stated previously, the Ral-PEG conjugate was prepared with a weight ratio of 1:2. From this ratio, it is thus possible to determine the concentration of raloxifene present in Ral-PEG, according to equation (5), in which $[Ral_PEG]$ corresponds to the concentration of Ral-PEG in a sample, and $[Ral]$ is the concentration of raloxifene present in that Ral-PEG.

$$[Ral_PEG] = 2.41 \times [Ral] \quad (5)$$

We are thus able to determine that the highest concentration of Ral in the release medium was at the 2-hour mark, being 5.2 ± 0.5 µg/mL for non-hollow spheres and 6.2 ± 2.0 µg/mL for hollow spheres. After the 48-hour mark, the cumulative mass of Ral increases at a rate of about 0.27 ± 0.16 µg/day for non-hollow spheres and 0.28 ± 0.13 µg/day for hollow spheres. At the end of 2 weeks, the measured cumulative mass of released Ral was determined to be around 14.5 ± 1.3 µg for non-hollow spheres and 15.8 ± 1.4 µg for hollow spheres.

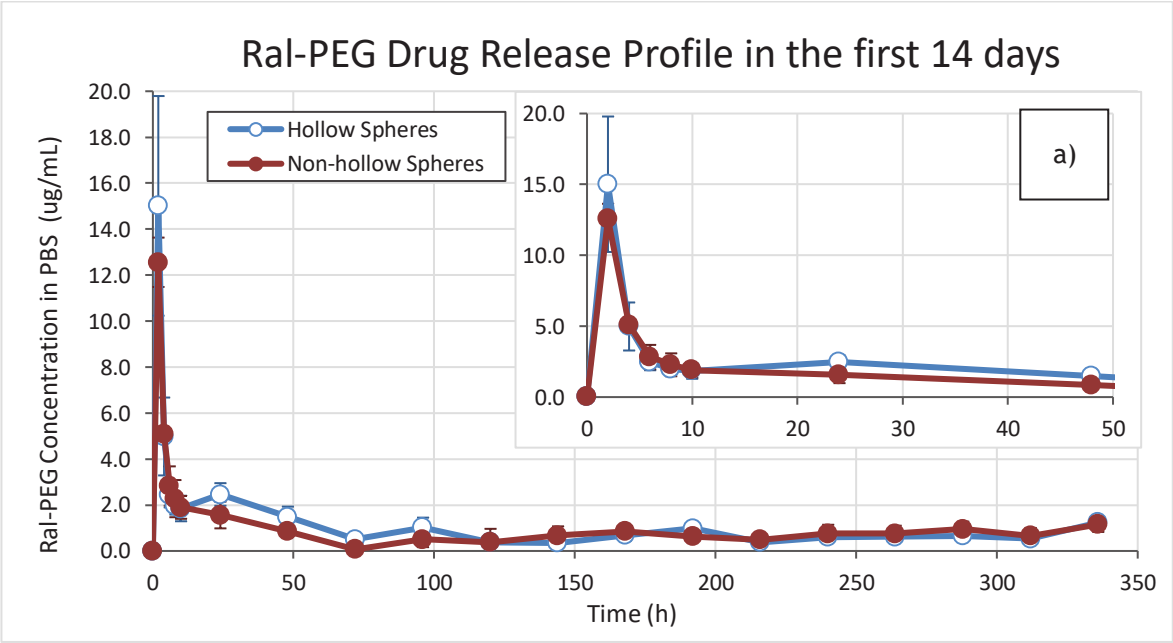


Figure 15 - Concentration of Ral-PEG in PBS release solution plotted against time, during the first week of release. This drug release corresponds to both hollow and non-hollow Hap microspheres that were previously loaded in a 1m/mL solution of Ral-PEG. Error bars indicate standard deviations in µg/mL. No statistical differences between plot values were observed at any time interval ($p < 0.05$). **a)** Detail of Ral-PEG concentration values in the first 48 hours.

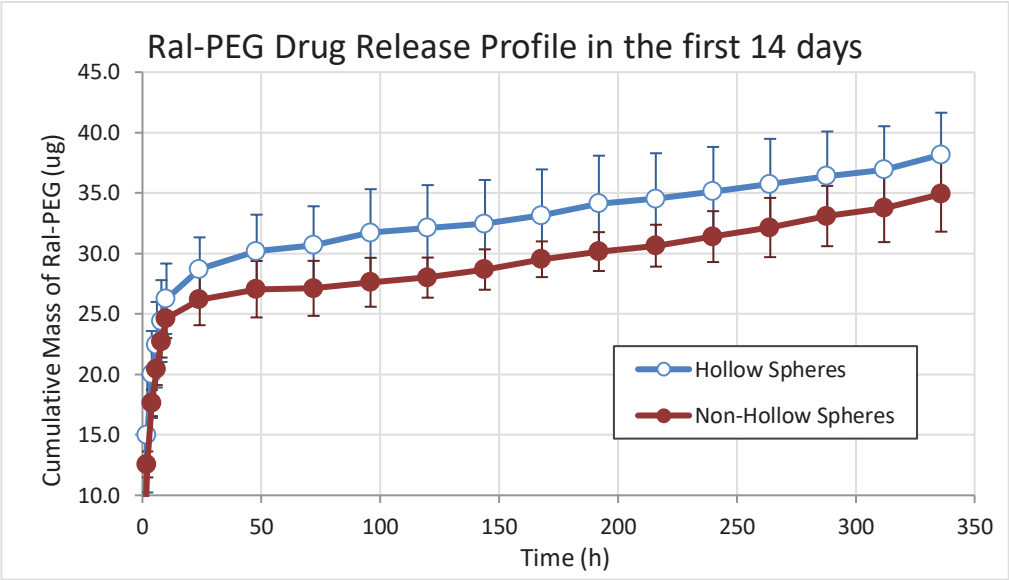


Figure 16 - Cumulative mass of Ral-PEG measured in the PBS release solution plotted against time, during the two weeks of release. This drug release corresponds to both hollow and non-hollow Hap microspheres that were previously loaded in a 1m/mL solution of Ral-PEG. Error bars indicate standard deviations in µg/mL. No statistical differences between plot values were observed at any time interval ($p < 0.05$).

The peak concentrations obtained at hour 2 go above 5.00 µg/mL for both Ral-PEG and Ral. This could result in the release solutions being potentially cytotoxic since, as a study by Kavas et al. [85] performed on adipose-derived mesenchymal stem cells from rats has shown, for concentrations of both Ral and Ral-PEG equal to 0.47 or 4.74 µg/mL, there was a noticeable cytotoxic effect on the cells after a period of 7 days, with relative cell viability remaining below 80 % even after a total of 14 days. There was no noticeable difference in viability between the Ral and the Ral-PEG tests, however, suggesting that the concentration of Ral is what ultimately lead to the development of a toxic medium, and that PEG did not have any noticeable influence in terms of cytotoxicity.

After Ral-PEG release stabilizes at around hour 48 (Figure 15), the average Ral concentration is about 0.3 µg/mL, a value that could potentially be non-cytotoxic, according to the study referenced above. However, a study by Lo Muzio et al. [86] showed that, after 7 days, MC3T3-E1 murine osteoblasts experienced cytotoxicity for Ral concentrations of 0.120 and 0.240 µg/mL, so a Ral concentration of 0.3 µg/mL still presents a risk of inducing cytotoxicity. To solve these issues with cytotoxicity, it would be recommended to use a loading solution with a much smaller concentration than 1 mg/mL of Ral-PEG.

As was previously described, 30 mg of microspheres were able to encapsulate about 50 % of 1 mg of Ral-PEG in a 1 mg/mL solution. After a period of 2 weeks, about 35 to 38 µg of Ral-PEG were released from an equal mass of microspheres, and, according to Figure 18, it appears that the cumulative mass of Ral-PEG would have a tendency to slowly increase even after the 2-week time period. If we assume that the 30 mg of microspheres encapsulated a total of 500 µg of Ral-PEG, and that the release rate after 2 weeks continued to be around 0.66 µg/day, then the spheres would be completely exhausted of Ral-PEG after a total of about 705 days (around 2 years). If Ral-PEG release can in fact be sustained for such a long time period, then the entire process of bone healing is likely

to always be supplied with Ral. However, it would be erroneous to not take the continual degradation of the Hap microspheres into account, when trying to envision more realistic results. Since Hap has a relatively slow degradation rate and no apparent changes in Hap structure and diameter were seen after a 2-week period of drug release in PBS, a much more extensive release period would have to be applied to understand the rate of degradation of the Hap microspheres (for both non-hollow and hollow spheres), and at what point does a more noticeable degradation takes place.

4.4. Cell Culture Studies

Cell culture studies were performed to test if the drug quantities released by the microspheres had an actual impact in an *in vitro* environment. For the release of gentamicin, the purpose was to mainly observe its antibacterial effects, whereas for the release of Ral-PEG, the purpose was to determine if the released drug quantities were cytotoxic and, if not, if they affected cell metabolism in a positive manner.

4.4.1. Effects of Gentamicin – Indirect Studies

For the gentamicin assays performed with the *E. coli* ATCC 25922 strain bacteria, the desired result was that the gentamicin-loaded hollow Hap microspheres were capable of significantly reducing the bacteria's viability, deterring their proliferation and growth.

A dose dependency assay was first performed, wherein filter disks embedded with 5 µL of gentamicin release solutions (which were obtained during the drug release tests described in *4.3.1. Gentamicin*) were placed on petri dish with Mueller-Hinton agar cultivated with *E. coli*. For a loading concentration of 2 mg/mL (Figure 17-a), there were only halos present in the disks that were imbibed with the release solution of hour 2, showing a distance of about 1 mm from the disk's border to the halo's limit. For a loading concentration of 3 mg/mL (Figure 17-b), halos were observed for release solutions of both hours 2 and 4, with the hour 2 samples displaying distances of 2 to 3 mm between disk and halo's borders, and distances of about 1 mm for hour 4. This is in line with the results obtained in the release profiles, that show that microspheres loaded with 3 mg/mL of gentamicin eventually led to release solutions with a higher concentration of this drug (Figure 13), thus leading to a higher antibacterial activity towards *E. coli*.

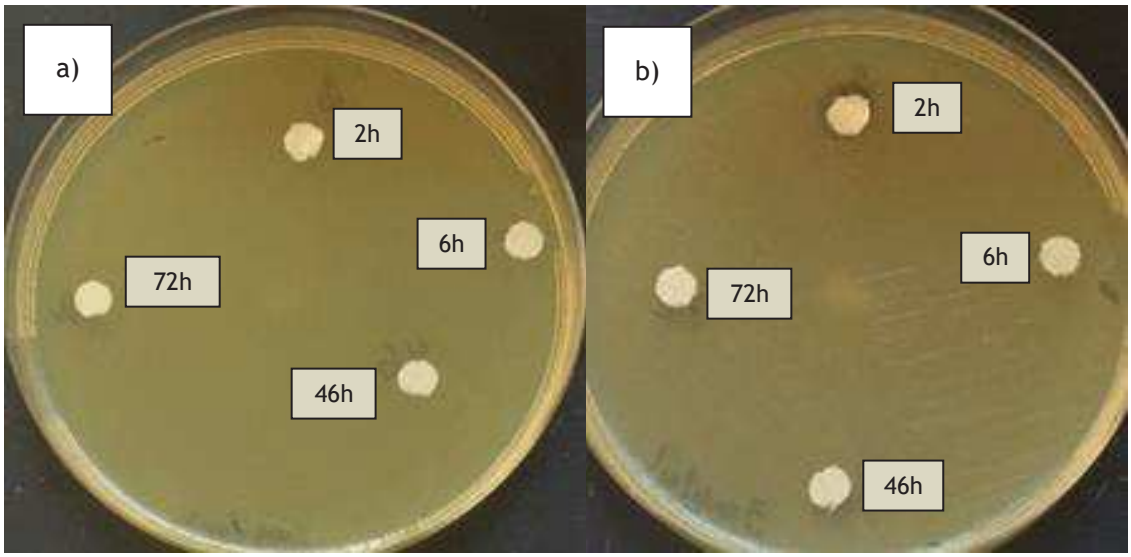


Figure 17 - Results of incubation of *E. coli* cultivated in Mueller-Hinton agar alongside filter disks imbibed with gentamicin release solutions. Tags near the disks indicate the instant at which the release solution in the disk was collected. a) Release solutions that originated from microspheres initially loaded with gentamicin solutions of 2 mg/mL and b) 3 mg/mL.

4.4.2. Effects of Gentamicin – Direct Studies

Besides the dose dependency studies, *E. coli* bacteria were also incubated alongside hollow Hap microspheres to determine if the spheres influenced bacterial viability. Mueller-Hinton petri dishes cultivated with *E. coli*, which were incubated alongside both hollow microspheres that had been supposedly depleted of gentamicin after a 3-day release, and fully loaded hollow microspheres (Figure 18). The results of this test show that microspheres loaded with gentamicin have a clearly visible effect on the reduction of *E. coli* viability, especially if they were loaded with a concentration of 3 mg/mL (Figure 18-b), corroborating previous results that indicated that a larger loading concentration resulted in the release of a larger quantity of gentamicin.

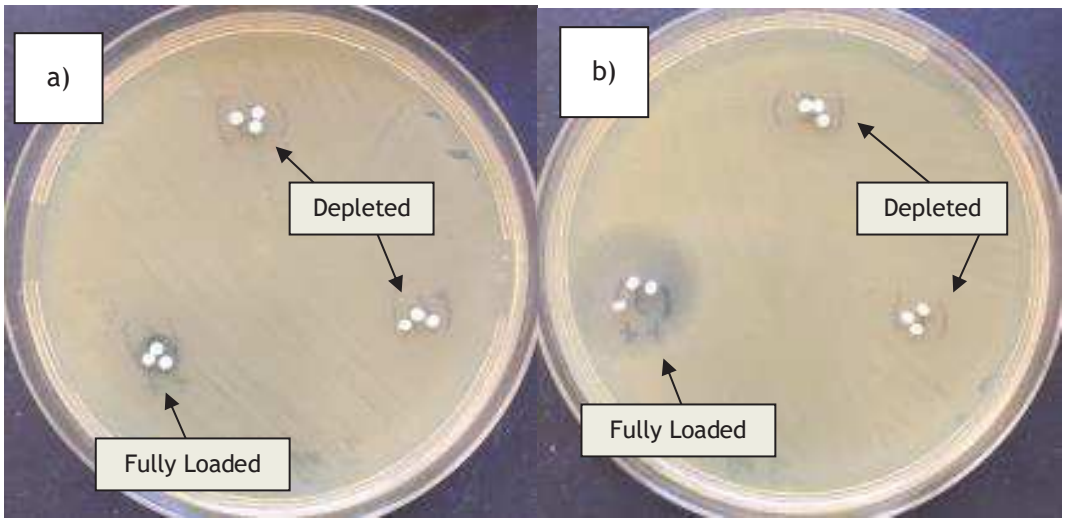


Figure 18 - Results of incubation of *E. coli* cultivated in Mueller-Hinton agar alongside hollow Hap microspheres that were either fully loaded with gentamicin or had been exhausted of it. Tags near the spheres indicate whether the groups of three spheres are loaded with gentamicin or depleted. a) Release solutions that originated from microspheres initially loaded with gentamicin solutions of 2 mg/mL and b) 3 mg/mL.

4.4.3. Effects of Ral-PEG

For the Ral-PEG experiments performed with the MG-63 – human osteoblast-like cells, the goal was to determine at which concentrations of Ral-PEG was this substance non-toxic for these cells, so that there could be some level of assurance that the Ral-PEG released by the microspheres was not potentially cytotoxic to the bone cells in a human organism.

During Ral-PEG drug release, two different release conditions were established, continuous and non-continuous, in order to study continuous drug release and store release solutions with different concentrations, and to be able to preserve spheres with different percentages of encapsulated drug. Ral-PEG release solutions resulting from continuous release were used to study dose-dependency of osteoblast-like cells' activity, as well as collagen production, while the microspheres resulting from non-continuous drug release were used in cell culture studies to analyse their potential cytotoxicity on osteoblast-like cells.

4.4.3.1. Dose Dependency

Firstly, to have a reference for the effects of different Ral-PEG concentrations on MG-63 cells, an MTT assay was conducted with solutions with known concentrations of Ral-PEG, which were incubated in 96-well microplates with a cell density of 10^4 cells/cm^2 of well surface. 9 different Ral-PEG concentrations were used, plus a solution that contained PBS with no Ral-PEG to verify if cell metabolism was affected by the used base PBS solution, and a positive control that contained only essential cell medium, which was used to then determine relative cell absorbance. The results are as presented in Figure 19.

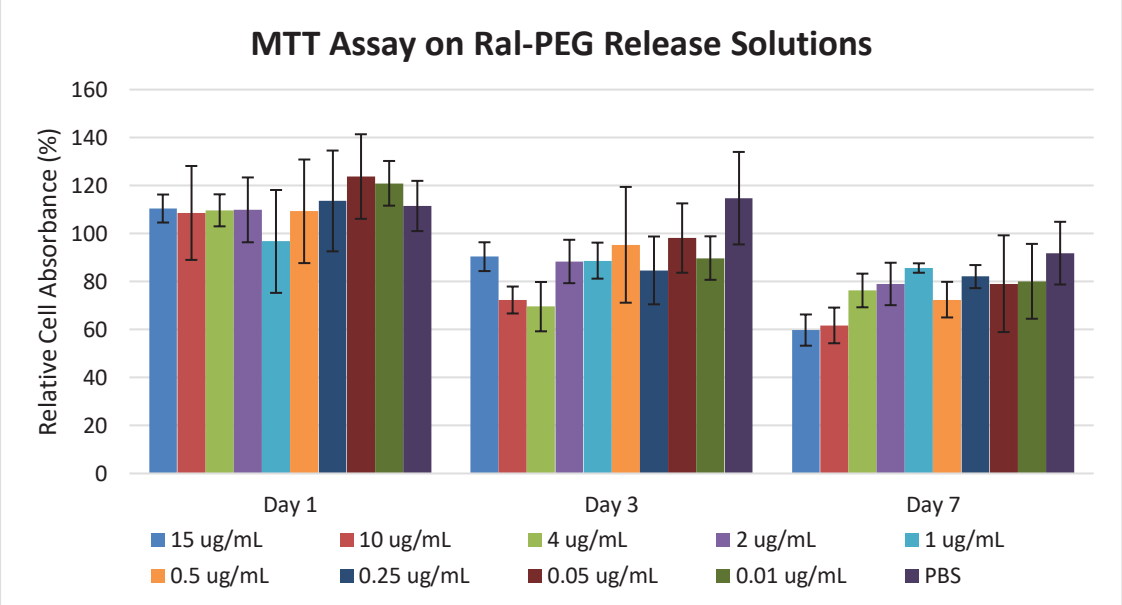


Figure 19 - Relative absorbance of MG-63 osteoblast-like cells in the presence of Ral-PEG solutions with different concentrations, at different days during the MTT assays. Error bars indicate standard deviations in %.

On Day 1, there is no statistical difference between the relative cell absorbance of all different concentrations, and they all appear to lead to the same level of metabolic activity as the control. On Day 3, however, the results for 4 μg/mL indicate that, at this concentration, relative cell absorbance is lower when compared to other concentrations, whereas the PBS solution displays the highest value of relative cell absorbance, and is thus potentially related to the highest cell metabolic activity on this day. On Day 7, there is no statistical difference between the relative cell absorbance of all different concentrations.

If the data is analysed according to the variations of each release solution along the different days, then for the concentration of 15 μg/mL, there is significant difference of relative cell absorbance along all time periods; for concentrations 10, 4, 2, 0.25 and 0.1 μg/mL, the values of absorbance decrease from Day 1 to Day 3, but are virtually identical from Day 3 to Day 7; for the concentration of 1 μg/mL and for the PBS solution, all absorbance values remain virtually identical throughout all time periods.

The results obtained for 15 μg/mL, the highest concentration, appear to indicate that a higher concentration of Ral-PEG leads to lower cell metabolic activity.

Given the abnormal behaviours seen for concentration 1 μg/mL when compared to lower and higher concentrations, it can be deduced that the results obtained for this concentration might be faulty, possibly due to the solution not having been prepared adequately, resulting in a concentration that is actually different than the one that is labeled. As for the behaviour seen in the PBS solution, the results seem to indicate that the PBS used to make the different solutions does not have any apparent effect on the cell metabolic activity on its own, as it was desired.

The Ral-PEG solutions resulting from continuous release were incubated in 96-well microplates with a cell density of 10^4 cells/cm^2 of well surface. 6 different types of Ral-PEG release solutions were used, corresponding to the time periods of 2, 4, 8, 24 and 72 hours and 7 days, plus and additional solution that contained PBS without any Ral-PEG, to act as a positive control. To analyse cell metabolism depending on the concentration of Ral-PEG of each release solution, MTT assays were performed for the duration of 1, 3 and 7 days. For each absorbance reading during an MTT assay, an additional solution consisting only of DMSO was used to act as a negative control.

Looking back at the Ral-PEG release profiles (Figures 15 and 16), in relation to hollow microspheres, between hour 2 and day 7, the concentration of released Ral-PEG in 1 mL of PBS varies between 0.35 ± 0.13 μg/mL (day 6) and 15.0 ± 4.8 μg/mL (hour 2). Regarding the incubation of the MG-63 cells for the MTT assays, the Ral-PEG release solutions in the microplates are diluted due to the addition of the cell suspensions – 50 μL of Ral-PEG solution diluted into a final volume of 100 μL. Thus, the concentration of Ral-PEG in the wells, from hour 2 to day 7, can be assumed to range from around 7.5 to 0.7 μg/mL – for the maximum value of these concentrations, this would imply a concentration of 3.1 μg/mL of raloxifene and 4.4 μg/mL of PEG in this solution.

The MTT assays, whose results are displayed in Figure 20, suggest that on Day 1, all drug release solutions had essentially the same level of effect on cell metabolism, increasing it by 30 to 90 % in relation to the control. On Day 3, there is a marked decrease in metabolic activity. Statistically speaking, the Ral-PEG solutions of hours 2 and 4 lead to a nearly identical and more marked decrease than the solutions of hours 24 and 72 and of day 7, which are considered to have had an identical effect when compared amongst themselves ($p < 0.05$). On this day, relative cell absorbance appears to vary between 30 to 50 % for the release solutions from hours 2 to 8, and between 50 to 70 % for the release solutions from hour 8 to day 7. Finally, on Day 7, all drug release solutions are considered to have statistically identical values of relative cell absorbance, with all relative absorbances roughly varying from 30 to 50 %. This seems to indicate that, regardless of the concentration of the Ral-PEG release solutions, the effect on cell metabolism will remain the same, if concentrations equal or below that of hour 2 are considered.

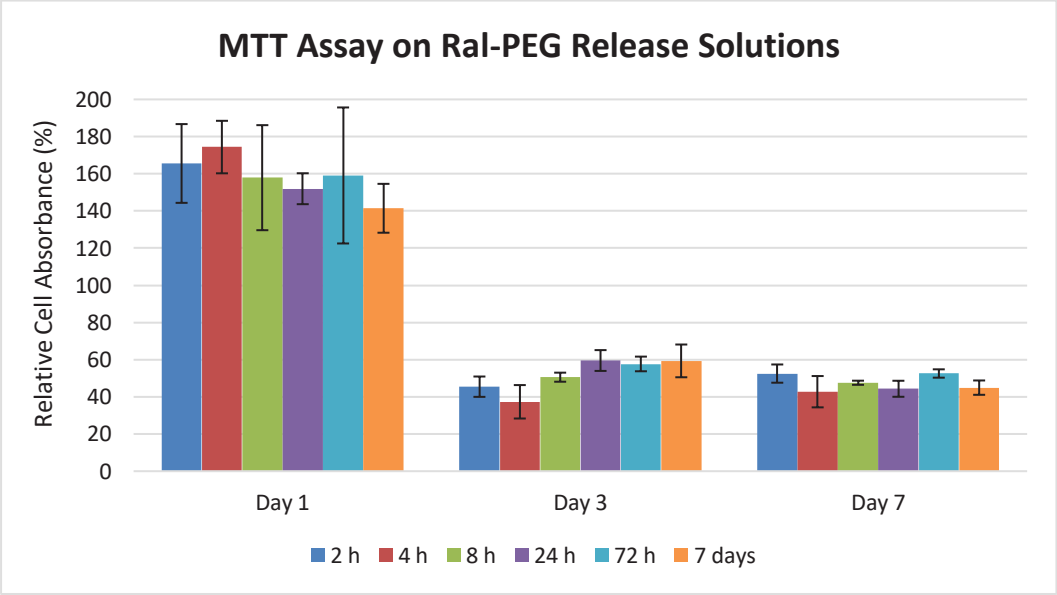


Figure 20 - Relative absorbance of MG-63 osteoblast-like cells in the presence of Ral-PEG release solutions with different concentrations, at different days during the MTT assays. Error bars indicate standard deviations in %.

If Figure 20 is analysed according to the variations of each release solution from Day 3 to Day 7, there is only statistical difference between the values obtained for hour 24 – around 60 % for Day 3 and 44 % for Day 7, whereas the remaining solutions are considered to lead to identical values of relative cell absorbance between those two days. Overall, though, it can be concluded that, between Day 3 and Day 7, there appears to be no significant changes in cell metabolic activity, regardless of the different release solutions.

The increase in absorbance values in relation to the control on Day 1 of incubation would seem to indicate that the presence of Ral-PEG increased cell metabolism, which could potentially be tied to cell proliferation and development. Yet, the notable decrease in absorbance on Day 3 of incubation seems to indicate that a notable decrease in cellular metabolic activity takes place. It can be hypothesised that the cells reached total confluence between the start of incubation and Day 3 – this

could be why they present higher cell metabolism than the control in Day 1, since they are still in a stage of proliferation and growth, while on Day 3, total confluence had been previously achieved, so the cells either started dying and then reached a point of numerical stability that is present until Day 7, or, upon reaching confluence, stopped being so metabolically active due to lack of space and nutrients for further cell growth, resulting in lower detected metabolic activity in relation to control, but not necessarily in a decrease in cell viability.

Since the only difference between the wells with the release solutions and the wells with the control is that 50 µL of PBS were added to the 50 µL of cell suspension, instead of 50 µL of released Ral-PEG, the obtained cell viabilities very likely suffered through those variations due to the presence of Ral-PEG. Some studies have shown that, although PEG based polymers are generally considered to be non-toxic, certain PEG with low molecular weights, especially PEG-based monomers, can be highly cytotoxic, some even at low concentrations [107-109]. However, a PEG with high molecular weight was used ($M_r \approx 16000$-24000), and a study that detailed the effect of both Ral-PEG and Ral on adipose-derived mesenchymal cells has shown that cell viability tended to decrease, at the same rate, with higher concentrations of either Ral-PEG or raloxifene [85], implying that the presence of PEG may not be much of a factor in terms of cytotoxicity, and that Ral may be the substance that is responsible. It should still be noted, though, that this study used concentrations of Ral-PEG and raloxifene that were significantly smaller than the ones used here, meaning that it is still possible for PEG to have a negative effect on cell viability when at higher concentrations.

Although there are several studies regarding raloxifene cytotoxicity on cancer cells [110-112], there appears to be a dearth of information regarding the potential cytotoxicity of both this drug and its conjugate with PEG on regular cells, so to determine if it is raloxifene, PEG or both substances that cause such a marked decreased in cell viability, further studies would be necessary.

4.4.3.2. Collagen Production

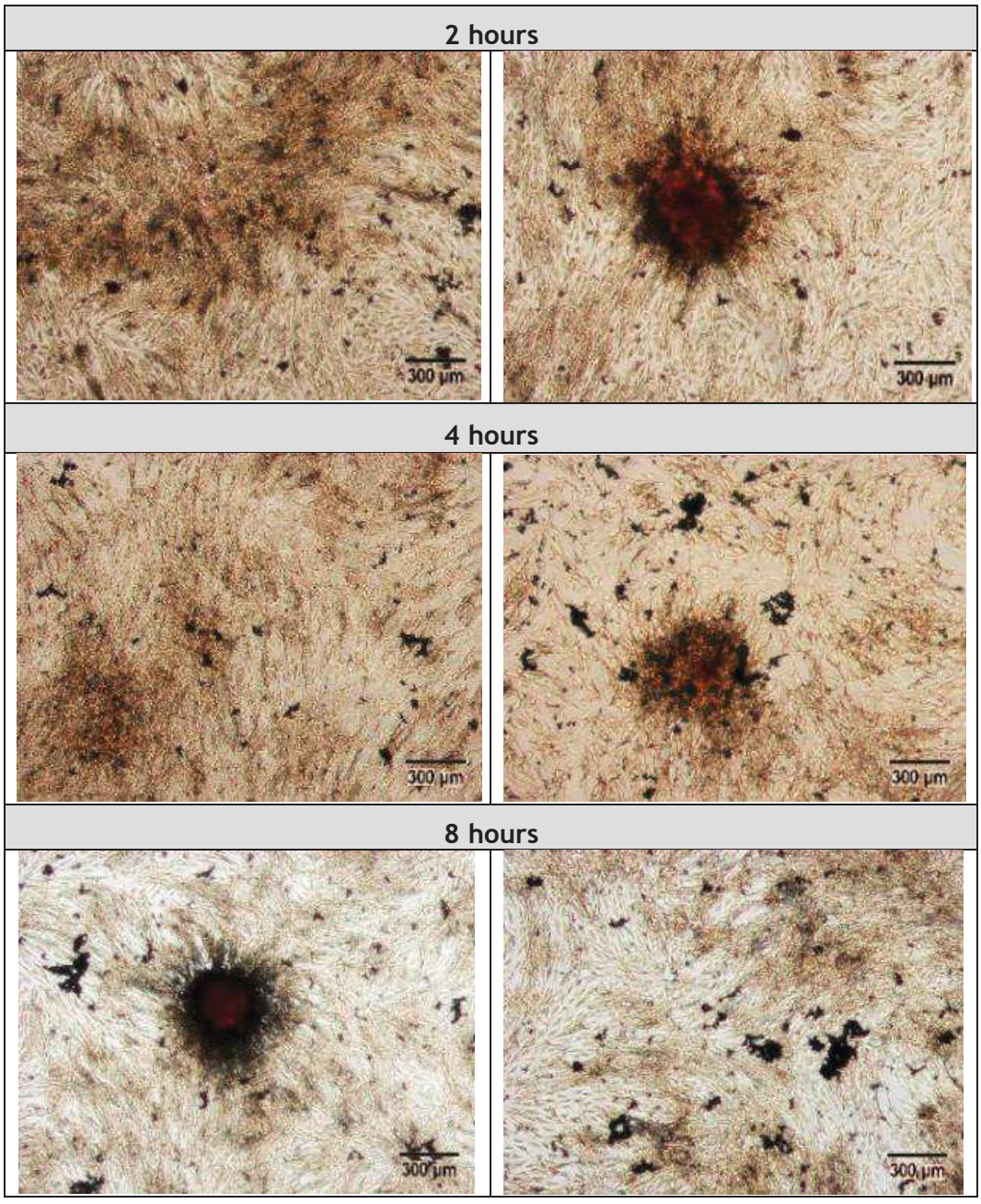
To analyse expression of the cells phenotype when exposed to the Ral-PEG release solutions, collagen synthesis of the MG-63 cells was studied; an increase in collagen biosynthesis can be a potential indicator of an increase in cell metabolism, and thus can potentially be linked to cell viability. As observed in a study by Arkaduisz et al. [113], raloxifene has the potential to promote collagen biosynthesis in human skin fibroblasts, meaning that this experiment presented an additional opportunity to test if raloxifene had the possibility to promote collagen biosynthesis in osteoblast-like cells.

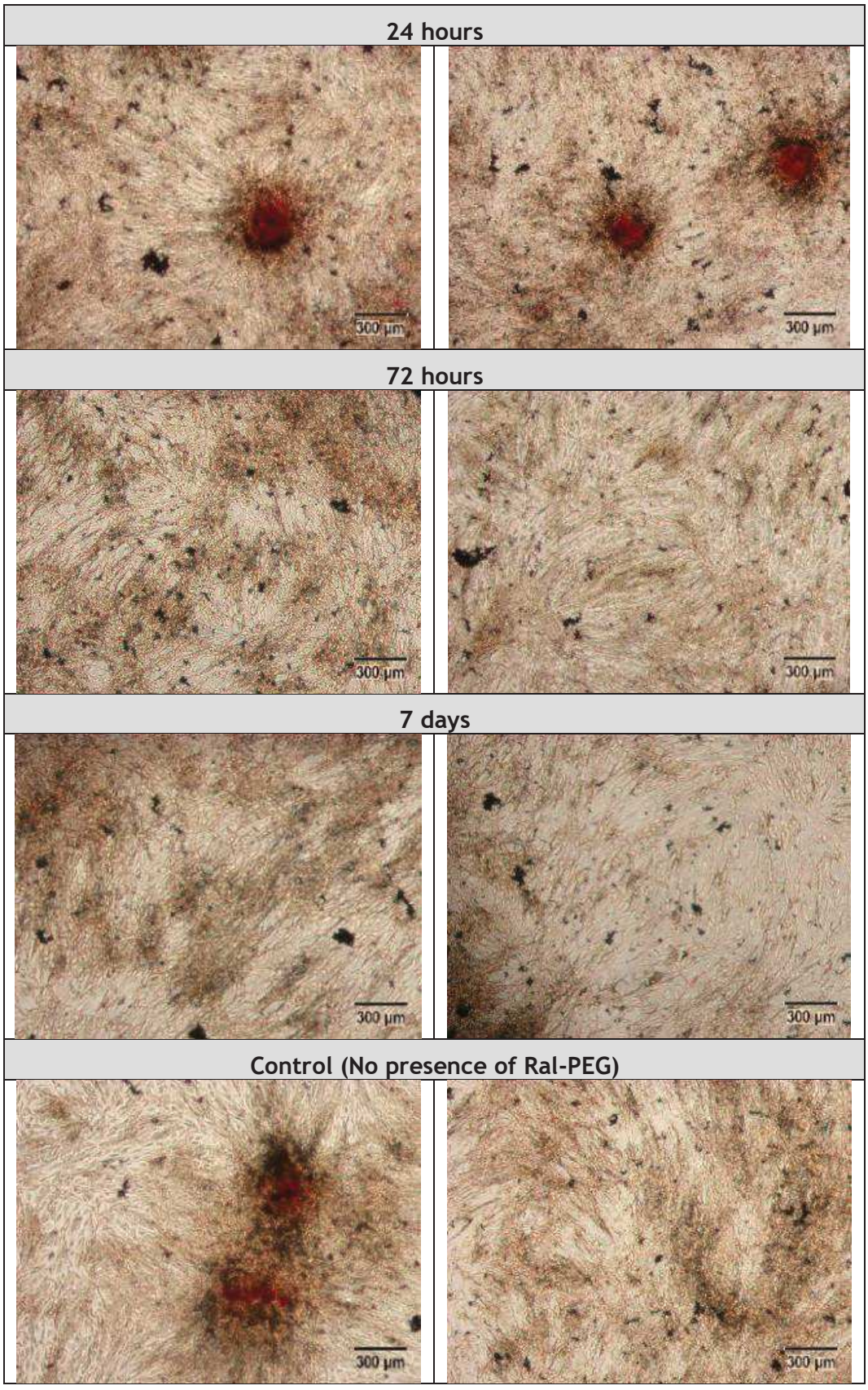
After incubating MG-63 cells in 48-well microplates, with a quantity of cells per well surface of 10^4 cells/cm^2, alongside different Ral-PEG release solutions for 8 days, a staining assay with Sirius Red was performed as described in *3.2.4.4.2. Effects of Ral-PEG on Collagen Production*, in order to observe the effects of collagen biosynthesis in the different release solutions. In Table 9, the results of the staining can be observed. Through a qualitative analysis, collagen biosynthesis seems to be on par with the control (obtained through the incubation of cells with added PBS without Ral-PEG) for

the release solutions of hours 2 to 8, with hour 24 appearing to present superior collagen biosynthesis to the control. Hour 72 and day 7, however, appear to show a slight decrease in collagen synthesis.

These results for collagen synthesis appear to be at odds with the results obtained through the MTT assay, since the latter suggest that the metabolism of the MG-63 cells appears to decrease with lower concentrations of Ral-PEG. However, if we accept the theory that total cell confluence was achieved some time between the incubation began and Day 3 and that, upon reaching this confluence, metabolic activity dropped due to lack of conditions for further cell growth, but cell viability did not necessarily decrease in the process, then the collagen results do match up.

Table 9 - Results of Sirius Red staining on wells containing MG-63 cells that were incubated alongside different Ral-PEG release solutions for seven days. **The darker and more reddish regions represent agglomerates of collagen.**





The correlation between cell metabolic activity and collagen synthesis is not very straightforward, as collagen biosynthesis is a very complex process [114]; from Day 1 to Day 7, collagen concentration

in the wells visibly increased, but cell metabolic activity decreased, according to the results in Figure 20. It is thus theorized that, upon reaching total confluence, cell activity decreased, so as not to completely exhausted all resources available for survival. Still, although the remaining viable cells stopped proliferating further, they still produced collagen, resulting in an increase in collagen concentration on the wells, while metabolic activity was lower (but not null).

4.4.3.3. Hollow Hap Microspheres

To determine if the viability of MG-63 cells was affected by the Hap microspheres themselves, resazurin assays were performed using the loaded hollow microspheres that were obtained from the non-continuous release of Ral-PEG.

The spheres were incubated in 96-well microplates with a cell density of $5x10^4$ cells/cm^2 of well surface. Microspheres that were loaded with 7 different concentrations of Ral-PEG were used, corresponding to the time periods of 0, 2, 4, 8, 24 and 72 hours and 7 days that the spheres underwent during Ral-PEG release, with an additional column with non-loaded microspheres in contact with the cellular suspension functioning as a positive control.

According to the resazurin assays, that were performed as was described in *3.2.4.4.3. Effects of Ral-PEG Loaded Microspheres*, and whose results can be observed on Figure 21, both cell metabolism and cell viability are essentially null in the presence of fully loaded microspheres (hour 0), regardless of the day. Given that the spheres were loaded in a 1 mg/mL Ral-PEG solution, and that 5 spheres were placed per well (about 14 mg of microspheres), with each well being seeded with only 100 µL of cell suspension, it is only normal that the concentration of released Ral-PEG would be so high to the point of being extremely toxic to the cells.

Apart from the results for the spheres at hour 0, all other spheres had virtually identical values of relative cell fluorescence for Day 1. On Day 4, however, there is a marked difference between the spheres of hours 2 and 4, and the spheres of hour 72 and day 7, with the latter showing higher values of relative cell fluorescence. However, on Day 8, this difference becomes accentuated only between the spheres of hour 2 and the ones of hour 72 and day 7.

If the data is analysed according to the variations of each different group of spheres along the different days, all groups of spheres have virtually identical values of relative cell fluorescence across all days, with the exception of hour 0 spheres (as previously mentioned) and hour 72 spheres, which, from Day 1 to Day 4 show a marked increase in relative cell fluorescence, followed by a decrease between Day 4 and Day 8.

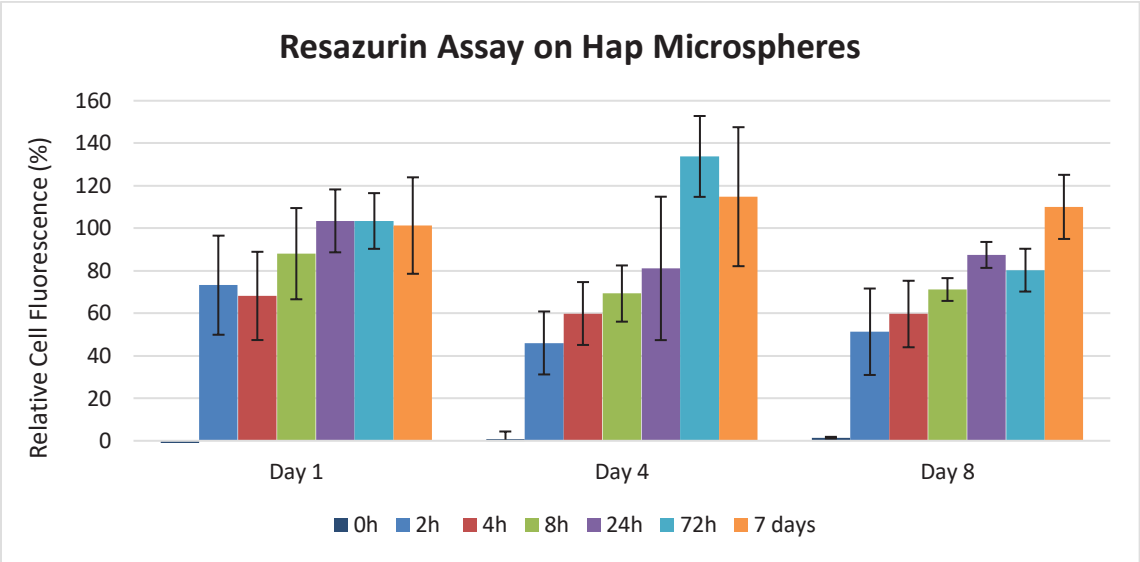


Figure 21 - Relative fluorescence of MG-63 osteoblast-like cells in the presence of hollow Hap microspheres loaded with different quantities of Ral-PEG, at different days during the resazurin assays. Error bars indicate standard deviations in %.

Compared to the results obtained in the MTT assay with the Ral-PEG release solutions, the results of the resazurin assay with the spheres appear to show a more defined relation between the effects of Ral-PEG on cell metabolic activity. The results suggest that, overall, lower quantities of Ral-PEG result in a higher metabolic activity for the MG-63 cells, and that concentrations of Ral-PEG that are too high, as in the case of the fully loaded microspheres (hour 0), can potentially result in total cell death. The MG-63 likely showed a more prolonged cell metabolic activity and better cell viability when in the presence of the hollow Hap microspheres, due to Hap generally being a good material for adhesion of bone cellular tissue, as well as due to the sphere's own structure – as a result from both its micro and macroporosity, the microsphere's outer surface, as well as its internal structure, may function as a matrix that allows for better cellular adhesion and growth, something which is lacking in the MTT assays, that were made with only liquid solutions. Additionally, baring the extreme conditions at hour 0, unlike the cells in the MTT assays, which are readily exposed to a Ral-PEG solution, in the resazurin assays there is likely an initial period were cellular interaction with Ral-PEG is lower, since the Ral-PEG molecules must first be removed from the microsphere's surface to then be dissolved into the cell suspension. A slower introduction of the drug into the cell medium can also be more favourable, since the concentration shock that the cells experience is lessened.

An important point that must be recalled is that the reaction of MG-63 cells towards certain concentrations of Ral has been examined in the past: a study by Lo Muzio et al. [86] showed that, for a duration of 7 days, MG-63 human osteoblast-like cells did not experience cytotoxicity for Ral concentrations of 0.120 and 0.240 μg/mL – in fact, for the former concentration, cell viability appeared to increase compared to the control, whereas for the latter concentration it remain identical to the control. Combined with the results observed in Figure 21, the idea that the MG-63 cell line in particular is highly compatible with Ral seems very likely, being able to withstand relatively

high concentrations of this drug, and even becoming more prolific in the presence of lower concentrations. Thus, to get a more complete picture of how cytotoxic both Ral and Ral-PEG can be for living human bone tissue, culture studies of different cell lines should be considered for this end.

Chapter 5

Conclusions

Synthetic bone substitutes have opened the door to novel ways to heal bone tissue more efficiently and with less drawbacks in terms of compatibility and availability. Ceramic calcium-phosphate derived bone substitutes have great potential in these regards, since they tend to present a high level of biocompatibility with host bone tissue. Since these substitutes must have a relatively high degree of porosity to allow for proper cell growth and migration, as well as tissue vascularization, this creates the possibility to incorporate drugs within the bone substitutes that can lead to a more successful post-operative recovery or to serve as a facilitator for the process of bone regeneration itself. To this end, hydroxyapatite microspheres were created and incorporated separately with two different types of drugs, leading to a group of spheres that were loaded with the antibiotic gentamicin, and another group that was loaded with the SERM raloxifene, which is known to promote bone healing largely through the decrease of osteoclastic activity.

The essential parameters to produce functional microspheres that were taken into consideration were its macropore size, interconnected porosity and pore volume, which was divided into closed and open porosity. Furthermore, two types of spheres were produced, non-hollow and hollow, wherein the latter had a hollow core in order to potentially lead to the encapsulation of higher drug volumes.

To induce porosity, a syringe-foaming method was employed, that is based around the introduction of foamed surfactant Pluronic® F-127 into a ceramic suspension of hydroxyapatite and sodium alginate, in order to create a ceramic foam that would be processed through a co-axial mould to create droplets, that would almost immediately undergo reticulation afterwards. The obtained microspheres had an overall spherical structure, although most non-hollow spheres were slightly ellipsoidal at one axis. Since the droplet's shape is greatly dependent of the action of gravity, this was likely due to a non-optimal distance between the exit point of the coaxial mould and the surface of the reticulation solution, meaning that this distance can be a key parameter in order to ensure maximum sphericity.

In the case of hollow spheres, polystyrene was co-injected with the ceramic foam, so that a polymeric core would be formed inside the droplets, that could later be fully combusted through heat treatment and thus leave a hollow core. Some issues arose in this regard, mainly with the hollow core being misaligned in relation to the centre of the microspheres, which could later lead to difficulties in properly predicting their drug release kinetics. The polystyrene was dissolved in dichloromethane, which is highly volatile; if the polymer dries out to quickly, its proper placement at the centre of the

sphere may be affected, and thus it would be recommended to use a less volatile solvent that would also not interfere with the integrity of the ceramic foam.

In terms of the obtained porosity, macroporosity for hollow spheres was enough to theoretically allow for bone cell migration and growth of simple blood vessels but was likely too small to allow for complete vascularization during growth of new bone tissue. An adjustment of the concentration of the used surfactant is an option, in order to create air bubbles with larger volumes.

For the drug release studies, it was shown that gentamicin loaded microspheres were capable of releasing quantities of the antibiotic that were good to stave off bacterial infections, while not being cytotoxic for the human host tissue. However, the spheres were only capable of releasing the drug for about 3 days, instead of the desired period of one week. However, this does not mean that these microspheres have no potential applications: for sites of injury that are relatively small or that do not require surgery that is too deeply invasive, a 3-day release of gentamicin can potentially be efficient.

Regarding Ral-PEG release, the microspheres were able to incorporate a sizeable quantity of raloxifene and release it for at least 2 weeks, as was desired. However, the released values of Ral-PEG might potentially be cytotoxic for the human host tissue, and the cell line used for cytotoxic studies might not have been the most appropriate in terms of predicting living bone tissue behaviour in the presence of Ral-PEG, since the used MG-63 cell line appears to have a particularly favourable affinity towards raloxifene. Studies with microspheres loaded with Ral-PEG solutions with lower concentrations are thus recommended, as well as the use of additional cell lines to create a more accurate understanding of the cytotoxicity of this drug.

Chapter 6

Future Works

Future works should strive to improve the microspheres' parameters that are crucial for complete bone growth and vascularization, mainly the spheres' porosity properties. As suggested previously, the use of a different foaming agent, such as Tween-80, during syringe foaming, is a viable alternative to try to induce higher macroporosity and better pore interconnectivity.

In the case of gentamicin, if a more prolonged release is desired, one aspect to consider would be to increase the strength of adsorption of gentamicin onto the hydroxyapatite carrier or add a barrier, in order to lead to a slower release. Furthermore, release studies should be performed in a medium that closer to that of human physiological fluids, so, instead of distilled water, PBS or even simulated body fluid should be used.

For Ral-PEG, lower loading concentrations should be considered, as well as the application of different cell lines for cytotoxicity studies. However, to more accurately analyse the effect that Ral-PEG could have on actual bone tissue, what is recommended is a study of Ral-PEG with a co-culture of human osteoblasts and osteoclasts, to observe the joint effects that the drug has on both of these cell types, since, as previously mentioned, raloxifene decreases both osteoclast activity and production, while also potentially stimulating osteoblast activity.

References

[1] JONES, J. R. (2005). 19 - Scaffolds for tissue engineering. In L. L. Hench & J. R. B. T.-B. Jones Artificial Organs and Tissue Engineering (Eds.), *Woodhead Publishing Series in Biomaterials* (pp. 201–214). Woodhead Publishing. https://doi.org/https://doi.org/10.1533/9781845690861.4.201

[2] Drake, R. L., Vogl, W., Mitchell, A. W. M., & Gray, H. (2005). Gray's anatomy for students. Philadelphia: Elsevier/Churchill Livingstone.

[3] Heaney, R. P. (2006). Bone as the Calcium Nutrient Reserve. In C. M. Weaver & R. P. Heaney (Eds.), Calcium in Human Health (pp. 7–12). Totowa, NJ: Humana Press. https://doi.org/10.1007/978-1-59259-961-5_2

[4] Alberts, B., Johnson, A., Lewis, J., Raff, M., Roberts, K., & Walter, P. (2002). Molecular biology of the cell. New York: Garland Science.

[5] Clarke B. (2008). Normal bone anatomy and physiology. Clinical journal of the American Society of Nephrology: CJASN, 3 (Supplement 3) S131-S139. https://doi.org/10.2215/CJN.04151206

[6] Commons.wikimedia.org. (2019). File: Bone cross-section.svg - Wikimedia Commons. [online] Available at: https://commons.wikimedia.org/wiki/File:Bone_cross-section.svg [Accessed 10 Feb. 2019].

[7] Pal, S. (2014). Design of artificial human joints & organs. Design of Artificial Human Joints & Organs, 9781461462552, 1–419

[8] Chen, Y., Wang, W., Ding, S., Wang, X., Chen, Q., & Li, X. (2018). A multi-layered poroelastic slab model under cyclic loading for a single osteon. *BioMedical Engineering OnLine*, *17*(1), 97. https://doi.org/10.1186/s12938-018-0528-y

[9] OpenStax, Anatomy & Physiology. OpenStax CNX. 30/07/2014 http://cnx.org/contents/14fb4ad7-39a1-4eee-ab6e-3ef2482e3e22@6.27. [Accessed 28 March 2020].

[10] Warriner, A. H., Patkar, N. M., Curtis, J. R., Delzell, E., Gary, L., Kilgore, M., & Saag, K. (2011). Which fractures are most attributable to osteoporosis?. Journal of clinical epidemiology, 64(1), 46–53. https://doi.org/10.1016/j.jclinepi.2010.07.007

[11] Plotkin, L. I., Aguirre, J. I., Kousteni, S., Manolagas, S. C., & Bellido, T. (2005). Bisphosphonates and estrogens inhibit osteocyte apoptosis via distinct molecular mechanisms downstream of extracellular signal-regulated kinase activation. Journal of Biological Chemistry, 280(8), 7317–7325. https://doi.org/10.1074/jbc.M412817200

[12] Khosla, S., Oursler, M. J., & Monroe, D. G. (2012). Estrogen and the skeleton. Trends in endocrinology and metabolism: TEM, 23(11), 576-81.

[13] Smith, E. L., & Gilligan, C. (1996). Dose-response relationship between physical loading and mechanical competence of bone. Bone, 18(1 SUPPL.), S45–S50. https://doi.org/10.1016/87563282(95)00379-7

[14] Curiel, Manuel & Poyatos R, Sierra. (2016). Bone Cell Response to Physical Activity. Journal of Osteoporosis and Physical Activity. 4. 10.4172/2329-9509.1000184. Curiel, Manuel & Poyatos R, Sierra. (2016). Bone Cell Response to Physical Activity. Journal of Osteoporosis and Physical Activity. 4. 10.4172/2329-9509.1000184.

[15] Osteoporosis Overview. (2018). Retrieved from https://www.bones.nih.gov/health-info/bone/osteoporosis/overview [Accessed 03 May 2020].

[16] Facts and Statistics. (2017). Retrieved from https://www.iofbonehealth.org/facts-statistics [Accessed 23 May 2020].

[17] Johnell, O., & Kanis, J. A. (2006). An estimate of the worldwide prevalence and disability associated with osteoporotic fractures. *Osteoporosis international : a journal established as result of cooperation between the European Foundation for Osteoporosis and the National Osteoporosis Foundation of the USA*, *17*(12), 1726–1733. https://doi.org/10.1007/s00198-006-0172-4

[18] Who are candidates for prevention and treatment for osteoporosis?. (1997). *Osteoporosis international : a journal established as result of cooperation between the European Foundation for Osteoporosis and the National Osteoporosis Foundation of the USA*, *7*(1), 1–6. https://doi.org/10.1007/BF01623453

[19] Riggs, B. L., & Melton, L. J. (1995). The worldwide problem of osteoporosis: Insights afforded by epidemiology. Bone, 17(5, Supplement 1), S505–S511. https://doi.org/https://doi.org/10.1016/8756-3282(95)00258-4

[20] Broken Bones, Broken Lives. (2018). Retrieved from https://www.iofbonehealth.org/broken-bones-broken-lives [Accessed 23 May 2020].

[21] Roberts, S. E., & Goldacre, M. J. (2003). Time trends and demography of mortality after fractured neck of femur in an English population, 1968-98: database study. *BMJ (Clinical research ed.)*, *327*(7418), 771–775. https://doi.org/10.1136/bmj.327.7418.771

[22] Teng, G. G., Curtis, J. R., & Saag, K. G. (2008). Mortality and osteoporotic fractures: is the link causal, and is it modifiable?. *Clinical and experimental rheumatology*, *26*(5 Suppl 51), S125–S137.

[23] Christiansen, B. A., Harrison, S. L., Fink, H. A., Lane, N. E., & Study of Osteoporotic Fractures Research Group (2018). Incident fracture is associated with a period of accelerated loss of hip

BMD: the Study of Osteoporotic Fractures. *Osteoporosis international : a journal established as result of cooperation between the European Foundation for Osteoporosis and the National Osteoporosis Foundation of the USA*, *29*(10), 2201–2209. https://doi.org/10.1007/s00198-018-4606-6

[24] Marsell, R., & Einhorn, T. A. (2011). The biology of fracture healing. *Injury*, *42*(6), 551–555. https://doi.org/10.1016/j.injury.2011.03.031

[25] Al-Rashid, M., Khan, W., & Vemulapalli, K. (2010). Principles of fracture fixation in orthopaedic trauma surgery. *Journal of perioperative practice*, *20*(3), 113–117. https://doi.org/10.1177/175045891002000305

[26] Einhorn T. A. (1998). The cell and molecular biology of fracture healing. *Clinical orthopaedics and related research*, (355 Suppl), S7–S21. https://doi.org/10.1097/00003086-199810001-00003

[27] Schubert, R., & Knipe, H. (2020). Fracture healing: Radiology Reference Article. Retrieved from https://radiopaedia.org/articles/fracture-healing [Accessed 26 June 2020].

[28] Aiyer, A. (2020). Fracture Healing. Retrieved from https://www.orthobullets.com/basic-science/9009/fracture-healing [Accessed May 25 2020].

[29] Sohn, H. S., & Oh, J. K. (2019). Review of bone graft and bone substitutes with an emphasis on fracture surgeries. Biomaterials research, 23, 9. https://doi.org/10.1186/s40824-019-0157-y

[30] Samarawickrama, K. (2018). A Review on Bone Grafting, Bone Substitutes and Bone Tissue Engineering. https://doi.org/10.1145/3239438.3239457

[31] Pape, H. C., Evans, A., & Kobbe, P. (2010). Autologous bone graft: properties and techniques. Journal of orthopaedic trauma, 24 Suppl 1, S36–S40. https://doi.org/10.1097/BOT.0b013e3181cec4a1

[32] Cascalho, M., & Platt, J. L. (2008). Challenges and potentials of xenotransplantation. Clinical Immunology, 1215–1222. https://doi.org/10.1016/B978-0-323-04404-2.10081-8

[33] Ranjan Dahiya, U., Mishra, S., & Bano, S. (2020). Application of Bone Substitutes and Its Future Prospective in Regenerative Medicine. https://doi.org/10.5772/intechopen.85092

[34] Pryor, L. S., Gage, E., Langevin, C. J., Herrera, F., Breithaupt, A. D., Gordon, C. R., Afifi, A. M., Zins, J. E., Meltzer, H., Gosman, A., Cohen, S. R., & Holmes, R. (2009). Review of bone substitutes. Craniomaxillofacial trauma & reconstruction, 2(3), 151–160. https://doi.org/10.1055/s-0029-1224777

[35] Kalita, S. J., Bhardwaj, A., & Bhatt, H. A. (2007). Nanocrystalline calcium phosphate ceramics in biomedical engineering. Materials Science and Engineering: C, 27(3), 441–449. https://doi.org/https://doi.org/10.1016/j.msec.2006.05.018

[36] Woesz, A. (2008). Rapid Prototyping to Produce POROUS SCAFFOLDS WITH CONTROLLED ARCHITECTURE for Possible use in Bone Tissue Engineering BT - Virtual Prototyping & Bio Manufacturing in Medical Applications. In B. Bidanda & P. Bártolo (Eds.) (pp. 171–206). Boston, MA: Springer US. https://doi.org/10.1007/978-0-387-68831-2_9

[37] Yarosh, E. B., Dmitrevskii, B. A., Naryzhnyi, V. P., & Tsvetkov, S. K. (2001). Some Characteristics of Synthetic Hydroxyapatite. Russian Journal of Applied Chemistry, 74(6), 1058–1060. https://doi.org/10.1023/A:1013080431495

[38] Sossa, P. A. F., Giraldo, B. S., Garcia, B. C. G., Parra, E. R., & Arango, P. J. A. (2018). Comparative study between natural and synthetic Hydroxyapatite: structural, morphological and bioactivity properties . Matéria (Rio de Janeiro), 23(4), e12217. https://doi.org/10.1590/s1517-707620180004.0551

[39] Kantharia, N., Naik, S., Apte, S., Kheur, M., Kheur, S., & Kale, B. (2014). Nano-hydroxyapatite and its contemporary applications. Journal of Dental Research and Scientific Development, 1, 15. https://doi.org/10.4103/2348-3407.126135

[40] Liu, C., Wang, W., Shen, W., Chen, T., Hu, L., & Chen, Z. (1997). Evaluation of the biocompatibility of a nonceramic hydroxyapatite. Journal of endodontics, 23(8), 490–493. https://doi.org/10.1016/S0099-2399(97)80307-X

[41] Blokhuis, T. J., Termaat, M. F., den Boer, F. C., Patka, P., Bakker, F. C., & Haarman, H. J. (2000). Properties of calcium phosphate ceramics in relation to their in vivo behavior. The Journal of trauma, 48(1), 179–186. https://doi.org/10.1097/00005373-200001000-00037

[42] Bohner, M. (2019). Bone Substitute Materials. In R. B. T.-E. of B. E. Narayan (Ed.) (pp. 513–529). Oxford: Elsevier. https://doi.org/https://doi.org/10.1016/B978-0-12-801238-3.00224-5

[43] Klawitter, J. J., & Hulbert, S. F. (1971). Application of porous ceramics for the attachment of load bearing internal orthopedic applications. Journal of Biomedical Materials Research, 5(6), 161–229. https://doi.org/10.1002/jbm.820050613

[44] Van der Stok, J., Van Lieshout, E. M., El-Massoudi, Y., Van Kralingen, G. H., & Patka, P. (2011). Bone substitutes in the Netherlands - a systematic literature review. Acta biomaterialia, 7(2), 739–750. https://doi.org/10.1016/j.actbio.2010.07.035

[45] Fernandez de Grado, G., Keller, L., Idoux-Gillet, Y., Wagner, Q., Musset, A. M., Benkirane-Jessel, N., Bornert, F., & Offner, D. (2018). Bone substitutes: a review of their characteristics, clinical use, and perspectives for large bone defects management. Journal of tissue engineering, 9, 2041731418776819. https://doi.org/10.1177/2041731418776819

[46] Mansour, F. R., Waheed, S., Paull, B., & Maya, F. (2020). Porogens and porogen selection in the preparation of porous polymer monoliths. Journal of Separation Science, 43(1), 56–69. https://doi.org/10.1002/jssc.201900876

[47] Chevalier, E., Chulia, D., Pouget, C., & Viana, M. (2008). Fabrication of porous substrates: a review of processes using pore forming agents in the biomaterial field. Journal of pharmaceutical sciences, 97(3), 1135–1154. https://doi.org/10.1002/jps.21059

[48] Seitz, H., Rieder, W., Irsen, S., Leukers, B., & Tille, C. (2005). Three-dimensional printing of porous ceramic scaffolds for bone tissue engineering. Journal of biomedical materials research. Part B, Applied biomaterials, 74(2), 782–788. https://doi.org/10.1002/jbm.b.30291

[49] Wang, xi, Ruan, J.-M., & Chen, Q.-Y. (2009). Effects of surfactants on the microstructure of porous ceramic scaffolds fabricated by foaming for bone tissue engineering. Materials Research Bulletin - MATER RES BULL, 44, 1275–1279. https://doi.org/10.1016/j.materresbull.2009.01.004

[50] Jabeen, F. (2018). Chapter 34 - Polymer–ceramic nanocomposites for controlled drug delivery. In Inamuddin, A. M. Asiri, & A. B. T.-A. of N. M. in D. D. Mohammad (Eds.), Woodhead Publishing Series in Biomaterials (pp. 805–822). Woodhead Publishing. https://doi.org/https://doi.org/10.1016/B978-0-12-813741-3.00035-2

[51] Paul, W., & Sharma, C. (2003). Ceramic Drug Delivery: A Perspective. Journal of Biomaterials Applications, 17, 253–264. https://doi.org/10.1177/0885328203017004001

[52] Mouriño, V., & Boccaccini, A. R. (2010). Bone tissue engineering therapeutics: controlled drug delivery in three-dimensional scaffolds. Journal of the Royal Society, Interface, 7(43), 209–227. https://doi.org/10.1098/rsif.2009.0379

[53] Colilla, M., Manzano, M., & Vallet-Regí, M. (2008). Recent advances in ceramic implants as drug delivery systems for biomedical applications. International journal of nanomedicine, 3(4), 403–414. https://doi.org/10.2147/ijn.s3548

[54] Parent, M., Baradari, H., Champion, E., Damia, C., & Viana-Trecant, M. (2017). Design of calcium phosphate ceramics for drug delivery applications in bone diseases: A review of the parameters affecting the loading and release of the therapeutic substance. Journal of Controlled Release, 252, 1–17. https://doi.org/https://doi.org/10.1016/j.jconrel.2017.02.012

[55] Santos, C., Martins, M. A., Franke, R.-P., Almeida, M. M., & Costa, M. E. V. (2009). Calcium phosphate granules for use as a 5-Fluorouracil delivery system. Ceramics International, 35(4), 1587–1594. https://doi.org/10.1016/j.ceramint.2008.08.015

[56] Queiroz, A. C., Santos, J., & Monteiro, F. (2005). Development of a system to adsorb drugs onto calcium phosphate materials. Journal of Materials Science. Materials in Medicine, 16, 641–646. https://doi.org/10.1007/s10856-005-2535-3

[57] Gubernator, J., Drulis-Kawa, Z., & Kozubek, A. (2006). A simply and sensitive fluorometric method for determination of gentamicin in liposomal suspensions. International journal of pharmaceutics, 327(1-2), 104–109. https://doi.org/10.1016/j.ijpharm.2006.07.039

[58] Pfizer New Zealand Limited. (2019). Gentamicin Solution for injection. https://www.medsafe.govt.nz/profs/Datasheet/g/Gentamicininj.pdf

[59] Andrews J. M. (2001). Determination of minimum inhibitory concentrations. The Journal of antimicrobial chemotherapy, 48 Suppl 1, 5–16. https://doi.org/10.1093/jac/48.suppl_1.5

[60] Che Seman, C. (2011). In vitro elution and dissolution of tobramycin and gentamicin from calcium phosphate. African Journal of Pharmacy and Pharmacology, 5. https://doi.org/10.5897/AJPP11.591

[61] Birt, M. C., Anderson, D. W., Bruce Toby, E., & Wang, J. (2017). Osteomyelitis: Recent advances in pathophysiology and therapeutic strategies. Journal of Orthopaedics, 14(1), 45–52. https://doi.org/https://doi.org/10.1016/j.jor.2016.10.004

[62] Gomes, D., Pereira, M., & Bettencourt, A. F. (2013). Osteomyelitis: an overview of antimicrobial therapy . Brazilian Journal of Pharmaceutical Sciences, 49(1), 13-27. https://doi.org/10.1590/S1984-82502013000100003

[63] Sigma-Aldrich (2020) Product Comparison Guide. Gentamicin Sulfate. Retrieved from https://www.sigmaaldrich.com/catalog/substance/gentamicinsulfate12345140541011?lang=en&region=GB [Accessed 20 June 2020].

[64] Rathbone, C. R., Cross, J. D., Brown, K. V., Murray, C. K., & Wenke, J. C. (2011). Effect of various concentrations of antibiotics on osteogenic cell viability and activity. Journal of orthopaedic research : official publication of the Orthopaedic Research Society, 29(7), 1070–1074. https://doi.org/10.1002/jor.21343

[65] Ince, A., Schütze, N., Karl, N., Löhr, J. F., & Eulert, J. (2007). Gentamicin negatively influenced osteogenic function in vitro. International orthopaedics, 31(2), 223–228. https://doi.org/10.1007/s00264-006-0144-5

[66] Chang, Y., Goldberg, V. M., & Caplan, A. I. (2006). Toxic effects of gentamicin on marrow-derived human mesenchymal stem cells. Clinical orthopaedics and related research, 452, 242-249. https://doi.org/10.1097/01.blo.0000229324.75911.c7

[67] Cho, C. H., & Nuttall, M. E. (2001). Therapeutic potential of oestrogen receptor ligands in development for osteoporosis. Emerging Drugs, 6(1), 137-154. https://doi.org/10.1517/14728214.6.1.137

[68] Nilsson, S., & Koehler, K. F. (2005). Oestrogen Receptors and Selective Oestrogen Receptor Modulators: Molecular and Cellular Pharmacology. Basic & Clinical Pharmacology & Toxicology, 96(1), 15-25. https://doi.org/10.1111/j.1742-7843.2005.pto960103.x

[69] An, K.-C. (2016). Selective Estrogen Receptor Modulators. Asian Spine J, 10(4), 787-791. https://doi.org/10.4184/asj.2016.10.4.787

[70] Randolph, J.F. (2006). Current Management of the Menopause, Christian Lauritzen, John Studd (Eds.). Taylor & Francis, Hilton Park, Abingdon, Oxfordshire, United Kingdom (2005), 1-448.

[71] Delmas, P. D., Bjarnason, N. H., Mitlak, B. H., Ravoux, A. C., Shah, A. S., Huster, W. J., Draper, M., & Christiansen, C. (1997). Effects of raloxifene on bone mineral density, serum cholesterol concentrations, and uterine endometrium in postmenopausal women. The New England journal of medicine, 337(23), 1641-1647. https://doi.org/10.1056/NEJM199712043372301

[72] Black, L. J., Sato, M., Rowley, E. R., Magee, D. E., Bekele, A., Williams, D. C., Cullinan, G. J., Bendele, R., Kauffman, R. F., & Bensch, W. R. (1994). Raloxifene (LY139481 HCI) prevents bone loss and reduces serum cholesterol without causing uterine hypertrophy in ovariectomized rats. *The Journal of clinical investigation*, *93*(1), 63-69. https://doi.org/10.1172/JCI116985

[73] Sliwiński, L., Folwarczna, J., Nowińska, B., Cegieła, U., Pytlik, M., Kaczmarczyk-Sedlak, I., … Trzeciak, H. I. (2009). A comparative study of the effects of genistein, estradiol and raloxifene on the murine skeletal system. Acta Biochimica Polonica, 56(2), 261—270. Retrieved from http://europepmc.org/abstract/MED/19401787

[74] Maximov, P. Y., Lee, T. M., & Jordan, V. C. (2013). The discovery and development of selective estrogen receptor modulators (SERMs) for clinical practice. Current clinical pharmacology, 8(2), 135-155. https://doi.org/10.2174/1574884711308020006

[75] Rey, J. R., Cervino, E. V., Rentero, M. L., Crespo, E. C., Alvaro, A. O., & Casillas, M. (2009). Raloxifene: mechanism of action, effects on bone tissue, and applicability in clinical traumatology practice. The open orthopaedics journal, 3, 14-21. https://doi.org/10.2174/1874325000903010014

[76] Fontana, M. C., Beckenkamp, A., Buffon, A., & Beck, R. C. (2014). Controlled release of raloxifene by nanoencapsulation: effect on in vitro antiproliferative activity of human breast cancer cells. International journal of nanomedicine, 9, 2979-2991. https://doi.org/10.2147/IJN.S62857

[77] National Center for Biotechnology Information. PubChem Database. Raloxifene, CID=5035, https://pubchem.ncbi.nlm.nih.gov/compound/Raloxifene#section=2D-Structure [Accessed 21 June 2020]

[78] Grese, T. A., Sluka, J. P., Bryant, H. U., Cole, H. W., Kim, J. R., Magee, D. E., Sato, M. (1996). Benzopyran selective estrogen receptor modulators (SERMs): Pharmacological effects and structural correlation with raloxifene. Bioorganic & Medicinal Chemistry Letters, 6(7), 903-908. https://doi.org/https://doi.org/10.1016/0960-894X(96)00141-2

[79] Bryant, H. U., Glasebrook, A. L., Yang, N. N., & Sato, M. (1996). A pharmacological review of raloxifene. Journal of Bone and Mineral Metabolism, 14(1), 1–9. https://doi.org/10.1007/BF01771666

[80] Jilka, R. L., Hangoc, G., Girasole, G., Passeri, G., Williams, D. C., Abrams, J. S., Boyce, B., Broxmeyer, H., & Manolagas, S. C. (1992). Increased osteoclast development after estrogen loss: mediation by interleukin-6. Science (New York, N.Y.), 257(5066), 88–91. https://doi.org/10.1126/science.1621100

[81] Gianni, W., Ricci, A., Gazzaniga, P., Brama, M., Pietropaolo, M., Votano, S., Patanè, F., Aglianò, A. M., Spera, G., Marigliano, V., Ammendola, S., Agnusdei, D., Migliaccio, S., & Scandurra, R. (2004). Raloxifene modulates interleukin-6 and tumor necrosis factor-alpha synthesis in vivo: results from a pilot clinical study. The Journal of clinical endocrinology and metabolism, 89(12), 6097–6099. https://doi.org/10.1210/jc.2004-0795

[82] Yang, N. N., Venugopalan, M., Hardikar, S., & Glasebrook, A. (1996). Identification of an Estrogen Response Element Activated by Metabolites of 17β-Estradiol and Raloxifene. Science, 273(5279), 1222 LP – 1225. https://doi.org/10.1126/science.273.5279.1222

[83] Kumar, V., Green, S., Stack, G., Berry, M., Jin, J. R., & Chambon, P. (1987). Functional domains of the human estrogen receptor. *Cell*, *51*(6), 941–951. https://doi.org/10.1016/0092-8674(87)90581-2

[84] Taranta, A., Brama, M., Teti, A., De luca, V., Scandurra, R., Spera, G., Migliaccio, S. (2002). The selective estrogen receptor modulator raloxifene regulates osteoclast and osteoblast activity in vitro. *Bone*, *30*(2), 368–376. https://doi.org/https://doi.org/10.1016/S8756-3282(01)00685-8

[85] Kavas, A., Keskin, D., Altunbas, K., & Tezcaner, A. (2016). Raloxifene-/raloxifene-poly(ethylene glycol) conjugate-loaded microspheres: A novel strategy for drug delivery to bone forming cells. International Journal of Pharmaceutics, 510. https://doi.org/10.1016/j.ijpharm.2016.06.053

[86] Muzio, L. L., Santarelli, A., Orsini, G., Memè, L., Mattioli-Belmonte, M., De Florio, I., … Bambini, F. (2013). MG63 and MC3T3-E1 Osteoblastic Cell Lines Response to Raloxifene. European Journal of Inflammation, 797–804. https://doi.org/10.1177/1721727X1301100322

[87] Eli Lilly and Company (2018) EVISTA- raloxifene hydrochloride tablet. Retrieved from https://uspl.lilly.com/evista/evista.html#top [Accessed 21 June 2020]

[88] Vásquez Niño, A. F., & Santos, L. A. L. dos. (2016). Preparation of an Injectable Macroporous α-TCP Cement. Materials Research, 19(4), 908-913. Epub July 18, 2016. https://doi.org/10.1590/1980-5373-MR-2016-0229

[89] Vásquez, A. F., Domínguez, S., & Loureiro dos Santos, L. A. (2017). α-TCP cements prepared by syringe-foaming: Influence of Na2HPO4 and surfactant concentration. Materials Science and Engineering: C, 81, 148–155. https://doi.org/https://doi.org/10.1016/j.msec.2017.07.056

[90] Zhang, J., Liu, W., Gauthier, O., Sourice, S., Pilet, P., Rethore, G., … Weiss, P. (2016). A simple and effective approach to prepare injectable macroporous calcium phosphate cement for bone repair: Syringe-foaming using a viscous hydrophilic polymeric solution. Acta Biomaterialia, 31, 326–338. https://doi.org/https://doi.org/10.1016/j.actbio.2015.11.055

[91] Bandela, J. J., & Anupama, C. H. (2009). Advanced PEGylation for the development of raloxifene hydrochloride, BCS class II drug. Journal of Young Pharmacists, 1. https://doi.org/10.4103/0975-1483.59316

[92] Patravale, V., Dandekar, P., & Jain, R. (2012). 4 - Nanotoxicology: evaluating toxicity potential of drug-nanoparticles. In V. Patravale, P. Dandekar, & R. B. T.-N. D. D. Jain (Eds.), Woodhead

Publishing Series in Biomedicine (pp. 123–155). Woodhead Publishing. https://doi.org/https://doi.org/10.1533/9781908818195.123

[93] Vega-Avila, E., & Pugsley, M. K. (2011, January). An overview of colorimetric assay methods used to assess survival or proliferation of mammalian cells. In Proc West Pharmacol Soc (Vol. 54, No. 10, p. 4).

[94] Ishikawa, K., Miyamoto, Y., Kon, M., Nagayama, M., & Asaoka, K. (1995). Non-decay type fast-setting calcium phosphate cement: composite with sodium alginate. Biomaterials, 16(7), 527–532. https://doi.org/https://doi.org/10.1016/0142-9612(95)91125-I

[95] Lee, G.-S., Park, J.-H., Shin, U. S., & Kim, H.-W. (2011). Direct deposited porous scaffolds of calcium phosphate cement with alginate for drug delivery and bone tissue engineering. Acta Biomaterialia, 7(8), 3178–3186. https://doi.org/https://doi.org/10.1016/j.actbio.2011.04.008

[96] Boguń, M. (2009). Rheological Properties of Sodium Alginate Spinning Solutions with Ceramic Nanoadditives. Fibres and Textiles in Eastern Europe, 17, 17–22.

[97] Valle, S. del, Miño, N., Muñoz, F., González, A., Planell, J. A., & Ginebra, M.-P. (2007). In vivo evaluation of an injectable Macroporous Calcium Phosphate Cement. Journal of Materials Science: Materials in Medicine, 18(2), 353–361. https://doi.org/10.1007/s10856-006-0700-y

[98] MITCHELL, J. R., & BLANSHARD, J. M. V. (1976). RHEOLOGICAL PROPERTIES OF ALGINATE GELS. Journal of Texture Studies, 7(2), 219–234. https://doi.org/10.1111/j.1745-4603.1976.tb01263.x

[99] Montufar, E. B., Traykova, T., Gil, C., Harr, I., Almirall, A., Aguirre, A., … Ginebra, M. P. (2010). Foamed surfactant solution as a template for self-setting injectable hydroxyapatite scaffolds for bone regeneration. Acta Biomaterialia, 6(3), 876–885. https://doi.org/https://doi.org/10.1016/j.actbio.2009.10.018

[100] Xu, H. H. K., Weir, M. D., Burguera, E. F., & Fraser, A. M. (2006). Injectable and macroporous calcium phosphate cement scaffold. Biomaterials, 27(24), 4279–4287. https://doi.org/https://doi.org/10.1016/j.biomaterials.2006.03.001

[101] Takagi, S., & Chow, L. C. (2001). Formation of macropores in calcium phosphate cement implants. Journal of Materials Science: Materials in Medicine, 12(2), 135–139. https://doi.org/10.1023/A:1008917910468

[102] Prakasam, M., Locs, J., Salma-Ancane, K., Loca, D., Largeteau, A., & Berzina-Cimdina, L. (2015). Fabrication, Properties and Applications of Dense Hydroxyapatite: A Review. Journal of functional biomaterials, 6(4), 1099–1140. https://doi.org/10.3390/jfb6041099

[103] Peon, E., Fuentes, G., Delgado, J. A., Morejon, L., Almirall, A., & García, R. (2004). PREPARATION AND CHARACTERIZATION OF POROUS BLOCKS OF SYNTHETIC HYDROXYAPATITE, 228, 225–228.

[104] Marchi, Juliana, Ribeiro, Christiane, Bressiani, Ana Helena de Almeida, & Marques, Márcia Martins. (2013). Cell response of calcium phosphate based ceramics, a bone substitute material. Materials Research, 16(4), 703-712. Epub April 23, 2013. https://doi.org/10.1590/S1516-14392013005000058

[105] Mutsuddy, B. C., & Ford, R. G. (1994). Ceramic Injection Molding. Springer US. Retrieved from https://books.google.pt/books?id=7_N11G5sAVkC

[106] Unosson, J., Montufar, E. B., Engqvist, H., Ginebra, M.-P., & Persson, C. (2016). Brushite foams—the effect of Tween® 80 and Pluronic® F-127 on foam porosity and mechanical properties. Journal of Biomedical Materials Research Part B: Applied Biomaterials, 104(1), 67–77. https://doi.org/10.1002/jbm.b.33355

[107] Biondi, O., Motta, S., & Mosesso, P. (2002). Low molecular weight polyethylene glycol induces chromosome aberrations in Chinese hamster cells cultured in vitro. Mutagenesis, 17(3), 261–264. https://doi.org/10.1093/mutage/17.3.261

[108] Razzazan, A., Atyabi, F., Kazemi, B., & Dinarvand, R. (2016). Influence of PEG Molecular Weight on the Drug Release and In vitro Cytotoxicity of Single-Walled Carbon Nanotubes-PEG-Gemcitabine Conjugates. Current drug delivery, 13(8), 1313–1324. https://doi.org/10.2174

[109] Biondi, O., Motta, S., & Mosesso, P. (2002). Low molecular weight polyethylene glycol induces chromosome aberrations in Chinese hamster cells cultured in vitro. Mutagenesis, 17(3), 261–264. https://doi.org/10.1093/mutage/17.3.261

[110] Nikolic, I., Andjelkovic, M., Zaric, M., Zelen, I., Milosavljevic, Z., Canovic, P., & Mitrovic, M. (2018). Enhanced cytotoxicity and apoptosis by raloxifene in combination with estrogen and methotrexate in human endometrial stromal cells. *Chemical biology & drug design*, *91*(4), 885-892. https://doi.org/10.1111/cbdd.13152

[111] Fryar, E. B., Das, J. R., Davis, J. H., Desoto, J. A., Laniyan, I., Southerland, W. M., & Bowen, D. (2006). Raloxifene attenuation of 5-FU/methotrexate cytotoxicity in human breast cancer cells: the importance of sequence in combination chemotherapy. Anticancer research, 26(3A), 1861–1867.

[112] Taurin, S., Nimick, M., Larsen, L., & Rosengren, R.J. (2015). A novel curcumin derivative increases the cytotoxicity of raloxifene in estrogen receptor-negative breast cancer cell lines. International Journal of Oncology, 48, 385-398. https://doi.org/10.3892/ijo.2015.3252

[113] Surazynski, A., Jarzabek, K., Haczynski, J., Laudanski, P., Palka, J., & Wolczynski, S. (2003). Differential effects of estradiol and raloxifene on collagen biosynthesis in cultured human skin fibroblasts. International journal of molecular medicine, 12(5), 803–809.

[114] Last, J. A., & Reiser, K. M. (1984). Collagen biosynthesis. Environmental Health Perspectives, 55, 169–177. https://doi.org/10.1289/ehp.8455169